SLAC-R-751

SLAC-ABC-42

B-Factory Contributions to the 1991 Particle Accelerator Conference

Stanford Linear Accelerator Center, Stanford University, Stanford, CA 94309

Work supported by Department of Energy contract DE–AC02–76SF00515.

PHYSICS AND TECHNOLOGY CHALLENGES OF $B\bar{B}$ FACTORIES*

Michael S. Zisman
Accelerator & Fusion Research Division, Lawrence Berkeley Laboratory, Berkeley, CA 94720

Abstract

An e^+e^- collider designed to serve as a B factory requires a luminosity of 3×10^{33} cm^{-2} s^{-1}—a factor of 20 beyond that of the best present collider (the CESR ring)—and thus presents a considerable challenge to the accelerator builder. To optimize the experiment, it is necessary that the $B\bar{B}$ system have a moving center-of-mass, which implies different energies for the two beams (hence an "asymmetric" collider). This feature dictates that a two-ring configuration be used. Accelerator physics issues that arise in such a design are related to the need to tightly focus the beams to a vertical beta function on the order of 1 cm, to bring the beams from two different rings into collision and then cleanly separate them again, and to mask the detector region sufficiently to permit measurements with very large beam currents passing through the interaction region. In addition, the process of optimizing the luminosity for asymmetric collisions breaks new ground.

Because the luminosity is limited by the beam-beam interaction, any large improvement must come from considerably increasing both the beam current and the number of bunches in the ring. These choices place many demands on accelerator technology as well as accelerator physics. Vacuum systems must be designed to handle the thermal load from a multi-ampere beam of 8–9 GeV and to maintain an adequate running pressure (below 10 nTorr) in the face of a large gas load from synchrotron radiation induced photodesorption. An RF system capable of supporting the high beam currents must be developed. To reduce the growth of potentially strong multibunch instabilities, the cavity higher-order modes (HOMs) must be highly damped to $Q \leq 70$. Even with a well-optimized RF system, the high beam currents typically mean that wideband multibunch feedback systems (both longitudinal and transverse) are needed to maintain beam stability. Effective approaches to deal with these issues have been identified by the various B factory design groups, and representative examples will be mentioned.

I. INTRODUCTION

There has been growing interest in the past several years in the design of a high-luminosity e^+e^- collider, operating at the $\Upsilon(4S)$ resonance, to serve as a "B factory." The primary physics motivation for such a facility is to determine the origins of *CP* violation. This phenomenon is expected to be easily observable in the B system, and determining its origins will provide a stringent test of the Standard Model. *CP*-violation studies benefit considerably from having a moving center of mass for the $B\bar{B}$ system, so an asymmetric collider is preferred. The physics capability of such a facility is not restricted solely to *CP*-violation studies; rich programs in rare B decays, Υ spectroscopy, charm and tau physics, and two-photon physics will also be available.

Although both dual-storage-ring [1–6] and linac-plus-storage-ring [7] designs have been studied, the focus here will be on the former configuration, storage-ring-based systems. All presently active proposals have chosen this design approach.

II. REQUIREMENTS

To study *CP* violation at the $\Upsilon(4S)$ resonance with an asymmetric collider, a peak luminosity of 3×10^{33} cm^{-2} s^{-1} is needed [8]. The actual figure-of-merit for the collider, however, is not the peak but the *integrated* luminosity. This is because the physics measurements require the study of an abundant sample of B decays to obtain statistically significant results. It is in this sense that we refer to the collider as a "factory."

The luminosity can be expressed in terms of the appropriate collider parameters as [5]

$$\mathcal{L}\left[\text{cm}^{-2}\text{s}^{-1}\right] = 2.17 \times 10^{34} \xi \left(1 + r\right) \left(\frac{I \cdot E}{\beta_y^*}\right)_{+,-} \qquad (1)$$

where I is the total beam current (A), β_y^* is the vertical beta function at the interaction point (cm), r is the beam aspect ratio (σ_y^*/σ_x^*, i.e., 0 for flat, 1 for round beams), E is the beam energy (GeV), and ξ is the beam-beam tune shift parameter. The subscript on the rightmost factor in Eq. (1) signifies that it can be evaluated using the parameters from either the electron (–) or positron (+) ring. The beam-beam tune shift parameter is not really under our control, and the beam energy is constrained by the need to run at the $\Upsilon(4S)$ resonance, requiring that $E_+ \cdot E_- = 28$ GeV^2.

It is clear from inspection of Eq. (1) that a twentyfold increase in luminosity compared with existing colliders requires high beam currents and small beta functions at the interaction point (IP). The requirement for low beta functions leads to some practical difficulties. For example, low beta functions are produced by strong quadrupoles, and these make the chromaticity correction difficult. Moreover, to take advantage of the low beta functions, there is a concomitant need for short bunches, such that $\sigma_l \leq \beta^*$. To produce the short bunches takes a high RF voltage, and thus considerable RF hardware. Taken together, these considerations imply a practical limit corresponding to $\beta_y^* = 1$–2 cm.

Because of the limitation from the beam-beam interaction, that is, the limit on the maximum value of ξ, a large increase in beam current implies the use of many more bunches than is typical of today's colliders. (Clearly it is possible to put high current in fewer bunches, but the single-bunch intensity is limited by the transverse mode-coupling instability, and the

* This work was supported by the Director, Office of Energy Research, Office of High Energy and Nuclear Physics, High Energy Physics Division, U.S. Department of Energy, under Contract No. DE-AC03-76SF00098.

beam-beam limit pushes the design towards an unreasonably large emittance.) Given little maneuvering room, it is reasonable for the designer to choose the number of bunches to be sufficiently large that *the parameters of a single bunch remain relatively standard.* This is the approach followed by essentially all B factory design groups. Typical parameter ranges for the designs considered here appear in Table 1.

Table 1
Typical B Factory Parameter Ranges

Parameter	Value
Total current, I (A)	1–3
Single-bunch current, I_b (mA)	1–5
No. of bunches, k_B	100–2000
Horizontal emittance, ε_x (nm·rad)	100
Bunch length, σ_L (cm)	1
Energy, E_-/E_+ (GeV)	8/3.5 or 9/3.1
Luminosity, $\mathcal{L}$ ($cm^{-2}\ s^{-1}$)	$1–3 \times 10^{33}$

III. PHYSICS CHALLENGES

The design of a high-luminosity asymmetric B factory leads to physics challenges primarily in the areas of lattice design and the beam-beam interaction. In the first area, the issues are related to the production of low β_y^* values, the separation of the two beams, and the design of the masking system. In the second area, the physics issues are centered around the techniques for optimizing the luminosity for the new parameter regime of asymmetric collisions.

Lattice Design

Low beta function. To provide the required luminosity, it is necessary to produce low β_y^* values, on the order of 1 cm, without introducing excessive chromaticity into the lattice. To accomplish this, the low-beta quadrupoles must be located as close as possible to the IP, as shown in Fig. 1 for the SLAC/LBL/LLNL design [5]. Although the permissible chromaticity can only be determined by actual particle tracking simulations, a good rule to apply is that β/s_Q should be less than 100, where s_Q is the distance of the quadrupole from the IP and β is the beta function at the quadrupole location. As can be seen in Fig. 1, the low-energy beam (LEB) focusing does not present a problem, but the high-energy beam (HEB) is more difficult. To locate the HEB quadrupole closer to the IP, it is designed as a superconducting Panofsky-style septum quadrupole. Equivalent design approaches with conventional magnets have been followed by other groups [2, 3, 4].

Because the LEB focusing quadrupoles are close to the IP, they lie within the solenoidal field of the detector. This restricts the choice of technology to either permanent magnets or superconducting magnets. Solutions using one or both of these technologies have been adopted by various designers. An example of an interaction region layout based on superconducting magnets is shown in Fig. 2, taken from Ref. [4]. In this case, the solenoid field is compensated by means of "anti-solenoid" windings to avoid coupling the horizontal and vertical beam motions. When using permanent magnets, as in Fig. 1, coupling is compensated with skew quadrupoles located outside the detector region. The placement and dimensions of the low-beta quadrupoles are restricted by the "detector stay-clear" area, usually defined as a 300 mrad cone.

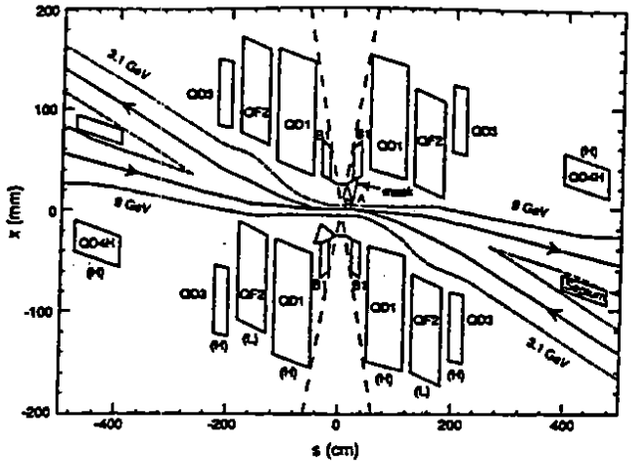

Figure 1. Anamorphic plan view of a B Factory interaction region for head-on collisions [5].

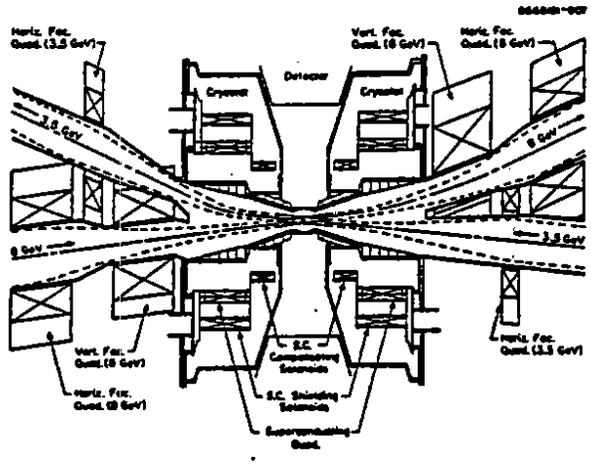

Figure 2. Configuration of a B factory interaction region (for a non-zero crossing angle geometry) with superconducting magnets [4].

Beam separation. The technique used for beam separation in an asymmetric B factory depends in large measure on the design approach. For the commonly adopted head-on collision case, the separation is accomplished by means of dipoles located close to the IP followed by offset quadrupoles. The separation dipoles could either be run in a symmetric or an asymmetric configuration; the latter case, illustrated in Fig. 1, is referred to as an "S-bend" geometry. The advantages of the S-bend geometry are that it decouples the masking solutions for the two rings, and it permits the synchrotron radiation fans generated by the separation magnets to exit the interaction region without creating severe background problems. It is worth noting here that an S-bend layout of the type shown in Fig. 1 lends itself well to being converted into a non-zero crossing angle scheme (cf. Fig. 2) without major hardware rearrangements.

Masking. A successful masking scheme must take into account all sources of backgrounds, including synchrotron radiation from the separation magnets and offset quadrupoles, lost particles from beam-gas interactions, and lost particles during injection [9]. It is also important that the solution adopted be insensitive to the details of the beam tail distribution and to small displacements of masks, magnets, and beam orbits. In general, backgrounds are never completely understood, so it is desirable to aim for safety margins of more like a factor of ten than a factor of two. It is good practice for designers of high luminosity accelerators to have close involvement with the detector users. The machine-detector interface is one of the most crucial aspects of the machine design, and the effort and care spent on it are evident in the various design reports that are now available [1–6].

Beam-Beam Interaction

Choice of Tune Shift. The beam-beam tune shift in the case of an asymmetric collider has not been studied experimentally. In the absence of such data, most design groups have taken guidance from the existing body of data on symmetric collisions [10]. It can be seen from such data that the beam-beam tune shift parameter ξ lies in the range from 0.02 to 0.06 for present colliders. Because most machines have reached $\xi = 0.03$, this value has generally been adopted by B factory design groups as a prudent target figure. (The KEK group [2] has adopted a larger tune shift value of 0.05, based on their choice to use very short bunches, 0.5 cm.) Note that this value is *not* intended to represent a beam-beam limit, it is merely a design parameter. To stay closer to the existing body of knowledge, head-on collisions are the initial design choice of all but one group [4]. For each case, beam-beam simulations are being carried out to demonstrate that the design choice is a realistic one. Thus far, it is fair to say that no new physics issues have arisen that are related to the asymmetry itself.

Energy Transparency. At present, most designers have adopted some set of conditions intended to make the asymmetric beam-beam collisions behave similarly to the well-studied symmetric case. The so-called "energy transparency" conditions postulated by Chin [11] require equality of beam-beam parameters, beam sizes, tune modulation from synchrotron oscillations at the IP, and damping decrements, $\lambda = T_0/\tau_{SR}$. Thus, we choose parameters such that

$$\xi_{x,+} = \xi_{x,-} \text{ and } \xi_{y,+} = \xi_{y,-}$$

$$\sigma_{x,+} = \sigma_{x,-} \text{ and } \sigma_{y,+} = \sigma_{y,-}$$

$$\left(\frac{\sigma_l V_\epsilon}{\beta^*_{x,y}}\right)_+ = \left(\frac{\sigma_l V_\epsilon}{\beta^*_{x,y}}\right)_-$$

$$\lambda_+ = \lambda_-$$

Further constraints have been put forth by Krishnagopal and Siemann [12] and these "equal tuneprint" conditions have been adopted in some designs [2,4]. The present view is that such symmetrization attempts are convenient (in the sense of restricting the parameter space available), but may not be entirely necessary. It is also unclear whether the restricted parameters corresponding to the symmetry conditions guarantee the optimum luminosity. It has been shown in one case [5] that the effects of parasitic collisions intrinsically tend to break the symmetry between the two beams anyway. This aspect of the parameter optimization needs further work.

Crab Crossing. To permit a non-zero crossing angle while avoiding the excitation of synchrobetatron resonances, it is attractive to consider the possibility of crab crossing. This scheme [13] involves the use of a transverse deflecting mode of crab RF cavities, located at a phase difference of

$$\Delta\phi = (n \pm 1/4)\, 2\pi$$

from the IP, to rotate the head and tail of the bunches such that they collide head-on at the IP, but in a transversely moving reference frame.

The voltage required to perform the rotation is given by

$$V_c = \frac{(E/e)\phi\lambda_c}{2\pi\sqrt{\beta_{xc}\beta^*_x}} \qquad (2)$$

For typical parameters, V_c is about 2 MV. Simulations done to date [4,5] suggest that voltage and phase tolerances are reasonable, so the technique should be viable. Nonetheless, prudence dictates that a small crab angle, on the order of 10 mrad, is the best choice. Such an angle is sufficiently small that it does not obviate the need for common quadrupoles for the two beams, as shown in Fig. 2. It is clear that crab crossing is a promising technique, though it has not yet been tested. Because of the absence of separation dipoles, the synchrotron radiation liberated near the IP is reduced with the crab crossing scheme compared with the head-on case; this should be of benefit in terms of detector backgrounds.

IV. TECHNOLOGY CHALLENGES

The physics issues discussed in Section III make certain implicit assumptions about the hardware capabilities in a B factory. For example, beam lifetime estimates assume that the average pressure in the storage rings will remain below about 10 nTorr (N_2 equivalent) despite the high gas loads associated with possibly several amperes of circulating beam. Similarly, luminosity estimates assume that these high beam currents can be supported without melting anything. The assessment of growth times for coupled-bunch instabilities is based on the ability to damp the dangerous HOMs of the RF cavities to $Q \leq 70$. Perhaps most importantly, we assume that the integrated luminosity can be maintained, that is, that the reliability of the components is such that the collider does not "spend all of its time in the shop."

In this section we discuss the technology areas where the main challenges arise. These include the vacuum system, the RF system, and the feedback system. It is worth commenting here that some other items, such as the separation magnets indicated in Figs. 1 and 2 (and the equivalent components in each of the other interaction region designs), are nontrivial design tasks as well.

Vacuum System

There are two main challenges for a B factory vacuum system:

- withstanding the high thermal flux from the synchrotron radiation power
- maintaining a low pressure in the face of considerable synchrotron radiation induced gas desorption

The average linear power density for the chamber is given by

$$P_L = \frac{P_{SR}}{2\pi\rho} \propto \frac{E^4 I}{\rho^2} \qquad (3)$$

This quantity varies widely among the various designs, as it depends on both the beam current requirement and the bend radius of the ring magnets. The lowest power density is that of the KEK design [3], 1.5 kW/m; the highest value, 25 kW/m comes from the "hard-bend" region of the Cornell design [4]. In terms of thermal management, the more important quantity is the areal density. The height of the synchrotron radiation fan at the chamber wall is typically about 0.4 mm, in which case the areal power densities range from 0.4 to 5.6 kW/cm^2.

The photodesorption gas load in the B factory rings can be written as

$$Q_{gas} = 2.42 \times 10^{-2}\, E_{[GeV]}\, I_{[mA]}\, \eta_F \quad [\text{Torr}\cdot\text{L/s}] \qquad (4)$$

where the desorption coefficient, η_F, represents the number of molecules produced per incident photon. The desorption coefficient depends on the chamber material, its history, and the photon dose to which the material has been exposed. After exposure to a few hundred ampere-hours of beam, values of low-to-mid 10^{-6} are expected for a copper chamber.

The two approaches that can be adopted for the B factory are a standard chamber shape, with a pumping channel on the inner radius, or an antechamber design in which the synchrotron radiation photons exit through a slot in the wall into an external pumping chamber. For cases where the design pressure can be achieved with a pumping speed of S = 100 L/s/m, no antechamber is needed. For cases where S ≥ 500 L/s/m is required, standard distributed ion pumps will not suffice. Then the system of choice is to use non-evaporable getter (NEG) or titanium sublimation pumps (TSPs). In a difficult case, such as the hard-bend region of the Cornell design, where the photon flux is high and where the pressure has been held to 1 nTorr to reduce backgrounds, both types of pumps are used with an antechamber configuration (see Fig. 3) to give a total pumping speed of about 2500 L/s/m.

Most designers favor a chamber made from copper or a copper alloy, similar to the chamber installed in the electron ring at HERA. In addition to the low desorption coefficient mentioned above, copper has good thermal properties and is self-shielding for the synchrotron radiation emitted by the beams (thus obviating the need for a lead liner on the outside of the chamber).

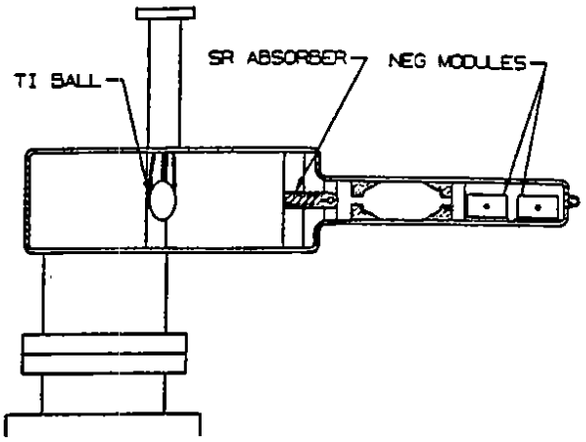

Figure 3. Vacuum chamber for the transition region [4] where the bend radius is only 45 m and the pressure must be held to less than 1 nTorr of CO and CO_2.

RF System

The main challenges for the RF system include:

- replacing the large synchrotron radiation power loss
- minimizing the HOM impedance per cell

The synchrotron radiation losses for an 8 or 9 GeV beam in the high-energy ring of a B factory could be 5 MW at a design luminosity of 3×10^{33} cm^{-2} s^{-1}. The issue is not the power per se, however, but is related to the need for controlling the HOM impedance by reducing the number of cavities. This results in a requirement for high input power through the cavity window—up to 500 kW for a room-temperature system. (To put this value in context, it is only half of the power transmitted through the output window of a modern klystron.) Special windows are being designed to handle this power level. It is also important to minimize the HOM impedance of an individual cavity by damping techniques in order to ensure practical parameters for the feedback system.

Both room-temperature [1–3,5] and superconducting [4] cavity designs are being actively developed for B factory use. In the room-temperature case, single- [1,3,5] or two-cell [2] cavities are being considered. Waveguides or slots in the cavity body are used to couple out the dangerous HOMs. With this technique, damping to a Q of about 30 has been demonstrated (at low power) in a pillbox cavity [5]. It is not possible to use the waveguide technique with superconducting cavities, but in this case it is not necessary to optimize the shunt impedance of the cavity and a large beam aperture is acceptable. In the Cornell approach, the aperture is sufficiently large that the HOMs propagate to a room-temperature ferrite load on the inner surface of the beam tube. Calculated damping to the level of Q = 70 is obtained [4].

The choice of superconducting technology will minimize the number of RF cells required. However, in the heavily beam loaded regime of a B factory, the advantage is only about 30% (assuming the same limitation on cavity window power as in the room-temperature case). In designs involving crab cavities, the use of superconducting technology is likely to be

preferred. For this application the requirements are high voltage and low power, which match well with the strengths of superconducting RF. To serve as a crab cavity, the cell must be driven at a transverse deflecting mode (TM110) rather than at the fundamental.

Feedback System

The requirement here is to control the growth of potentially strong coupled-bunch instabilities driven by the HOMs of the RF system. Due to the high beam current and large number of bunches, the instabilities can grow rapidly (≈ 1 ms), and the bandwidth requirements can be high (≈ 100 MHz). It is worth noting that the response of the feedback system to injection transients may dominate the power requirements. This issue favors an injection system that is phase-locked to the ring RF systems. It also helps to inject the beam in many small portions rather than large amounts of charge all at once.

A promising approach is to use a bunch-by-bunch system operating in the time domain [14]. An advantage of this choice is that the system can damp dipole motion from any source, including injection transients and beam-beam disturbances as well as coupled-bunch instabilities

V. SUMMARY AND OUTLOOK

The construction of a high-luminosity asymmetric B factory provides excellent scientific opportunities, combining first-rate particle physics incentives (to study the origins of *CP* violation) with equally exciting challenges in both the accelerator physics and accelerator technology areas. Challenges in accelerator physics include:

- development of lattices to collide and then cleanly separate two unequal energy beams
- achieving high luminosity in asymmetric beam-beam collisions
- designing effective masking techniques to protect the detector

Challenges in accelerator technology include:

- designing vacuum systems capable of handling large thermal loads, providing adequate pumping speed, and having acceptable impedance characteristics
- designing RF systems capable of handling high beam power and providing greatly reduced HOM impedance
- designing wideband bunch-by-bunch feedback systems

Effective approaches to all of these challenges have been identified and R&D activities are being vigorously pursued at many laboratories to optimize designs and finalize design choices. Extensive simulation studies of accelerator physics issues are also being carried out to better understand the beam-beam interaction and beam instabilities.

It is recognized by the various B factory design groups that making a large jump in luminosity will not be an easy task. Perhaps the most important ingredient in ensuring the success of a B factory will be to constantly remember to treat these challenges with proper respect.

ACKNOWLEDGMENTS

I would like to thank my many "co-conspirators" in B factory design, not only at LBL, SLAC, Caltech, and LLNL, but at CERN, Cornell, DESY, KEK, Novosibirsk, and PSI, for numerous profitable interactions. I would especially like to acknowledge my colleague Swapan Chattopadhyay, who dragged me kicking and screaming into this exciting endeavor.

REFERENCES

[1] K. Balewski, et al., "Study of an Asymmetric B-Factory," *Beam Dynamics Issues of High-Luminosity Asymmetric Collider Rings*, in AIP Conf. Proc. 214, Berkeley, CA, August 1990, p. 565-574.

[2] "Accelerator Design of a KEK B Factory," ed. by S. Kurokawa et al., KEK Report 90-24, March 1991.

[3] "Feasibility Study for a B-Meson Factory in the CERN ISR Tunnel," ed. by T. Nakada, CERN 90-02, PSI PR-90-08, March 1990.

[4] K. Berkelman, et al., "CESR-B: Conceptual Design for a B Factory Based on CESR," CLNS 91-1050, January 1991.

[5] "An Asymmetric B Factory Based on PEP," Conceptual Design Report, LBL PUB-5303, SLAC-372, CALT-68-1715, UCRL-ID-106426, UC-IIRPA-91-01, February 1991.

[6] A. Zholents, "Novosibirsk B-Factory," *Beam Dynamics Issues of High-Luminosity Asymmetric Collider Rings*, in AIP Conf. Proc. 214, Berkeley, CA, August 1990, pp. 592-593.

[7] P. Grosse Wiesmann, et al., "A Linac-on-Ring Collider B-Factory Study," *Beam Dynamics Issues of High-Luminosity Asymmetric Collider Rings*, in AIP Conf. Proc. 214, Berkeley, CA, August 1990, p. 602-615.

[8] "The Physics Program of a High-Luminosity Asymmetric B Factory at SLAC," ed. by D. Hitlin, SLAC-353, LBL-27856, CALT-68-1588, October 1989.

[9] H. DeStaebler, "Interaction Region Considerations," *Beam Dynamics Issues of High-Luminosity Asymmetric Collider Rings*, in AIP Conf. Proc. 214, Berkeley, CA August 1990, p. 59-80.

[10] D. Rice, "Beam-Beam Interaction: Experimental," *Beam Dynamics Issues of High-Luminosity Asymmetric Collider Rings*, in AIP Conf. Proc. 214, Berkeley, CA August 1990, p. 219-234.

[11] Y.H. Chin, "Symmetrization of the Beam-Beam Interaction in an Asymmetric Collider," *Beam Dynamics Issues of High-Luminosity Asymmetric Collider Rings*, in AIP Conf. Proc. 214, Berkeley, CA August 1990, p. 424-433.

[12] S. Krishnagopal and R. Siemann, Phys. Rev. D **41**, 1741 (1990).

[13] K. Oide and K. Yokoya, Phys. Rev. A **40**, 315 (1989).

[14] F. Pedersen, "Feedback Systems," *Beam Dynamics Issues of High-Luminosity Asymmetric Collider Rings*, in AIP Conf. Proc. 214, Berkeley, CA, August 1990, p. 246-269.

LBL-30857
ESG Note-140

PEP-II: An Asymmetric *B* Factory Based on PEP*

A. Hutton
Stanford Linear Accelerator Center, Stanford University, Stanford, CA 94309, USA
M. S. Zisman
Lawrence Berkeley Laboratory, Berkeley, CA 94720, USA
for the SLAC/LBL/LLNL *B* Factory Design Group

INTRODUCTION

An Asymmetric *B* Factory to be installed in the PEP tunnel has been under study at SLAC, LBL, and LLNL for several years [1-4]. A mature design for a 9 GeV × 3.1 GeV electron-positron collider with a design luminosity of 3×10^{33} $cm^{-2}s^{-1}$ is presented. Solutions now exist for all the technical problems, including issues related to high currents (e.g., beam instabilities, feedback systems, vacuum chamber design, lifetime degradation, and radiation power dissipation in the interaction region) and those related to the different energies of the beams (e.g., beam separation, beam-beam interaction, and detector requirements). The status of this project, which is being proposed for funding in FY 1993, will be discussed.

MAIN PARAMETER CHOICES

B Factory Physics Requirements

The PEP-II *B* Factory is a two ring e^+e^- collider designed to operate at the $\Upsilon(4S)$ resonance (center-of-mass energy 10.6 GeV). To enhance the study of *CP* violations, different energies for the two beams have been adopted (9.0 GeV for the electrons and 3.1 GeV for the positrons). The important detection requirement is to differentiate and separately identify the decay products of the *B* and the $\bar{B}$ mesons. This means a vertex resolution of about 60 microns, requiring that the inner radius of the vertex chamber be about 2.5 cm. Although the magnitude of the *CP* violation is expected to be large in the *B*-meson system, the cross sections of the important processes are small, so the design luminosity of the *B* Factory is 3×10^{33} $cm^{-2}s^{-1}$.

Machine Design Strategy

The luminosity of an asymmetric collider is given by [1]

$$\mathcal{L} = 2.17 \times 10^{34} (1+r) \left\{ \frac{I \, E \, \xi_y}{\beta_y^*} \right\}_{+,-} \quad cm^{-2} \, s^{-1} \qquad (1)$$

where r is the aspect ratio, I is the beam current in amperes, E is the beam energy in GeV, ξ_y is the beam-beam tune shift and β_y^* is the vertical beta function in cm. The expression in brackets can be evaluated for either beam.

Work supported by U.S. Department of Energy contracts DE-AC03-76SF00098, DE-AC03-76SF00515, DE-AC03-81-ER40050, W-7405-Eng-48 and DE-AS03-76ER70285.

The basic strategy is to choose single-bunch parameters (Table 1) similar to those obtained routinely in existing storage rings. This ensures that the beam-beam interaction is similar, the machine optics problems are tractable, and the single-bunch instabilities are manageable. New problems are:

1) Interaction region layout (two rings, backgrounds).
2) Vacuum chamber design (high currents).
3) RF and feedback systems (multibunch instabilities).

Design challenges are restricted to high-current and multi-bunch problems, which are either engineering problems or, in the case of the multibunch feedback system, in an area where there have been enormous improvements in the electronics available on the market. This means that, for the most part, no new accelerator physics issues must be addressed that would be less likely to provide definitive solutions.

TABLE 1. PARAMETER LIST

	Electron	Positron	
Energy	9.0	3.1	GeV
Luminosity	3×10^{33}		$cm^{-2}s^{-1}$
Tune shift ξ	0.03		
No. of bunches	1658†		
Bunch spacing	1.26		m
β_y^*	3.0	1.5	cm
β_x^*	75.0	37.5	cm
Separation	Horizontal		
Beam current	1.48	2.14	A
Bunch current	0.89	1.29	mA
σ_y^*	7.4		μm
σ_x^*	186		μm

†allows for 5% gap for ion clearing

INTERACTION REGION

The interaction region (Fig. 1) has been laid out to be compatible with either a head-on or a crossing-angle configuration [5]. Our initial choice is head-on collisions with flat beams, separated magnetically. This configuration is closest to that of conventional circular colliders so our luminosity estimates are the most reliable. Since the magnetic separation produces synchrotron radiation from which the detector must be shielded, the detector masking is easier with a crossing angle, and this option is maintained for a future upgrade. Permanent magnets are used for the LER focusing; a septum quadrupole is needed for the first HER quadrupole, 4 m from the IP.

Background conditions are one to two orders of magnitude better with flat beams than with round beams, because the quadrupoles are weaker, the beam angular divergence is smaller (so that the beam size in the quadrupoles is smaller), and the separation angle can be smaller [6].

Completely satisfactory masking solutions for the head-on case have been obtained using an "S-bend" geometry to reduce backgrounds. The synchrotron radiation conditions are acceptable, and particle background rates from bremsstrahlung and beam-gas interactions have been evaluated and demonstrated to be acceptable [7].

FIGURE 1. THE INTERACTION REGION LAYOUT

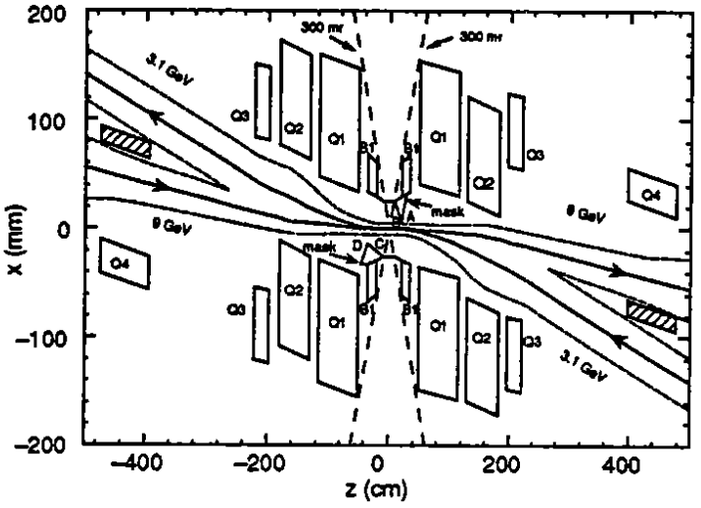

We now have a detailed layout of the IP region, including all magnets, supports, collimators, and the innermost detector elements. The permanent-magnet bends and quadrupoles for the LER are based on Sm_2Co_{17} (which has the best radiation hardness and temperature stability) and meet all of the aperture and strength requirements. The synchrotron radiation power density on the masks and collimators is reasonable and preliminary engineering designs have been made, including thermal and stress analyses. All of these elements, as well as the vertex detector, fit inside a 31.2-cm diameter support tube that spans the entire detector. All elements will be prealigned within this tube prior to its installation into the detector.

We are studying two different solutions to the septum quadrupole for the HER. We have a detailed design for a superconducting Panofsky septum quadrupole, which would be just outside the detector and is compatible with all of the constraints. We also have a conceptual design for a room-temperature, Collins-type septum quadrupole, which we are in the process of engineering.

RING LAYOUT

The PEP-II *B* Factory will be based on the present PEP ring [8], taking advantage of the existing components and infrastructure. This leads to significant reductions in the cost and the scheduling uncertainties usually associated with conventional construction.

The HER arcs have a completely regular periodic structure containing 12 identical cells [9]. These cells are slightly longer than in PEP (15.125 m instead of 14.35 m) allowing room for vacuum flanges (PEP had only one 14.35-m vacuum chamber per cell). There are two dispersion suppressor cells at the ends of each arc, each slightly longer than the arc cells (16.013 m). The straight sections consist of 8 FODO cells, each 15.125 m long, except in the special straights.

The LER layout is based on that of the HER. The length of the standard period is exactly the same as the HER (15.125 m) and the quadrupoles are stacked vertically to simplify installation. The short (1-m) bend magnets increase the radiation damping. Each bend is placed close to its quadrupole on a common support raft, and is always down-beam from the quadrupole so that its synchrotron radiation strikes the chamber wall downstream of the bend.

The HER magnets are recuperated from PEP: 192 5.4-m dipoles, 20 low-field dipoles, 192 quadrupoles, and 144 sextupoles. All of these magnets will be taken from the PEP tunnel and the coils removed and refurbished. The mechanical shape of every magnet will be measured in an automated measurement facility and some fraction (≈20%) will also be measured magnetically and the results compared with the original data to confirm the validity of the procedure.

The LER magnets (and some HER magnets) are new and will be based on the designs used for the PEP magnets.

VACUUM CHAMBER

The vacuum chamber, which is based on the HERA approach [10], is designed for a maximum current of 3 A, corresponding to ≈10 kW/m or ≈2 kW/cm^2 (PEP was designed for 10 kW/m). A phosphor-bronze alloy with 2% tin is being considered for the beam tube and the pumping channel. An octagonal shape beam chamber with 5 mm walls is completely self shielding. Temperature profiles across the chamber and thermal stresses have been evaluated. The photodesorption rate should be ten times lower than aluminum [11-13]. A copper test chamber will be built this year and its synchrotron radiation outgassing properties confirmed at BNL.

In the HER, lumped ion pumps will be used as well as distributed ion pumps in both bends and quadrupoles. In the LER, only lumped pumps will be used, as there is no magnetic field in the region where the gas load is greatest.

RF SYSTEM

The RF cavities will be powered from 1-MW commercial klystrons at the *B*-Factory frequency of 476 MHz. Each klystron will be attached to two cavities via a circulator. This will require windows capable of transmitting 500 kW, which we are developing. We are also studying the possibility of modifying the present PEP klystron design to produce 500 kW at 476 MHz. If this is successful, the klystrons could be built at SLAC.

The cavity design is such that trapped higher-order modes are strongly coupled to outside loads using waveguides that are beyond cutoff for the fundamental accelerating mode [14]. We are adopting a copper cavity with "noses," similar to the Daresbury and ALS designs. This choice maximizes the cavity shunt impedance and minimizes the RF power required to establish the voltage. A computational method has been developed for estimating the shunt impedance of the fundamental mode in the presence of the waveguide couplers, and this technique is being used to optimize the cavity design. A model (pill-box) cavity has been built to measure waveguide coupling, check the computations, and investigate the practical difficulties involved. Calculations of the higher-order-mode damping and measurements on the model cavity agree, and show that damping of the higher-order modes to a Q of 30 is achievable.

The mechanical design of the cavity is proceeding with calculations of the thermal loading. Other cavity components, such as the tuners and couplers, are also being studied. We have funds for the design and construction of a high-power cavity to investigate the manufacturing issues.

FEEDBACK

The feedback system detects the phase offset of each bunch and feeds back after 90° of synchrotron oscillation (about 7 turns later). A front-end detection circuit has been built to evaluate signal-to-noise capabilities of a fast detection system [15], and a tracking program has been developed incorporating all longitudinal effects (including those of the feedback system) [16]. Analytic calculations and simulations have been performed to understand the effects of limiting the output power of the kicker amplifier.

The results show that our concept works and that only 2 kW are required to stabilize the beams. The front-end detection circuits have demonstrated the capability to measure phase errors of 0.5° at 476 MHz, with 27 dB rejection between adjacent bunches.

SLC AS INJECTOR

The injection system (Table 2) is based on the transfer of single bunches of electrons and positrons on each pulse of SLC into single buckets in each ring [17]. These bunches contain 20% of the total required charge when filling from scratch, but only contain 4% when topping up. Bypass lines will be added to the linac so that the *B*-Factory beams need not traverse the full length of the linac accelerating structure, which would lead to energy jitter and emittance degradation.

Adjustable collimators will be provided in the arcs to limit the acceptance to $\pm 10\sigma$. Adjustable collimators will also be provided in the straight section upstream of the detector, set to $\pm 12.5\sigma$. The physical apertures in the interaction region allow $\pm 15\sigma$ and an additional 2 mm for closed-orbit errors. We have tracked injected particles with large energy and transverse position errors for 20,000 turns in the ring and find no particles being lost in the interaction region.

TABLE 2. INJECTION PARAMETERS

Ring energies			
HER (e^-)	9 GeV		(10 max, 8 min)
LER (e^+)	3.1 GeV		(4 max, 2.8 min)
Ring currents			
HER	1.48 A	—	6.9×10^{13} e^-
LER	2.12 A	—	9.7×10^{13} e^+
Ring particles/bunch (with 5% gap)			
HER			$\approx 4 \times 10^{10}$ e^-
LER			$\approx 6 \times 10^{10}$ e^+
Linac repetition rate (pps)			60 – 120
Linac current ($e^{\pm}$/bunch/pulse)†			$0.2 - 1 \times 10^{10}$
Time between bunches (ns)			4.2
Ring kicker pulse (start-to-finish)			≤ 300 ns
Topping-off time (from 80 to 100%)			3 minutes
Filling time (from zero)			6 minutes

†*SLC presently operates with* $2 - 3 \times 10^{10}$

SUMMARY

We have a conservative design that achieves all of our goals. Key technical aspects of the design have successfully undergone independent technical reviews. The budget (Table 3) has been evaluated in great detail, and has been validated by the DOE. There is no technical impediment to starting in 18 months and we are aggressively seeking funding.

TABLE 3. BUDGET

ED& I	$ 32,241,000
M&S and Labor	$101,537,000
Total	$133,778,000
Contingency	≈ 25%
Construction time could be 42 months	

REFERENCES

[1] LBL PUB-5244, SLAC-352, CALT-68-1589 (1989).
[2] SLAC-353, LBL PUB-5245, CALT-68-1588 (1989).
[3] LBL PUB-5263, SLAC-359, CALT-68-1622 (1990).
[4] LBL PUB-5303, SLAC-372, CALT-68-1715, UCRL-ID-106426, UC-IIRPA-91-01 (1991).
[5] A. Garren and M. Sullivan, this conference, USC 4.
[6] A. Hutton, in AIP Conf. Proc. 214 (1989) p.284.
[7] H. DeStaebler, this conference, IGR 3.
[8] PEP Design Handbook (1977) H. Wiedemann, ed.
[9] M. Donald and A.A. Garren, this conference, USC 3.
[10] DESY HERA 80 /01 (1980).
[11] C.L. Foerster et al., 1970. J. Vac. Sci. Tech. A 8(3), 2856.
[12] O. Gröbner et al., 1983. Vacuum 33, 397.
[13] A. Mathewson et al., 1990. S. Ueda et al., Proc. Second Topical Conference on Vacuum Design of Synchrotron Light Sources, Argonne National Laboratory, Nov 1990.
[14] R. Rimmer et al., this conference, HRA 77.
[15] D. Briggs et al., this conference, KTH 6.
[16] D. Briggs et al., this conference, KTH 7.
[17] E. Bloom et al., this conference, HTP 31.

SLAC–PUB–5542
LBL–PUB–30730
April 1991
(A)

APIARY B-Factory Separation Scheme*

A. GARREN

Lawrence Berkeley Labs, University of California at Berkeley, Berkeley, CA 94720
and
M. SULLIVAN

Inter-campus Institute for Research at Particle Accelerators—Stanford Linear Accelerator Center, Stanford, CA 94309

Abstract

A magnetic beam-separation scheme for an asymmetric-energy B-Factory based on the SLAC electron-positron collider PEP is described that has the following properties: the beams collide head-on and are separated magnetically with sufficient clearance at the parasitic crossing points and at the septum, the magnets have large beam-stay-clear apertures, synchrotron radiation produces low detector backgrounds and acceptable heat loads, and the peak β–function values and contributions to the chromaticities in the IR quadrupoles are moderate.

I. INTRODUCTION

The APIARY B-Factory design calls for electrons and positrons to be stored in two rings, separated vertically, and located in the PEP tunnel. The 2-ring system is forced by the high currents and small bunch spacing required for high luminosity. The parameters of the system are shown in Table 1.

Table 1. APIARY Parameters

	Low Energy Beam	High Energy Beam	
Energy	3.1	9.0	GeV
Current	2.14	1.48	A
Betas at IP, β_x/β_y	37.5/1.5	75.0/3.0	cm
Emittance, ϵ_x/ϵ_y	96.5/3.9	48.2/1.9	nm-rad
Bunch separation	1.26	1.26	m
Vertical separation	0.895		m
Collision mode	head on		
Separation scheme	magnetic: horizontal, then vertical		
IP aspect ratio, σ_x:σ_y	25:1		
Luminosity	3×10^{33}		cm^{-2} sec^{-1}

The separation scheme must solve three interwoven problems: to separate the beams and lead them into the two rings, to focus the beams without unacceptable β–function values or chromaticity contributions, and to control the quantity and distribution of synchrotron radiation (SR) produced so that sensitive components can be shielded by the masking system.

II. DESCRIPTION OF THE SEPARATION SCHEME

The separation scheme is briefly as follows: the beams collide head-on and are separated after leaving the interaction point (IP) by the dipole magnet B1 starting 20 cm from the IP, a triplet common to both beams with quadrupoles QD1, QF2, and QD3 centered alternately on the high, low and high energy beams to increase the separation, a septum quadrupole QD4 focussing the high-energy beam (HEB) only, and a vertical septum dipole that deflects the low-energy beam (LEB) upwards, see Figs. 1–3. This dipole together with three others beyond bring the LEB to a level 89.5 cm above the HEB. Seven quadrupoles between these vertical bends focus the LEB and bring the horizontal and vertical dispersions to zero. Just beyond the vertical septum, the quadrupole QF5 focusses the HEB horizontally (see Fig. 4), and bending magnets begin the steering of that beam toward the arc and contribute to the dispersion suppression. Additional horizontal dipoles and quadrupoles in both beamlines complete the steering, dispersion matching, and matching of the beams to the β functions in the arcs.

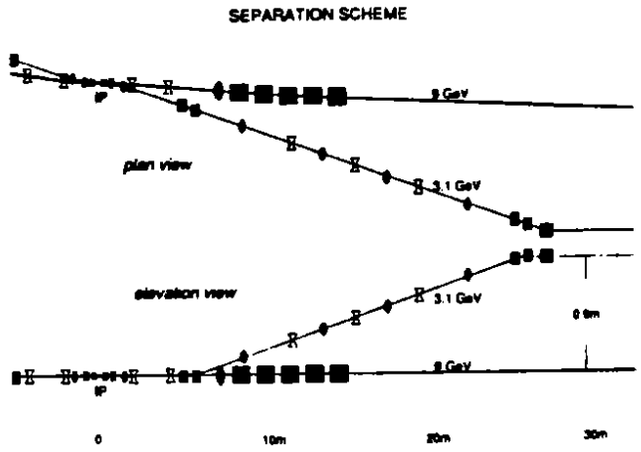

Figure 1. Schematic diagram of the APIARY separation scheme.

The system design satisfies the following constraints:

- The beam-stay-clear (BSC) in the interaction region (IR) magnets is defined to contain both beams with $15\sigma_{x,y}$ envelopes, plus 2 mm for orbit distortion, where σ_x, σ_y refer to uncoupled, fully-coupled beams respectively
- At least 2 mm spacing between SR fans and the nearest surface
- A 5 mm allowance for beam pipe, cooling, and trim coils between the BSC and SR fans and any magnetic material
- The ratio β_y^*/(distance to 1st quadrupole) $\sim$ 100, in order to keep the chromaticity reasonable
- 15 mm is allowed for the QF4 septum between the BSCs of the two beams

* Work supported by Department of Energy contract DE-AC03-76SF00515 and DE-AS03-76ER70285 and DE-AC03-76SF00098.

Contributed to the IEEE Particle Accelerator Conference, San Francisco, CA, May 6–9, 1991

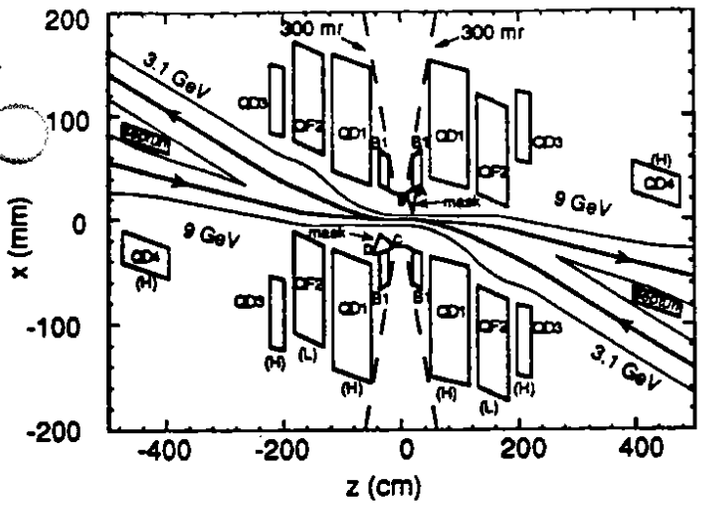

Figure 2. Plan view of the magnets and beamlines near the IP. Note the distorted scale.

III. Optics, Beam Matching and Steering

The four common elements B1, QD1, QF2, and QD3 are permanent magnets, with 1.05 T remnant fields, and inner radii satisfying the BSC and other constraints listed previously. Fig. 2 shows a diagram of the IR in plan view. The beamlines are shown as heavy lines, and the $15\sigma_x$ envelopes as light lines. The (H) or (L) near each magnet indicates on which beam (HEB or LEB) the quadrupole is centered.

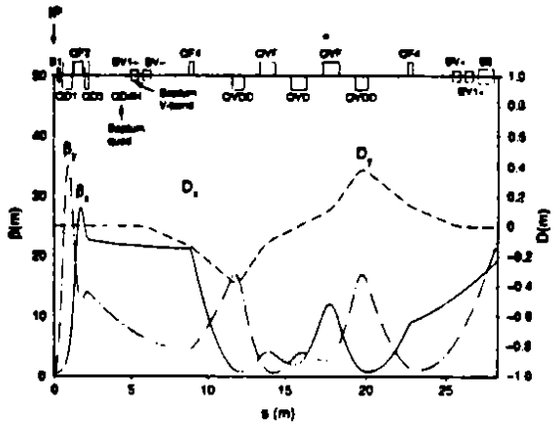

Figure 3. Lattice functions of the LEB from the IP to the end of the vertical step.

The triplet is adjusted to focus the LEB so that it is small at the QD4 septum and enters the vertical-step region in a nearly parallel state with small β–function values (see Fig. 5). The triplet is also quite useful for some initial focusing of the HEB. The quadrupole QD1, though centered on the HEB, is tilted with respect to it in order that one of the SR fans not strike its inner surface.

The first 'parasitic' bunch crossing point occurs 63 cm from the IP, just inside QD1, where the beamlines are separated by 7.5 times the largest σ-value of either beam (σ_x(LEB)).

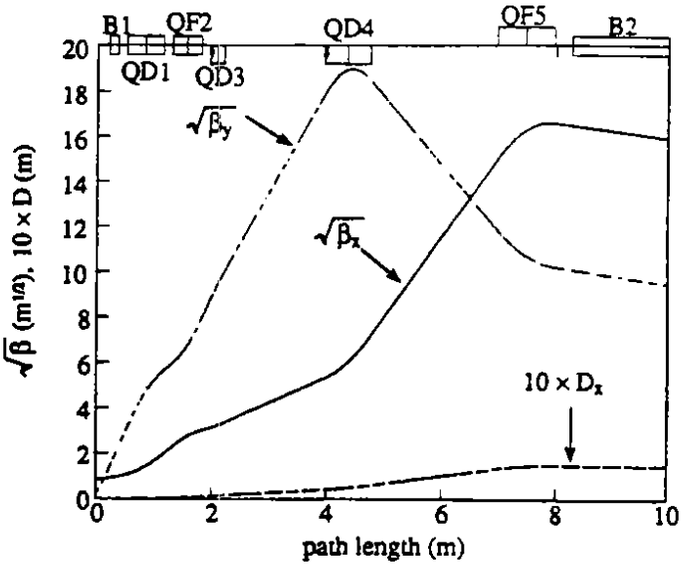

Figure 4. Lattice functions of the HEB within the first 10 m of the IP.

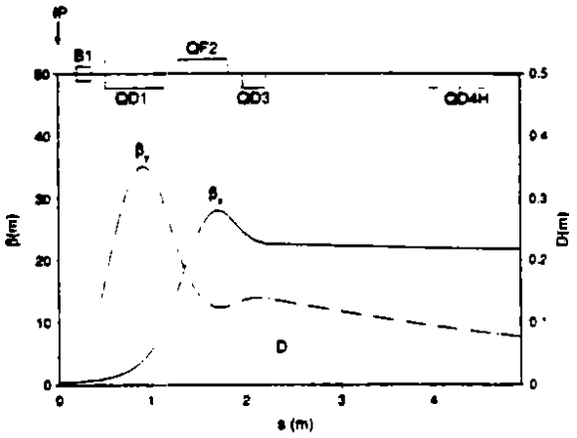

Figure 5. Lattice functions of the LEB through the common magnets and the septum quadrupole.

The horizontal bending pattern is antisymmetric about the IP, which produces an S-bend beamline—a geometry that is conducive to extracting the synchrotron radiation.

Figure 6 shows the first 60 m from the IP to the start of the arc for the HEB. The dispersion function D and its slope are brought to zero by the dipoles B2 and B3 whose bending is very weak ($\epsilon_{crit} \approx 1$ keV) to avoid problems with the SR in the IR. These dipoles are followed by quadrupoles QD6 and QF7 that match the β functions into the arc. Two additional dipoles in the dispersion suppressor at the end of the arc steer the HEB to the proper direction.

The strength of the B2 dipole of the LEB (originally set to bring D_x and its slope D_x' to zero at the end of B2). together with the strengths of three additional dipoles, are adjusted to steer the LEB from the arc to the IP with the correct radial position and slope, while preserving the dispersion matching. The remaining β–function matching for the LEB, is done with quadrupoles QD8-QF13, located between the end of the vertical step and the arc.

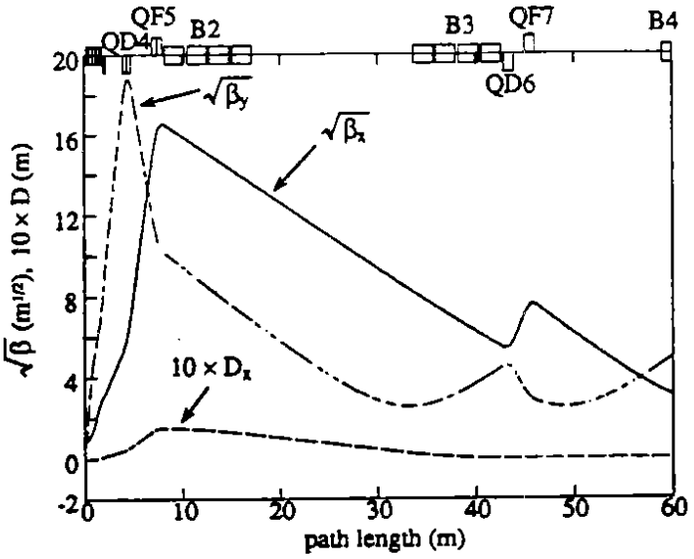

Figure 6. Lattice functions of the HEB from the IP to the begining of the arc.

Table 2. Properties of the synchrotron radiation generated within ±3 meters of the IP.

Magnet	Fan pwr (kW)	$N_\gamma(10^{10})$	ϵ_{crit}(keV)
LEB:			
Upstream QD3	0.84	3.1	2.3
Upstream QD1	0.83	5.4	1.3
Upstream B1	2.39	4.2	4.8
Downstream B1	2.39	4.2	4.8
Downstream QD1	0.96	5.2	1.4
Downstream QD3	0.91	3.1	2.4
subtotal	8.3	13	
HEB:			
Upstream QF2	28.3	7.5	32.1
Upstream QD1	2.3	2.7	7.3
Upstream B1	13.8	2.9	40.4
Downstream B1	13.8	2.9	40.4
Downstream QD1	1.1	1.8	5.1
Downstream QF2	26.1	7.3	30.5
subtotal	85.4	25	
Total	93.7	38	

IV. Control of the Synchrotron Radiation

The LEB generates SR fans as it passes through QD3, QD1 and B1 on its way to the IP. Figure 7 shows the LEB radiation fans near the IP. The mask labeled AB in Figs. 7 and 8 is designed to prevent any SR generated by the upstream magnets from directly striking the detector beam pipe. The QD1 magnet, in the LEB downstream direction, is tilted with respect to the HEB axis by 22 mrad, so that any SR generated by the LEB upstream magnets that goes by the AB mask tip clears the beampipe.

As can be seen in Fig. 7, the AB mask absorbs all of the fan radiation from the upstream QD3 magnet. The fans generated by the two B1 dipoles and by the downstream QD1 and QD3 magnets pass through the IR without striking any surfaces. The first surface that intercepts the QD1 fans is the "crotch mask" in front of the QD4 septum. Table 2 summarizes some of the properties of the LEB and HEB radiation fans.

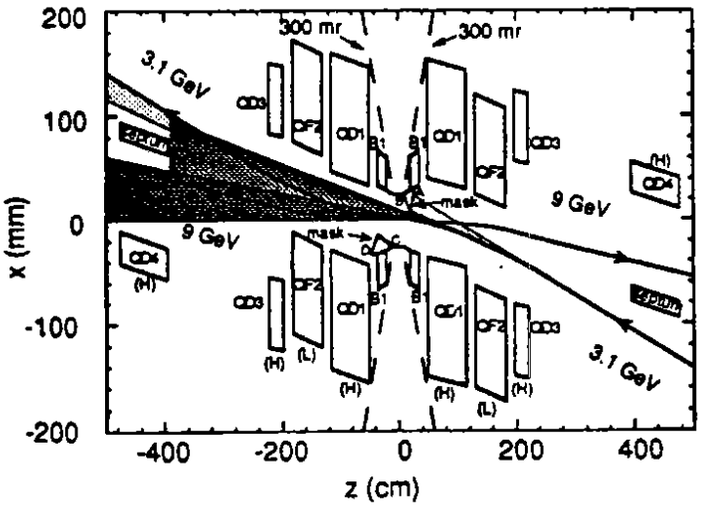

Figure 7. Radiation fans generated by the LEB near the IP. Darker shading indicates higher radiation intensity.

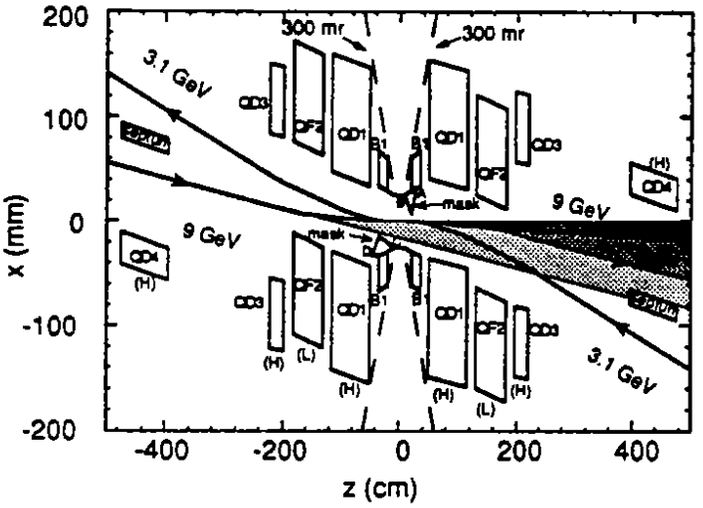

Figure 8. Radiation fans generated by the HEB near the IP.

The SR fans generated by the HEB as it passes through the QF2 and B1 magnets also pass through the detector region without striking any surfaces. Figure 8 shows the HEB radiation fans near the IP. The mask labeled CD in Figs. 7 and 8 is located to prevent quadrupole radiation produced by the HEB in QF5 and QD4 from directly striking the detector beam pipe. The CD mask tip is positioned 2 mm outside the upstream QF2 radiation fan that passes through the IR. The other QD1 magnet, in the HEB downstream direction, is tilted with respect to the HEB axis by 15 mrad, so that this fan clears the beampipe. Therefore the first surface struck by the upstream QF2 fan is the crotch mask in front of QD4.

Only 6% of the total generated SR strikes surfaces within 4 m of the IP: 4.3 kW on the crotch mask from the HEB and 1.2 kW on the AB mask from the LEB (see Table 2). This leads to an estimated detector background level that is 50 times lower than acceptable limits.

SLAC-PUB-5538
LBL-30669
April 1991
(A)

An Isochronous Lattice for PEP*

W.J. Corbett and M.H.R. Donald

Stanford Linear Accelerator Center, Stanford, CA 94309

and

A. A. Garren

Lawrence Berkeley Laboratory, Berkeley, California 94720

Abstract

With e^+e^- storage rings operating in a quasi-isochronous mode, it might be possible to produce short bunches with length $\sigma_z < 1$ cm. The unique characteristics of the short bunches could then be utilized for synchrotron radiation applications or colliders with mm-scale β^*. In principle, the design of a quasi-isochronous storage ring is relatively straight-forward, but experimental studies with electron storage rings in this configuration have not been carried out. The purpose of this paper is to demonstrate that an isochronous lattice design is compatible with PEP given a minimum of hardware modifications.

I. Introduction

In addition to being a prime candidate for a B Factory, [1] PEP is well recognized as a high brilliance synchrotron radiation source. [2] To further explore new directions in B Factory design and the capabilities of PEP as a light source, [3] we have begun to investigate the potential for short bunch operation in a quasi-isochronous, or low momentum-compaction mode. Since we are working under the constraint that magnets may not be moved, the configuration requires periodically driving the dispersion function negative throughout the arcs to compensate for positive values. Using this approach, a preliminary solution has been found for the present PEP magnet arrangement. Following further refinement of the design, valuable short-bunch machine studies of interest to both the high energy physics and synchrotron radiation communities might be possible.

The principle behind using a low momentum-compaction lattice for bunch length compression proceeds from the observation that for high energy electron storage rings the bunch length scales as [4,5]

$$\sigma_l \propto \sqrt{\alpha} \tag{1}$$

for a given RF voltage and frequency. Here, the momentum compaction factor

$$\alpha = \frac{\Delta L}{L} \times \frac{p}{\Delta p} = \frac{1}{\gamma_t^2} = 1/(2\pi R) \oint D_x/\rho \, ds \tag{2}$$

gives (to lowest order) the path length deviation due to small energy excursions from the central value. If α is made sufficiently small, the phase slip factor

$$\eta = \frac{1}{\gamma^2} - \frac{1}{\gamma_t^2} \tag{3}$$

tends to zero and the synchrotron oscillation amplitude is reduced. For PEP, the lowest value achieved to date is $\alpha = 1 \times 10^{-3}$ in a low-emittance configuration. [6] The isochronous condition implies a lattice with $\alpha = 1/\gamma^2 \approx 5 \times 10^{-5}$ at 10 GeV. In the following Section, a solution for a low-α lattice in PEP which maintains the proper phase advance between chromaticity correction sextupoles is discussed, and a two-family solution for sextupole strengths is found. In Section III, the bunch length is estimated based on an analysis of the longitudinal acceptance for a small, energy dependent, momentum compaction factor. [7,8]

The results are summarized in Section V along with recommendations for future work.

II. Lattice Design

The PEP lattice consists of six long straight sections, connected by 2-cell dispersion suppressors to arcs containing 12 FODO cells. The regular FODO structure of each arc is broken at its center to accommodate a short 5 m "symmetry" straight. In the "colliding beams" mode the insertion quadrupoles, close to the center of each long straight, focus the beams to low β values, while in the "low emittance" light source mode weak focussing is used across the interaction points. The basic constraint in designing any alternative lattice for PEP is not to move any magnets in the arcs. It is also advantageous not to exceed the power dissipation of the present magnets.

One way to obtain a low momentum compaction lattice [9,10] is to force the dispersion function D_x to negative values through some of the dipoles to compensate for the positive values of D_x in other dipoles. The requirement is that $\alpha = 1/(2\pi R) \oint D_x/\rho \, ds$ be close to zero for the whole ring. We achieve this by making super-cells, consisting of several FODO cells, that repeat in regular fashion through the arcs. We have found (so far) that the most suitable arrangement for PEP is a super-cell made of three PEP FODO cells and having betatron phase advance $\mu_x/(2\pi) = 0.75$ and $\mu_y/(2\pi) = 0.25$. There are thus four super-cells in one PEP arc. The phase advance is arranged so that self-compensating pairs of chromaticity correcting sextupoles can be placed with a phase advance of $(2n+1)\pi$ between them. The basic super-cell is shown in Fig. 1.

It was found that this particular super-cell matched nicely into the symmetry section and, through the disper-

* Work supported by Department of Energy contract DE-AC03-76SF00515 and DE-AC03-76SF00098.

Presented at the IEEE Particle Accelerator Conference, San Francisco, CA, May 6-9, 1991

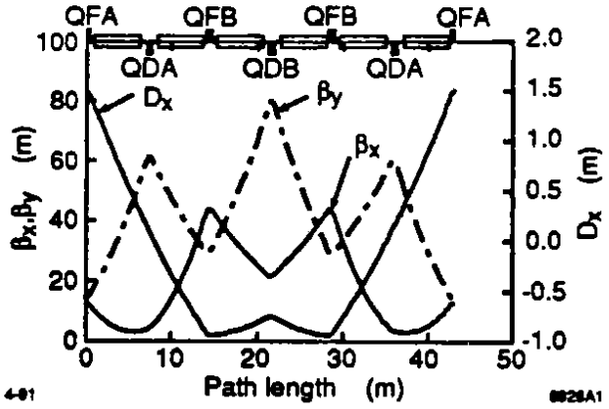

Figure 1. The standard supercell is made up of three FODO cells with symmetry about the middle of the center cell. The strong quadrupoles QFA drive the dispersion function through the center of QDA to negative values.

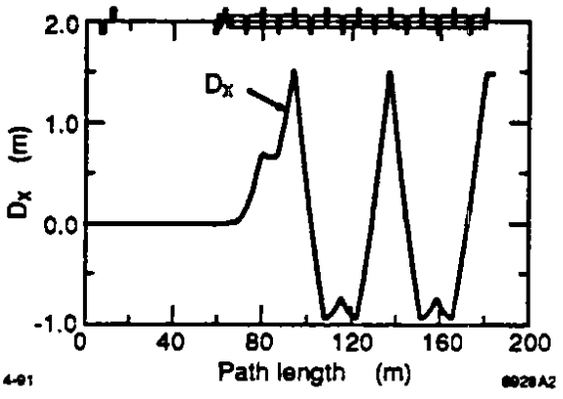

Figure 2. Dispersion Function for one half Superperiod.

sion suppressor, into the long straight sections (Figs. 2,3). The phase advance through the symmetry straight required an adjustment to the super-cell phase advance, so that the phase advance through the combination of super-cell and symmetry straight equalled $0.75(2\pi)$ and $0.25(2\pi)$. Figure 4 shows the phase advance between typical sextupole pairs.

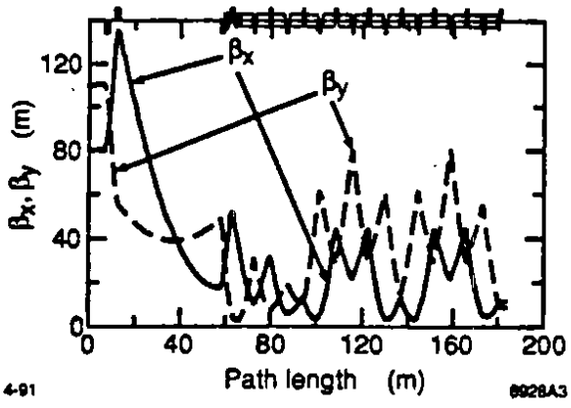

Figure 3. Beta Functions for one half Superperiod.The beta functions of the supercells match easily into the symmetry straight and into the long straight section.

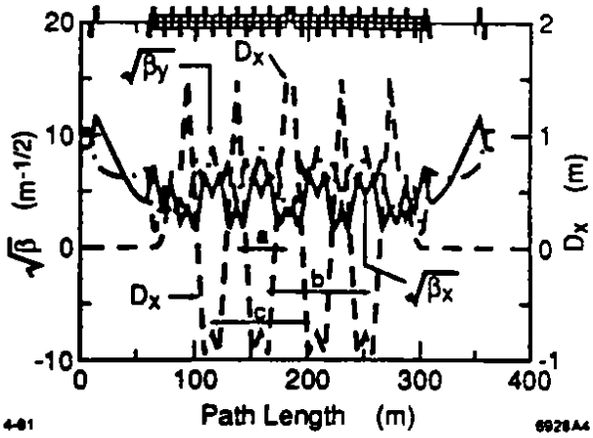

Figure 4. One of the six Sextants of PEP. (a) The phase advance is adjusted to be 90° and 270° across the supercell. (b, c) Chromaticity correcting sextupoles may be placed in pairs with phase advance of 0.5 and 1.5 times 2π.

Some lattice parameters for the 6 superperiod PEP ring are:

$P = 9$ GeV

$Q_x = 25.526$ $\quad Q_y = 15.861$ $\quad Q_s = 0.0022$

$\xi_x = -38.32$ $\quad \xi_y = -39.13$ (uncorrected)

$V_{RF} = 15\ MeV/rev$ $\quad \sigma_E = 0.06\%$ $\left(\frac{dp}{p}\right)$

Preliminary particle tracking results are promising, showing a dynamic aperture of $12\sigma_\beta$ for both on-momentum particles and those undergoing synchrotron oscillations with 6σ momentum deviation. The chromatic properties $(d\beta)/\beta)/(dp/p)$ and $(d\nu_{x,y})/(dp/p)$ were also good.

The lattice as shown is more of a demonstration of a lattice with zero α than a finished design. As explained in the following section, a lattice with α this small would not be stable in synchrotron motion at this energy deviation. A more realistic lattice design would have a larger value of α. In addition, we must explore alternative ways of changing the betatron tune of the machine, either by adding quadrupoles in the long straight sections or by having a conventional FODO lattice in one or more of the arcs.

III. Bunch Length Scaling

Analysis of the longitudinal dynamics for short bunches is inherently a non-linear problem and has been discussed by Pellegrini and Robin.[4, 7] In principle. since the bunch length scales as $\sigma \propto \sqrt{\alpha}$, a factor of > 100 reduction in momentum compaction is required to compress a 5 cm bunch into the range of interest for short bunch B Factory designs, or advanced synchrotron radiation applications. Expanding the momentum compaction as a function of energy deviation, $\alpha = \alpha_1 + \alpha_2\delta$ where

$$\alpha_1 = \frac{1}{2\pi R}\int D_x/\rho ds \quad , \quad \alpha_2 \approx \frac{1}{2\pi R}\int \frac{(D_x^{/2})}{\rho} ds$$

and $\delta = \Delta p/p$, the authors [4, 7] have found that the ratio α_1/α_2 gives a rough estimate of the longitudinal bucket

size along the energy axis. To estimate the lower bound on α_1, we assume the RF acceptance must exceed the energy spread of the bunch by a factor of 10 to preserve quantum lifetime.

Since D_x can be energy dependent, we use the computer program MAD [11] to find the off-energy closed-orbit and plot α as a function of energy deviation. For our lattice, including chromaticity sextupoles, we find $\alpha_2 = 0.027$, as shown in Fig. 5. Imposing the lifetime condition $\alpha_1/\alpha_2 \sim 10\delta$, the lower bound on α_1 is about 1.6×10^{-4}. The design bunch length is 3.3 mm for this lattice. By adding more families of sextupoles, it may be possible to reduce the longitudinal chromaticity (α_2) and thus obtain shorter bunches.

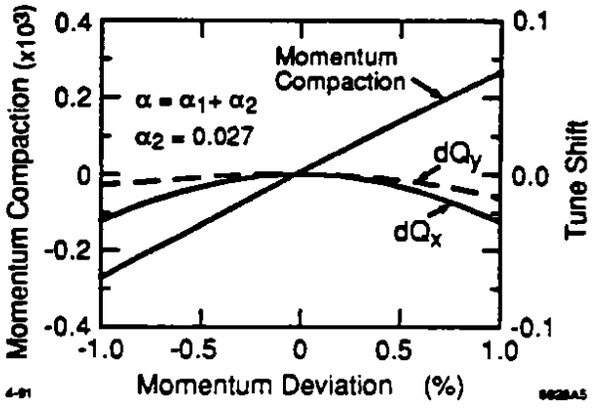

Figure 5. (1) α has an energy dependence $\alpha = \alpha_1 + \alpha_2 \frac{dr}{\rho}$ that governs the size of the RF bucket. (2) Two sextupole families (SD and SF) are used to correct chromaticity.

IV. Conclusions

We have demonstrated the design of a low momentum-compaction lattice for PEP. The configuration is based on a succession of supercells (3 FODO cells each) with regions of negative dispersion and betatron phase advance between pairs of compensating sextupoles fixed at $(2n+1)\pi$. Although the configuration must be regarded as preliminary, it requires no magnet re-locations, no quadrupole polarity reversals, and does not exceed power load ratings for a 9 GeV beam. Some new bus work is required. Prior to experimental verification of the low-α lattice, further study of chromatic properties (including tracking with synchrotron motion), injection and tuning procedures, and longitudinal dynamics would be required. At this stage, the theoretical bunch length is about 3.5 mm at 9 GeV (V_{RF} = 15 MV), but smaller values could in principle be reached by correcting the longitudinal chromaticity with additional sextupole families.

V. Acknowledgments

The authors would like to thank Max Cornacchia for initiating this study, and Claudio Pellegrini and David Robin for their non-linear bunch stability analysis. Heinz-Dieter Nuhn, Jim Spencer and Hermann Winick provided many useful comments throughout the course of this work.

References

[1] "An Asymmetric B Factory Based on PEP: Conceptual Design Report," LBL PUB-5303 (SLAC-372, CALT-68-1715, UCRL-ID-106426,UCIRRPA-91-01), 1991.

[2] A. Bienenstock, G. Brown, H. Wiedermann, H. Winick, "PEP as a Synchrotron Radiation Source," R. S. I. 60 (7), pp. 1393-1398, 1989.

[3] A. Fisher, et al., "Coherent Radiation for PEP," these proceedings.

[4] C. Pellegrini and D. Robin, "Quasi-Isochronous Storage Ring," NIM A301, pp. 27–36, 1991.

[5] M. Sands, "The Physics of Electron Storage Rings: An Introduction," SLAC–121, 1970.

[6] M. Donald, L. Rivkin, A. Hofmann, SSRL ACD Note 34, 1985.

[7] C. Pellegrini and D. Robin, "Quasi-Isochronous Storage Rings: A Possible Low Current High Luminosity Meson Flavor Factory," these proceedings.

[8] E. Ciapola, A. Hofmann, S. Myers, T. Risselada, "The Variation of γ_t with $\Delta p/p$ in the CERN ISR,' IEEE Trans. N. S., Vol. NS–26, 3, pp. 3571–3573, 1979.

[9] A. A. Garren, E. D. Courant, U. Wienands, "Low Momentum Compaction Lattice Study of the SSC Low Energy Booster," these proceedings.

[10] R. V. Servranckx, U. Wienands and M. K. Craddock, "Racetrack Lattices for the TRIUMF Kaon Factory," in Proc. IEEE PAC, Chicago, IL, pp. 1355–1357, 1989.

[11] H. Grote and F. C. Iselin, "The MAD Program (Methodical Accelerator Design)," Rev. 2. CERN/SL/90–13 (AP).

SLAC-PUB-5526
MAY 1991
(A)

THE PROPOSED INJECTION SYSTEM FOR AN ASYMMETRIC B FACTORY IN THE PEP TUNNEL

E. Bloom, F. Bulos, G. Loew, R. Miller, B. Sukiennicki, T. Mattison*
Stanford Linear Accelerator Center
Stanford University, Stanford, CA 94309
and
W. Barletta†
Lawrence Livermore National Laboratory
Livermore, CA 94551

I. ABSTRACT AND INTRODUCTION

The proposed asymmetric energy B Factory to be built in the PEP tunnel at SLAC will require a highly effective and profuse source of low emittance electron and positron bunches. The B Factory will consist of two rings of equal size, a 9 GeV electron ring and a 3.1 GeV positron ring, each with 1658 bunches with total circulating currents of 1.5 and 2.1 amperes respectively. As the luminosity lifetime of the collider is expected to be about two hours, the injector should be capable of filling the rings in a small fraction of an hour. It turns out that with some simple modifications, the SLC linac with its damping rings and positron source is ideally suited to fulfill this function effectively. The overall injection system is described below.

II. SYSTEM SPECIFICATIONS AND DESCRIPTION

The specifications and required parameters of the injection system are shown in Table I. It is seen that each of the 1658 stored bunches will require about 5×10^{10} particles. In the topping-off filling mode (80→100%), assuming that each bucket receives about 5 single bunches from the injector with 50% filling efficiency, the linac will have to provide single bunches of 4×10^9 particles/bunch as compared to $2\text{-}5 \times 10^{10}$ particles/bunch in the regular SLC mode. This should be very easy. In the full filling mode, the first 80% of each bucket will be filled, also with 5 linac bunches, but at the rate of 2×10^{10} particles/bunch, and the remaining 20% at the topping-off rate as above. Assuming that both rings are filled by alternate linac pulses, each at a 60 pps rate, it is easily seen that the filling operations will take on the order of 3 and 6 minutes respectively.

A schematic of the SLC injection system is shown in Fig. 1. The injector will consist of the first 19 sectors of the linac, the two damping rings and the positron source. The 3.1 GeV positrons will be extracted at the end of Sector 3 through a DC chicane which will let the electrons continue on, either to the end of Sector 7 for extraction at 9 GeV via a slowly pulsed magnet, or to Sector 19 at about 30 GeV for positron production. The remaining 11 sectors of the linac may be

*Work supported by Department of Energy, contract DE-AC03-76SF-00515.
†Work supported by Department of Energy, contract W-7405-ENG-48.

TABLE I

B FACTORY INJECTION SPECIFICATIONS AND PARAMETERS

Beam Energy:	
High-energy ring (HER) (e^-) [GeV]	9 [range: 8-10]
Low-energy ring (LER) (e^+) [GeV]	3.1 [range: 2.8-4]
Beam current:	
HER ring [A/$10^{10}e^-$]	1.48/6777
LER ring [A/$10^{10}e^+$]	2.14/9799
Particles per bunch:	
HER ring[$10^{10}e^-$]	4.1
LER ring [$10^{10}e^+$]	5.9
Linac repetition rate [pps]	60/120
Linac current [10^{10} $e^{\pm}$ per pulse]**	0.4-2
Invariant linac emittance [m-rad]	5×10^{-5}
Filling times:	
Topping-off (80-100%) [min]	3
Full Filling (0-100%) [min]	6
Magnet standardization time [min]	15
Ring circumference [m]	2199.318
Revolution period [μs]	7.336
Revolution frequency [kHz]	136.311
Bunch frequency [MHz]	476/2 = 238
Time between bunches [ns]	4.20
Harmonic number	3492
Number of bunches	1746 + 5%
(leaving 5% gap)	= 1658
Horizontal damping time:	
HER [ms]	38
LER with wigglers [ms]	36
LER without wigglers [ms]	150
Geometric beam emittance [nm-rad]:	
HER horizontal/vertical	48/1.9
LER horizontal/vertical	96/3.8

**Assuming 50% filling efficiency.

Presented at the IEEE Particle Accelerator Conference, San Francisco, CA., May 6-9, 1991.

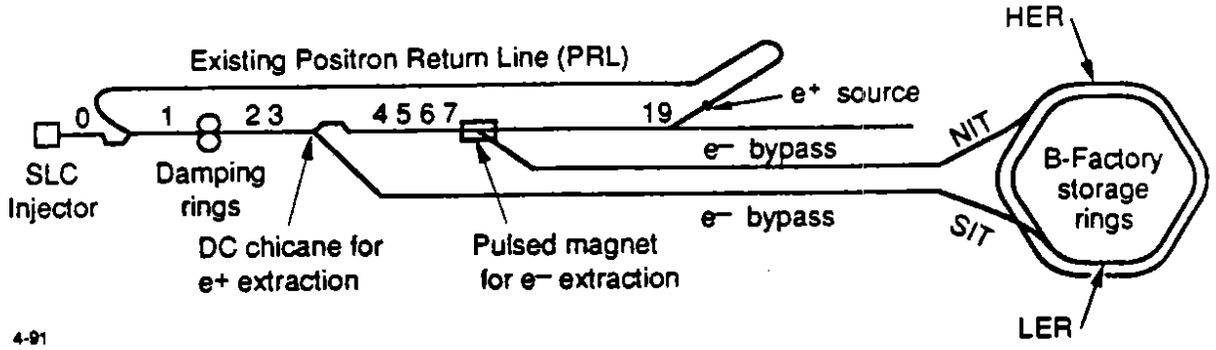

Fig.1. Schematic of the B Factory $e^{\pm}$ injection system, based on use of the SLC linac with bypass lines. The numbers along the linac indicate the location (not to scale) of each sector. Each of the 30 sectors is 100 m long.

turned off. Once extracted, the respective bunches of electrons and positrons will be transmitted through two separate bypass lines to the existing NIT and SIT lines presently used to fill PEP from the end of the linac. The NIT and SIT lines are well instrumented and will not be described in this paper. The advantages of the system proposed here are numerous: a) it preserves all other High Energy Physics opportunities at SLAC: b) the bunches leave the linac at the desired energy, thereby eliminating the need for backphasing and minimizing wakefields in unnecessary accelerator structures: c) by alternating e^+ and e^- pulses at 60 pps, only one bunch will be stored at a time in each damping ring: d) no additional fast kickers (often unreliable) will be needed: e) between filling times, it will be possible to "park" e^+ and e^- bunches at a low rate in NIT and SIT Faraday cups to optimize readiness for filling on demand: f) finally, by selecting a ring RF frequency of 476 MHz, i.e., 1/6 of the linac RF frequency of 2856 MHz, synchronization will be greatly simplified.

The bypass lines will consist of 10 cm-diameter aluminum pipe (for adequate pumping speed) with 2.5 cm-diameter constrictions every 50m where a FODO array of quadrupoles and beam position monitors will be located. These apertures will be fully adequate since the low-emittance beams will have σ_r's of less than 1.5 mm. A cross-section of the linac housing with the overhead-suspended quadrupoles showing the respective tilts of the extraction planes is given in Fig. 2. The existing positron return line (PRL) is shown for reference in the upper right-hand corner. Table II gives a list of the components in the bypass lines. The matching quadrupoles are part of 360 degree-phase advance achromatic bends joining the linac to the bypass lines, and these to NIT and SIT.

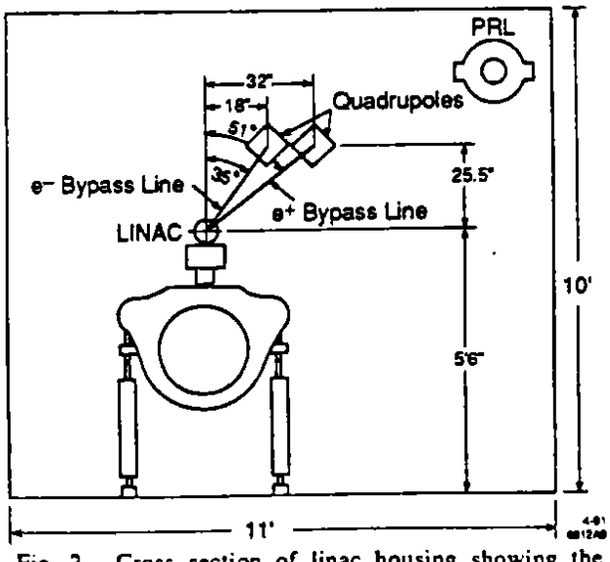

Fig. 2. Cross section of linac housing showing the location of the electron and positron FODO array quadrupoles. Note the tilts of the extraction planes.

TABLE II
LINAC BYPASS LINE COMPONENTS AND SPECIFICATIONS

	POSITRON LINE	ELECTRON LINE
Length (km)	~2.6	~2.2
Energy (GeV)	2.8-4	8-10
No. of quadrupoles		
Matching	24	24
FODO array	52	44
Steering correctors	64	56
Beam position monitors	64 (64 readouts)	56 (56 readouts)
Profile monitors	2	2
Pumps (120L/s)	29	23
Vacuum roughing connections	29	23
Fast valves	1	1
Isolation valves	14	13

III. INJECTION INTO THE HER AND LER

In contrast to the single PEP ring, for which the injection lines come down vertically into the plane of the ring and are tangent to the inside, the HER and LER injection lines will be brought down on the outside of the two rings - into the plane of the HER at IR-10 and into the plane of the LER at IR-8. The proposed method of injection is very similar to the one used in PEP. It assumes β_x = 80 m and β_y = 20 m in 40-m-long injection regions. Horizontal injection occurs as shown in Fig. 3. The closed orbit of the stored beam is temporarily distorted by means of four DC bump magnets and three kickers. Details of the horizontal phase space (x,x') for the stored and injected beam are shown at three sequential points in time following the turn-on of the DC bump magnets: (i) stored beam is moved by 0.5 cm to DC bumped position, $10\sigma_x$ away from the inner edge of the 3-mm septum: (ii) stored beam is within 6 σ_x of the septum inner edge: incoming beam from the linac is tangent to the stored-beam

orbit and within 2 σ_i of the outer septum edge; (iii) approximately four turns later, the stored beam is back to its DC bumped orbit: the incoming beam is inside the ring within $2\sigma_x$ of the inner septum edge, ready to damp and merge with the stored beam. It is assumed that the injected beam has a β_x of 30 m.

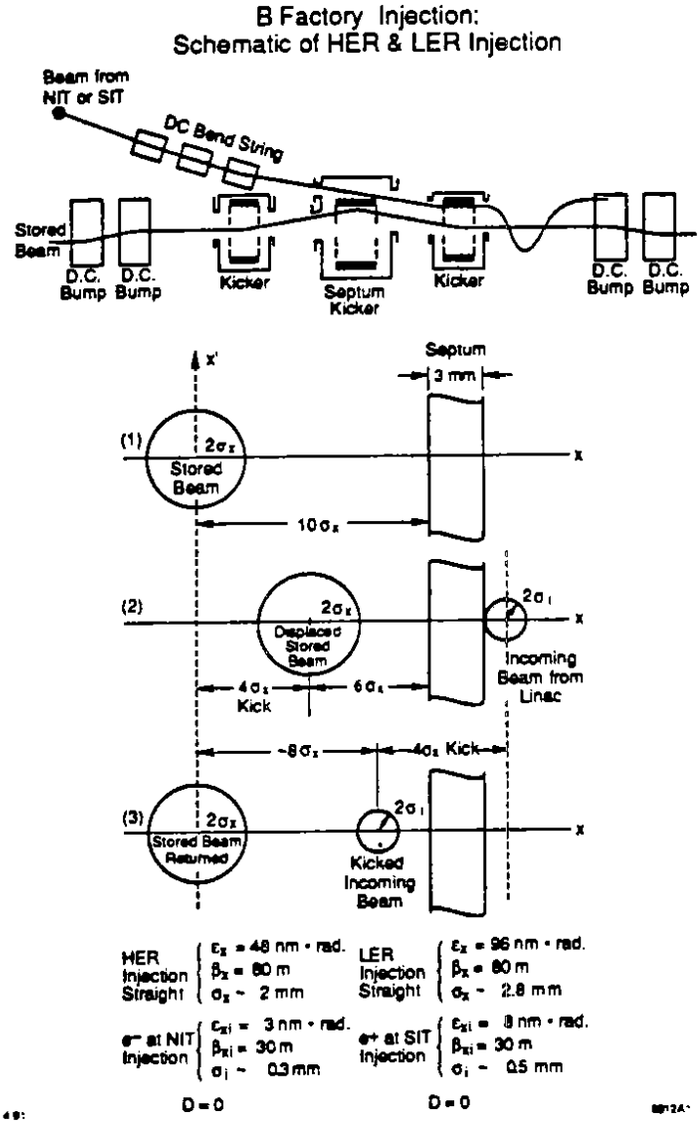

Fig. 3 Schematic of Injection Kicker System, and horizontal transverse phase space (x,x') of stored and incoming beams during three successive steps of the injection process (HER and LER). The diameters of the stored and incoming beams are not drawn to scale.

For injection purposes, each ring is divided into nine rotating "zones" of equal length as shown in Fig. 4. A zone has a length of about 244 m (or 815 ns) and contains 194 bunches. One of these zones in each ring will remain about half empty to leave a gap for ion control. We describe here the process for filling the LER at a 60Hz rate; the HER is filled in a similar way. The transverse damping time for the HER is 38 ms and for the LER 36 ms. If the damping contribution of the wigglers in the LER is ignored, a worst-case situation in terms of injection, then the LER has a damping time of 150 ms. The beginning of each zone is determined by the time onset of the kicker current pulses. All three kicker pulsers are identical, consisting of critically damped RLC circuits that rise and fall to practically zero within less than 1500 ns. The first bucket to be filled in zone n is located roughly 200 ns after the beginning of the kicker pulse so as to ride on the flat top where sensitivity to time jitter is minimized. Since the rise time of the pulse is much shorter than the fall time, bunches recently stored in zone n - 1 are unaffected. Bunches in zone n + 1 (at least 815 ns later) are kicked slightly, but since they have been in the ring for the longest time, their orbits are almost fully damped, and, to the extent that the kickers are matched, these bumps are closed. Thus, single buckets in zones 1 through 9 are filled in succession, after which, 9 times 1/60th of a second, or 150 ms later (that is, one damping time in the LER in the absence of wigglers), the next adjacent buckets (4.2 ns later) in each zone are filled, and so on. With this method, damping in the LER, even without wigglers, is adequate. The entire filling sequence will be computer controlled and automated for both rings.

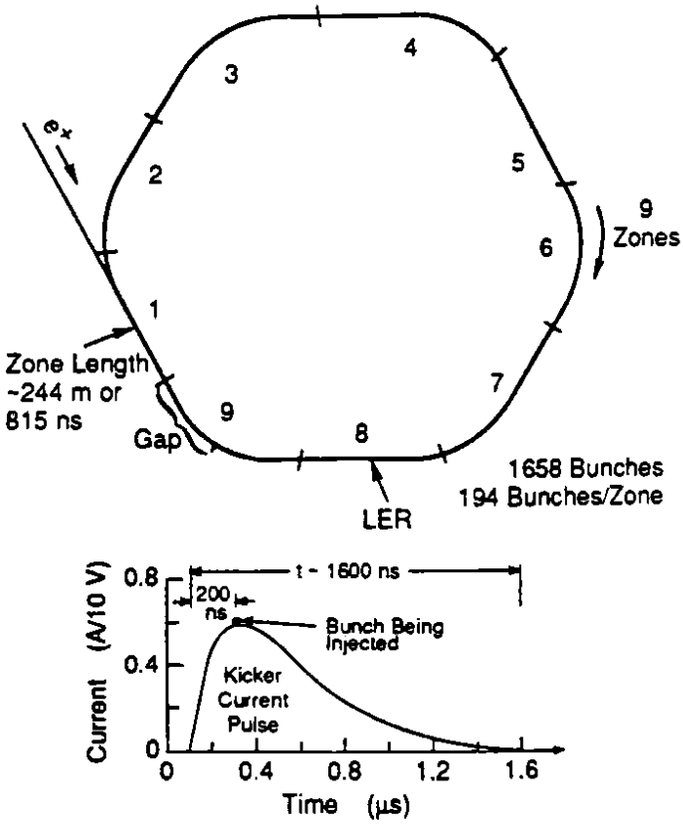

Zone Filling Sequence: 1,2,3,4,5,6,7,8,9 (partially), 1,etc. ...

Fig. 4 Azimuthal zone filling sequence for the LER, showing nine zones. The kicker pulse shown (equal for all kickers) was computed by assuming charged, critically damped RLC circuits [R = 2 (L/C) $^{1/2}$] in which the current reaches its maximum at t = 2 L/R after a thyratron is fired and allows the circuit to be discharged.

S.F. PAC
May 1991
LBL-30833

Hourglass Effects for Asymmetric Colliders *

Miguel A. Furman
Lawrence Berkeley Laboratory, Berkeley, CA 94720

Abstract

We give the expressions for the geometrical reduction factor of the luminosity and the geometrical beam-beam "aggravating factor" for the general asymmetric case, for tri-gaussian bunches colliding head-on. With these formulas we attempt a (limited) analytic understanding of the multiparticle tracking simulations carried out for the proposed SLAC/LBL/LLNL B factory [1] when parasitic crossings are ignored. We conclude the following: (a) the geometrical reduction in luminosity is $\sim$ 6% relative to the zero-bunch-length (nominal) value; (b) only the vertical beam-beam parameter of the LER is significantly altered by the hourglass effect: the geometrical enhancement of the central positron's vertical beam-beam parameter is $\sim$ 10% relative to the nominal value, and (c) the positrons at the head or tail of the bunch have vertical beam-beam parameters much larger than nominal. We discuss the electromagnetic disruption effect only qualitatively. This effect probably compensates (or overcompensates) the geometrical reduction of the luminosity, and it is possibly detrimental for the beam-beam parameters. This article summarizes Ref. [2].

I. Introduction

Although proposed B factories [1] call for designs that are asymmetric in energy, beam current and emittances, they also invoke to a greater or lesser degree a "transparency condition" by virtue of which the beam sizes are pairwise equal [3]. Because of the beam-beam interaction, however, the beams become different in size at least to some degree. Expressions available in the literature [4, 5, 6] for the hourglass factors for the luminosity and beam-beam parameters assume some sort of equality among the beam sizes or lattice functions. In this note we provide generalizations that are applicable to the most general asymmetric case, when the four beta-functions and the six rms beam sizes are arbitrary. With these formulas we attempt a (limited) analytic understanding of the multiparticle tracking results for the proposed SLAC/LBL/LLNL B factory [1] when parasitic collisions are ignored.

*Work supported by the Director, Office of Energy Research, Office of High Energy and Nuclear Physics, High Energy Physics Division, of the U.S. Department of Energy under Contract Number DE-AC03-76SF00098.

II. Luminosity

Consider two bunches moving in equal and opposite directions with speed c, with tri-gaussian particle distributions, such that the centers collide at the optical interaction point (IP, $s = 0$) with no displacement. We assume that the interaction region is a dispersionless drift section and that the IP is a symmetry point of the lattice. Then the transverse rms sizes σ_{x+}, σ_{y+}, σ_{x-} and σ_{y-} have an s dependence of the form $\sigma^2 = \sigma^{*2} \times (1 + s^2/\beta^{*2})$. The hourglass reduction factor for the luminosity is [2]

$$R(t_x, t_y) \equiv \frac{\mathcal{L}}{\mathcal{L}_0} = \int_{-\infty}^{\infty} \frac{dt}{\sqrt{\pi}} \frac{\exp(-t^2)}{\sqrt{(1 + t^2/t_x^2)(1 + t^2/t_y^2)}} \quad (1)$$

where $\mathcal{L}$ is the actual luminosity and $\mathcal{L}_0$ is the luminosity in the zero-bunch-length limit,

$$\mathcal{L}_0 = \frac{f_b N_+ N_-}{2\pi\sqrt{(\sigma_{x+}^{*2} + \sigma_{x-}^{*2})(\sigma_{y+}^{*2} + \sigma_{y-}^{*2})}} \quad (2)$$

where f_b is the bunch collision frequency, and t_x is defined by

$$t_x^2 = \frac{2(\sigma_{x+}^{*2} + \sigma_{x-}^{*2})}{(\sigma_{s+}^2 + \sigma_{s-}^2)\left(\sigma_{x+}^{*2}/\beta_{x+}^{*2} + \sigma_{x-}^{*2}/\beta_{x-}^{*2}\right)} \quad (3)$$

with a corresponding expression for t_y. The superscript $*$ refers to the IP and $\sigma_{s\pm}$ are the rms bunch lengths. We exhibit $R(t_x, t_y)$ in Fig. 1.

It is easy to see from Eq. (1) that R is always < 1, except that $R(\infty, \infty) = 1$, as it should.

If both beams are flat, with $\sigma_{x\pm} \gg \sigma_{y\pm}$, then $t_x \gg 1$ and (1) can be expressed in terms of a modified Bessel function. This result is of similar form to that of Ivanov *et al.* [5] but is of more general validity because it does not assume $\beta_{y+}^* = \beta_{y-}^*$ or $\sigma_{s+} = \sigma_{s-}$ or $\sigma_{y+}^* = \sigma_{y-}^*$.

If the beams are such that $t_x = t_y$ (which may happen naturally in a round-beam design), then (1) can be expressed in terms of the complementary error function.

III. Beam-Beam Parameters

We focus on a single particle, say a positron, as it passes through the opposing electron bunch. In a first-order calculation we can assume that the particle follows a straight line trajectory with constant speed c. We assume that this particle is close to the collision axis and is displaced longitudinally by a finite distance z from the center of its

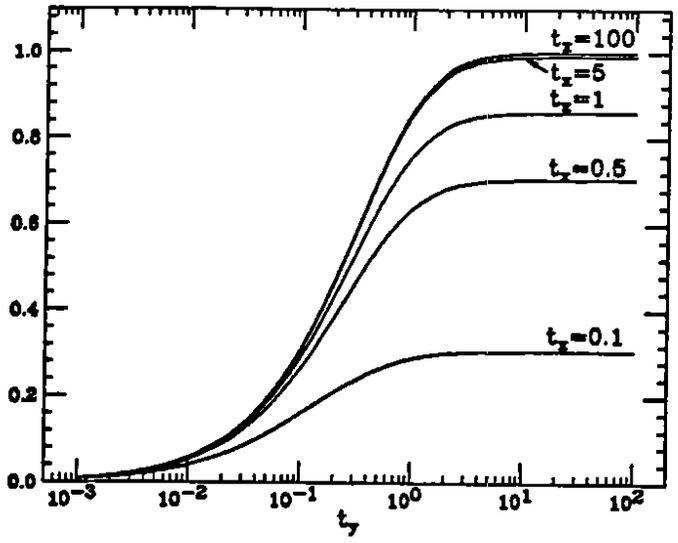

Figure 1: The luminosity reduction factor, Eq. (1), plotted *vs.* t_y for various values of t_x.

own bunch. We assume that z is constant during the collision process (or during several successive collisions), which is a very good approximation in practice. Then the "aggravating factor" [4] for the positron's vertical beam-beam parameter is [2],

$$R_{y+}(z) \equiv \xi_{y+}(z)/\xi_{0y+} =$$

$$\int_{-\infty}^{\infty} \frac{dt}{\sqrt{\pi}} \frac{(1+t^2/t_1^2)\exp(-(t-t_0)^2)}{\sqrt{1+t^2/t_2^2}\left(v\sqrt{1+t^2/t_2^2}+h\sqrt{1+t^2/t_3^2}\right)} \quad (4)$$

where $h = \sigma^*_{x-}/(\sigma^*_{x-}+\sigma^*_{y-})$, $v = \sigma^*_{y-}/(\sigma^*_{x-}+\sigma^*_{y-})$, $t_0 = z/\sqrt{2}\sigma_{s-}$, $t_1 = \sqrt{2\beta^*_{y+}}/\sigma_{s-}$, $t_2 = \sqrt{2\beta^*_{y-}}/\sigma_{s-}$ and $t_3 = \sqrt{2\beta^*_{x-}}/\sigma_{s-}$. The nominal (zero-bunch-length) vertical beam-beam parameter ξ_{0y+} of the central positron is

$$\xi_{0y+} = \frac{r_0 N_- \beta^*_{y+}}{2\pi\gamma_+\sigma^*_{y-}(\sigma^*_{x-}+\sigma^*_{y-})} \quad (5)$$

where r_0 is the classical electron radius and γ_+ is the usual relativistic factor. The expressions for the remaining three beam-beam parameters ξ_{x+}, ξ_{x-} and ξ_{y-} are obtained from Eqs. (4) and (5) by the substitutions $x \leftrightarrow y$ and/or $+ \leftrightarrow -$ in h, v and the t_i's.

It should be noted that the aggravating factors can be > 1 or < 1, as opposed to the luminosity reduction factor, which is always < 1. However, if $\beta^*_{x+} = \beta^*_{y+} = \beta^*_{x-} = \beta^*_{y-}$ we obtain

$$R_{x+}(z) = R_{y+}(z) = R_{x-}(z) = R_{y-}(z) = 1 \quad (6)$$

for all z regardless of the beam sizes. This allows, in principle, for the possibility of designing the lattice so that there is no hourglass effect on the beam-beam parameters.

If the beams are flat such that $\sigma_{x+} \gg \sigma_{y+}$, $\sigma_{x-} \gg \sigma_{y-}$, $\beta^*_{x+} \gg \beta^*_{y+}$ and $\beta^*_{x-} \gg \beta^*_{y-}$, Eq. (4) yields, for the central particle, $R_{x+}(0) \simeq R_{x-}(0) \simeq 1$, and

$$R_{y+}(0) \simeq \frac{t_2}{2\sqrt{\pi}} e^{t_2^2/2}\left[(2-\rho)K_0(t_2^2/2)+\rho K_1(t_2^2/2)\right] \quad (7)$$

where $\rho \equiv (t_2/t_1)^2$ and K_0, K_1 are Bessel functions. $R_{y-}(0)$ is obtained from (7) by exchanging $t_1 \leftrightarrow t_2$.

If $t_2 = t_3$ for both beams (such as for round beams), then $\beta^*_{x+} = \beta^*_{y+}$ and $\beta^*_{x-} = \beta^*_{y-}$; we allow, however, for the possibility that $\beta^*_{x+} \neq \beta^*_{x-}$ and we assume nothing about the six rms beam sizes. Then we find that

$$R_{x+}(0) = R_{y+}(0) = \rho + (1-\rho)\sqrt{\pi}\, t_2 \exp(t_2^2)\,\mathrm{erfc}(t_2) \quad (8)$$

where $\mathrm{erfc}(x)$ is the complementary error function. $R_{x-}(0) = R_{y-}(0)$ is obtained by exchanging $t_1 \leftrightarrow t_2$.

For particles away from the bunch center, Eq. (4) implies that $\xi(z) = \xi(-z)$ for each of the four beam-beam parameters. This means that the particles at the head and the tail of the bunch suffer the same beam-beam tune shift. This property follows from the assumed lattice symmetry about the IP and the assumed lack of bunch disruption.

The aggravating factors saturate [2] to a limit when $z \to \infty$. In practice this limit applies to particles with $|z| \gg \beta^*$, where β^* is here any of the four beta-functions at the IP; therefore this limit may or may not be sensibly reached in specific machine designs. Furthermore, this property follows from a first-order calculation; it may not hold in higher orders if $\xi(\infty)$ is large.

IV. The SLAC/LBL/LLNL B Factory

For nominal parameters of the APIARY 6.3-D design for the proposed SLAC/LBL/LLNL B factory [1] we obtain $t_x = 47.43$ and $t_y = 1.897$, so that $R = 0.945$. This implies that the luminosity is 5.5% smaller than the zero-bunch-length estimate.

We also obtain $R_{y+}(0) = 1.093$, so that the vertical beam-beam parameter of the central positron is 9.3% larger than the nominal value. The other three aggravating factors are slightly smaller than unity [2]. For particles away from the center of the bunch, R_{y+} grows almost linearly with z. Fig. 2 shows ξ_{y+} as a function of the positron's longitudinal distance away from the center of the bunch. The remaining three aggravating factors deviate significantly from unity only for $z \gtrsim 10\sigma_s$. Fig. 3 shows all four aggravating factors as a function of the particle's distance away from the center of the bunch.

A qualitative estimate of the electromagnetic bunch disruption can be obtained from results for multiparticle simulations for single-pass, symmetric, beam collisions [7]. For flat bunches that are uniform in x and gaussian in y and s, one obtains, from Chen's empirical fit, that the disruption is $H_D = 0.998$ with an estimated accuracy of $\pm 10\%$, for nominal APIARY 6.3-D parameters ($A = 0.53$ and $D = 0.20$). Since H_D takes into account both the geometrical and the electromagnetic disruption effects, we conclude, to this accuracy, that the geometrical reduction in luminosity is compensated by the pinching effect. This

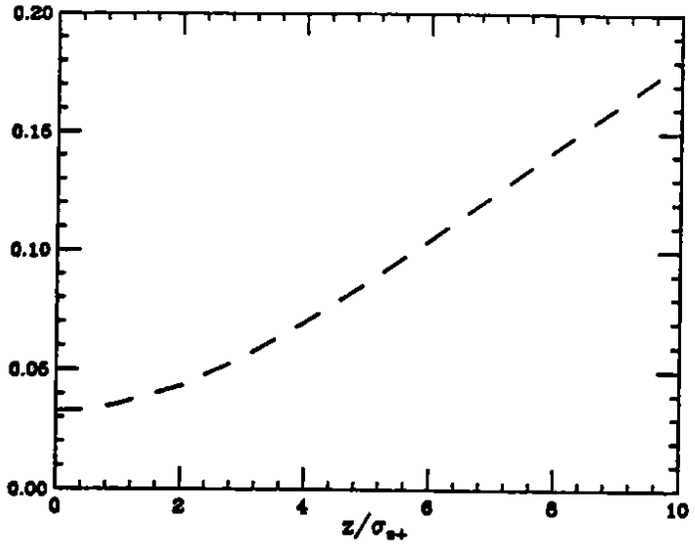

Figure 2: The vertical beam-beam parameter for the positron, $\xi_{y+}(z)$, for nominal APIARY 6.3-D parameters. The nominal value is $\xi_0 = 0.03$ for all four beam-beam parameters. The almost linear rise is explained in [2].

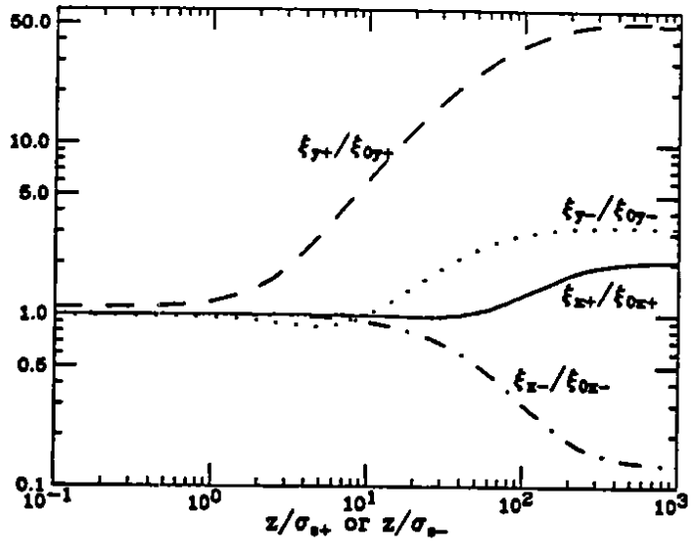

Figure 3: The aggravating factors for both beams for nominal APIARY 6.3-D parameters. The saturation property is seen at (unphysically) large values of z ($\sigma_{z\pm} = 1$ cm).

result is consistent with the multiparticle tracking simulation results for the SLAC/LBL/LLNL B factory when parasitic collisions are ignored [1]. One should keep in mind, however, that since Chen's results apply to single-pass collisions, a potentially important dependence on the tune of the machine may be missed in this interpretation.

V. Conclusions

As in the symmetric case, the luminosity reduction factor is a sensitive function of β^*/σ_z. Unlike the symmetric case, however, this factor depends explicitly on the transverse bunch sizes in addition to the bunch lengths and beta-functions.

A numerical application to the SLAC/LBL/LLNL B factory shows a 5.5% geometrical reduction of the luminosity and a 9.3% geometrical enhancement of the central positron's ξ_{y+} relative to the nominal values.

Positrons with $x \simeq y \simeq 0$ at the head or tail of the bunch have higher ξ_{y+} than the central positron due to the fact that they sample, on average, a higher β^*_{y+} during the collision process ($\beta^*_{y+} = 1.5$ cm is the smallest of the four β^*'s). Positrons with $|z| > 6\sigma_z$ have $\xi_{y+} > 0.1$; this number can be made smaller, however, by a modest increase in β^*_{y+} [2].

We estimate the electromagnetic pinching effect to be small, since it modifies the results of the geometrical calculations by $\sim \pm 10\%$. It is probably beneficial for the luminosity, and it is probably detrimental for the beam-beam parameters.

VI. Acknowledgments

I thank Pisin Chen, Yong-Ho Chin, Bill Fawley, Andrew Hutton, Jeff Tennyson and Mike Zisman for discussions.

VII. References

[1] LBL PUB-5303/SLAC-372/CALT-68-1715 /UCRL-ID-106426/UC-IIRPA-91-01, February 1991; CLNS 91-1050; KEK 90-24, March 1991.

[2] M. A. Furman, ABC-21/ESG-161, April 1991.

[3] Y. H. Chin, *AIP Conf. Proc.* **214**, 424 (1990); also Y. H. Chin, LBL-27665, 1989; M. A. Furman, ABC-25/ESG-161, February 1991.

[4] S. Milton, CBN 89–1.

[5] P. M. Ivanov, I. A. Koop, E. A. Perevedentsev, Yu. M. Shatunov and I. B. Vasserman, 1989 ICFA Workshop, Novosibirsk.

[6] J. T. Seeman, Springer-Verlag Lecture Notes in Physics no. 247, Sardinia, 1985.

[7] P. Chen, SLAC-PUB-4822, December 1988, Snowmass 1988; P. Chen and K. Yokoya, Phys Rev. D **38**, 987 (1988).

BECON-90
LBL-30225

Control of Coupled-Bunch Instabilities in High Current Storage Rings

G. Lambertson
Lawrence Berkeley Laboratory,
University of California
Berkeley, CA 94720

April 1991

* Work supported by the Director, Office of Energy Research, Office of High Energy Physics, Advanced Energy Projects Division, of the U.S. Department of Energy under Contract No. DE-AC03-76SF00098.

PARASITIC CROSSING AT AN ASYMMETRIC B FACTORY, APIARY*

Y.H. Chin
Accelerator & Fusion Research Division
Lawrence Berkeley Laboratory
Berkeley, CA 94720

Abstract

Effects of parasitic crossings ("near miss" collisions of two counter-rotating beams at unwanted positions near the IP) are studied in terms of computer simulations for an asymmetric B Factory, APIARY–6.3d. Beams are separated horizontally at the first parasitic crossing points by about 7.6 times the horizontal rms size of the low energy beam (the larger in size of the two beams), $\sigma_{0x,+}$. Simulations, including both the beam collision at the IP and parasitic crossings, have been performed for different separation distances, d. It is found that the ratio $d/\sigma_{0x,+}$ is a good scaling parameter of beam blowup behavior. The results show that beam blowup due to the parasitic crossings is diminished for $d \geq 7\sigma_{0x,+}$, in agreement with the bunch separation experiment at CESR. Thus, the nominal separation 7.6 $\sigma_{0x,+}$ turns out to be acceptable, but with only a small margin. Some methods to mitigate the effects of the parasitic crossings are discussed.

I. INTRODUCTION

The attainable luminosity in an asymmetric storage-ring collider for a B Factory will be determined to a large extent by the physics of the beam-beam interaction. Extensive studies of the beam-beam dynamics under asymmetric energy conditions have been done, and the idea of the so-called "energy transparency symmetry" was suggested to put the two beams on an equal footing as far as transverse dynamics is concerned [1]. Most of those studies consider only primary head-on collision of two beams at the IP. For the APIARY–6.3d, the bunch spacing is only 1.26 m, so that the bunches experience long-range collisions on the way into and out of the IP region (where both beams travel in a common vacuum pipe). These collisions are called "parasitic crossings." There are six parasitic crossings symmetrically located on either side of the IP. Of these, the first parasitic crossing (the one closest to the IP) on either side has the dominant effect on beam dynamics due to the small beam separation and the large vertical beta function. The nominal parameters at the IP and the first parasitic crossing point for the two rings of APIARY–6.3d are listed in Table 1. In this table, Δs is the distance between the IP and the first parasitic crossing, d is the separation distance between the two orbits at the parasitic crossing, $\Delta\nu$ is the tune advance between the IP and the first parasitic crossing, β is the beta function, and σ_0 is the rms nominal beam size. Horizontal and vertical quantities are denoted by the subscripts x and y, respectively.

Table 1
APIARY–6.3d nominal parameters at the IP and the first parasitic crossing

	Low Energy Ring (LER, e^+)		High Energy Ring (HER, e^-)	
Δs (m)	0.63			
d (mm)	2.82			
	IP	1st PC	IP	1st PC
$\Delta\nu_x$	0	0.1643	0	0.1111
$\Delta\nu_y$	0	0.2462	0	0.2424
β_x (m)	0.375	1.51	0.75	1.30
β_y (m)	0.015	25.23	0.03	13.01
σ_{0x} (μm)	186	373	186	245
σ_{0y} (μm)	7.4	302	7.4	153
d/σ_{x0}	—	7.6	—	11.5

Parasitic crossings have the potential to induce significant blowup in the vertical beam size of the low energy ring (LER), because they excite odd-order resonances and because the vertical long-range tune shift of the LER is as large as the head-on tune shift at the IP. Obviously, if the separation is large enough, effects of the parasitic crossings diminish. We carry out simulations to see if the present nominal separation $d = 7.6\ \sigma_{0x,+}$ gives acceptable performance. A more detailed description of the present study can be found in Ref. 2.

II. SIMULATION TECHNIQUE

Once the two rings are filled with bunches, pairs of collisions at the IP are fixed; that is, each bunch of one ring collides only with the same partner in the other ring. Therefore, the beam-beam dynamics can be simulated with one bunch per ring. However, when parasitic crossings are included, all the bunches can "talk" to each other directly or indirectly. A completely faithful simulation for APIARY–6.3d would require 1658 bunches per ring, pushing the CPU time beyond practical limits. If the coherent beam-beam oscillation does not play an important role in beam blowup, the "talk" between bunches may not need to be simulated exactly. At the same time, the particle distributions do not

* Supported by Director, Office of Energy Research, Office of High Energy and Nuclear Physics, High Energy Physics Division, of the U.S. Department of Energy under Contract No. DE-AC03-76SF00098.

differ much from bunch to bunch. Under these assumptions, we may adopt the following technique to allow us to use only one bunch per ring. Two bunches are counter-rotating in the two rings (see Fig. 1). When the e^- bunch is at the parasitic crossing PC+, the e^+ bunch is at the other parasitic crossing, PC–. To calculate the beam-beam force on the e^- bunch from the e^+ bunch at PC+, we use the particle distribution of the e^+ bunch at PC-. The same technique is applied to the e^+ bunch.

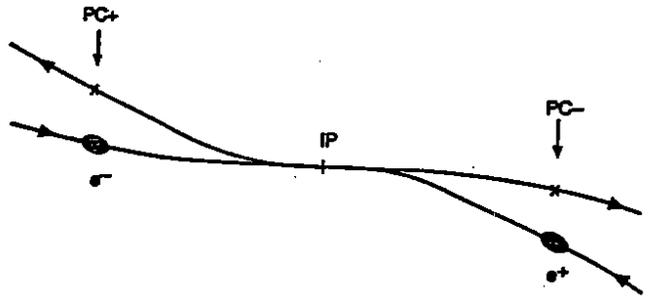

Figure 1. Schematic layout of the interaction region.

III. SIMULATION RESULTS

The main parameters of APIARY–6.3d used in the simulations are listed in Table 2.

Table 2
Main parameters of APIARY–6.3d

	LER (e^+)	HER (e^-)
Energy, E (GeV)	3.1	9
Circumference, C (m)	2200	2200
Nominal emittance, ε_{0x} (nm-rad) ε_{0y} (nm-rad)	92 3.6	46 1.8
Bunch length, σ_s (cm)	1.0	1.0
Damping time, $\tau_x = \tau_y$ (turns)	4400	5014
Bunch current, I_b (mA)	1.23	0.848
Synchrotron tune, Q_s	0.0403	0.0520
Nominal beam-beam tune shift, $\xi_{0x} = \xi_{0y}$	0.03	0.03

We have selected the fractional tunes of the working point to be $\nu_x = 0.09$ and $\nu_y = 0.05$ for both beams at the present time; a thorough tune scan remains to be carried out for actual operation. For these parameters, the primary simulation result without parasitic crossings shows 23% beam blowup in the vertical size in the LER. The other three beam sizes remain practically unchanged from their nominal values. Figure 2 shows the beam blowup factor as a function of the separation $d/\sigma_{0x,+}$ where all other parameters are kept fixed. The corresponding luminosity as a function of $d/\sigma_{0x,+}$ is shown in Fig. 3. From Fig. 2, it can be seen that the separation $d = 7\ \sigma_{0x,+}$ should be enough to consider that the effects of the parasitic crossings are negligible. Accordingly, the luminosity is only reduced by about 10% from its design value. This result agrees with the separation experiment at CESR [3] that concludes that at least 6 "effective" σ_{0x} (practically, 6 + 1 σ_{0x}) separation is required to maintain a one–hour beam lifetime.

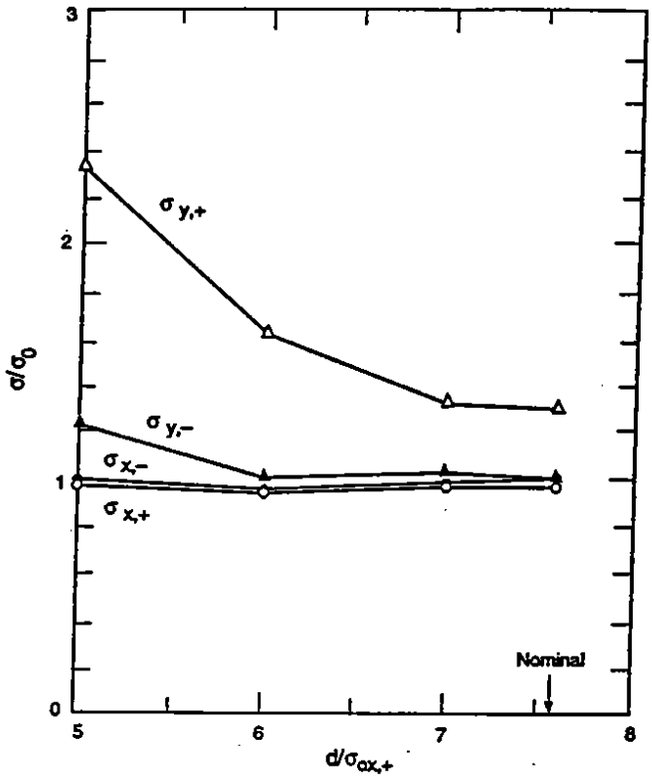

Figure 2. RMS beam sizes as a function of the relative separation $d/\sigma_{0x,+}$ for the nominal APIARY–6.3d parameters. The subscripts label HER (–) and LER (+). The nominal beam separation at the parasitic crossing is indicated by the arrow.

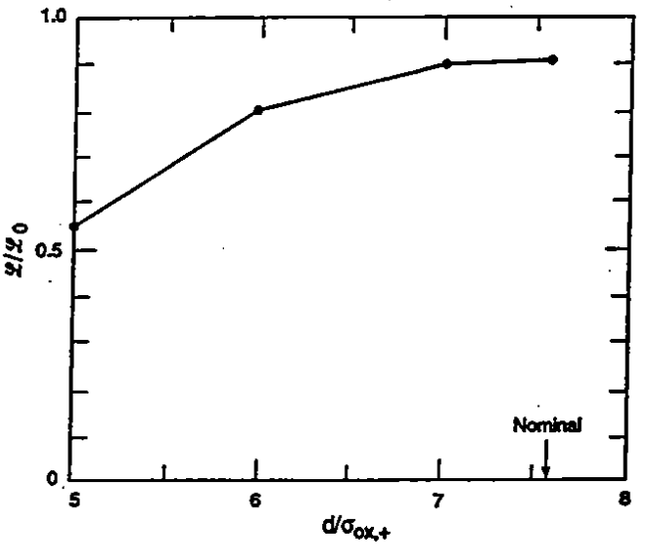

Figure 3. Luminosity as a function of $d/\sigma_{0x,+}$, for the nominal APIARY–6.3d parameters.

Although the nominal separation $d = 7.6\ \sigma_{0x,+}$ turns out to be large enough, the safety margin for closed–orbit

distortion and so forth is not that great. A simple solution for this would be to increase the separation distance, and that approach is now under study. Here, however, we intend to explore other possibilities in order to improve luminosity, particularly for a large value of ξ_0. The first such possibility is to increase the beta function at the IP, β^*, of the LER. The idea is to make the tune modulation due to the synchrotron motion at the IP closer to the energy transparency condition, and simultaneously to reduce the beta function of the LER at the parasitic crossing. Therefore, the beam size at the parasitic crossing is also reduced and the relative separation $d/\sigma_{0x,+}$ increases. The penalty is a large low-energy beam current. A preliminary simulation result without parasitic crossings shows that the two beams blow up more symmetrically and the luminosity gets closer to its nominal value.

Another possibility is to increase the bunch spacing from $2\lambda_{rf} = 1.26$ m to $3\lambda_{rf} = 1.89$ m by filling the rings with bunches every third rf bucket, instead of every second bucket, while other lattice parameters are kept fixed. Here, λ_{rf} is the rf wave length. This pushes the parasitic crossing farther away from the IP and the separation distance becomes larger. Now, the separation d at the first parasitic crossing increases from 2.82 mm to a considerably large value of 7.41 mm. The beta function at the parasitic crossing increases also, so that the relative separation $d/\sigma_{0x,+}$ increases from 7.6 to 9.2. In order to maintain the nominal ξ_0 and keep the luminosity constant, the bunch current and the emittance also must increase by 50%. These changes are still acceptable in terms of beam instability thresholds and dynamic aperture considerations. The simulation results are shown in Figs. 4 and 5. We can see practically no beam blowup at the nominal separation, and the luminosity is close to the nominal value. The safety margin of d is now sufficiently greater than the previous case (note that the beam size at the parasitic crossing increases by a factor of about 2). Good luminosity performance remains even for a larger $\xi_0 = 0.05$.

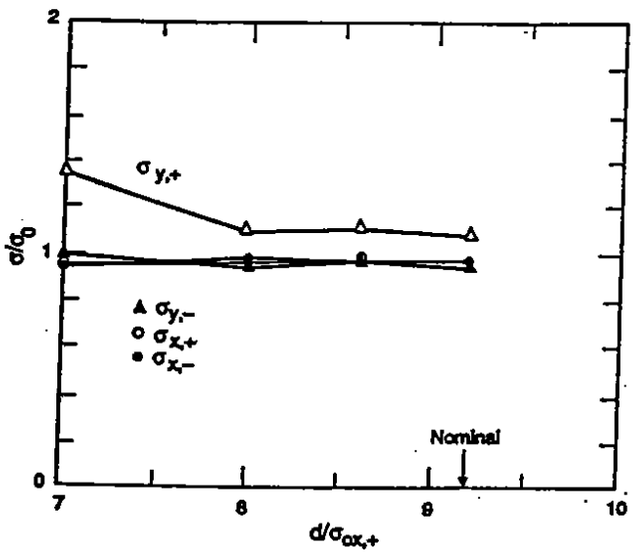

Figure 4. RMS beam sizes as a function of $d/\sigma_{0x,+}$ for APIARY–6.3d, in the case where bunches are filled every third bucket instead of every second bucket.

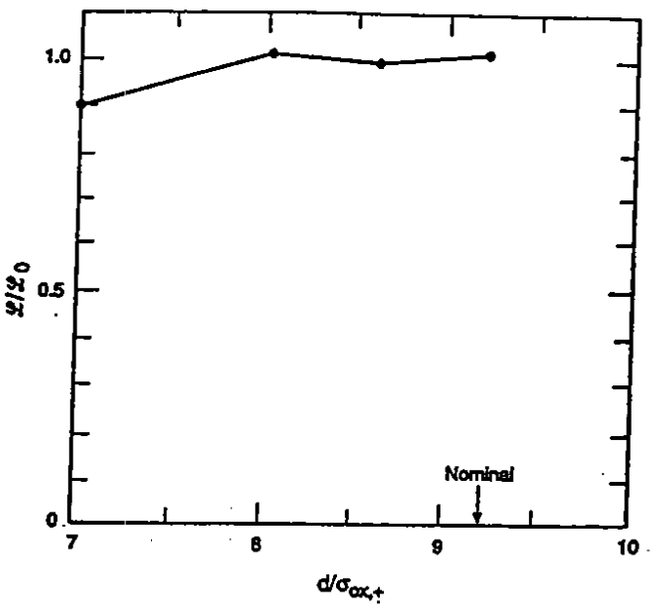

Figure 5. Luminosity as a function of $d/\sigma_{0x,+}$ for APIARY–6.3d, corresponding to Fig. 4.

IV. CONCLUSIONS

Simulation results including the effect of parasitic crossings for APIARY–6.3d show that the nominal separation is large enough that beam blowup due to the parasitic crossings disappears and the luminosity reduction is only 10% from its nominal value for $\xi_0 = 0.03$. However, the safety margin in terms of separation tolerance is low. To mitigate the effects of the parasitic crossings, one such possibility is to change the lattice parameters, such as the beta functions at the IP and at the parasitic crossing, so that the relative separation d/σ_{0x} increases. Another possibility is to increase the bunch spacing from $2\lambda_{rf} = 1.26$ m to $3\lambda_{rf} = 1.89$ m by filling the rings with bunches every third bucket rather than every second bucket. In this way, the optics parameters can be kept fixed. Preliminary simulation results for the case of filling every third bucket show improvement in the beam sizes and the luminosity.

The author would like to thank M. Zisman for helpful discussions and proofreading of the manuscript.

V. REFERENCES

[1] Y.H. Chin in *Beam Dynamics Issues of High Luminosity Asymmetric Collider Rings*, AIP Conf. Proc. 214, edited by A.M. Sessler, Berkeley, CA (1990), pp. 424-433.

[2] *An Asymmetric B Factory Based on PEP, Conceptual Design Report*, Lawrence Berkeley Laboratory Report LBL PUB-5303, February, 1991.

[3] D.H. Rice in *Beam Dynamics Issues of High Luminosity Asymmetric Collider Rings*, AIP Conf. Proc. 214, edited by A.M. Sessler, Berkeley, CA (1990), pp. 219-234.

Control of Coupled-Bunch Instabilities in High-Current Storage Rings*

G. Lambertson

Lawrence Berkeley Laboratory
1 Cyclotron Road
Berkeley, California 94720

ABSTRACT

Intense particle beams may be subject to coupled-bunch instabilities that would grow at rates greater than the bunch oscillation frequencies. The suppression of this growth requires both reduction of the driving impedances and active feedback of bunch motions. The shunt impedances of higher-order cavity resonances can be reduced by passive dampers and the beam impedance within the band of the fundamental resonance can be reduced by rf feedback around the cavity and power amplifier. The feedback of bunch motions composed of numerous coupled-bunch modes requires broad-band systems for which the amplifiers are costly. Examples proposed for electron storage rings are presented.

I. INTRODUCTION AND GENERAL RELATIONS

In the intense stored electron beams of light sources and large e^+-e^- colliders, the strongest collective instabilities are expected to be the coupled-bunch (c.b.) motions. This is largely a response to the presence of strong rf systems needed to produce the many short intense bunches. Suppression of c.b. growth calls for both reduction of the normal resonant impedances of rf cavities and the provision of strong broadband feedback of longitudinal and transverse bunch motions.

The fact that the bunch length is usually much shorter than the wave length of the highest resonances below the beam tube cutoff frequency simplifies some relations. The effective driving voltages for the rigid-body motions, which grow most rapidly, are simply the voltages excited in high-Q resonators by the bunch motions. A longitudinal mode amplitude $\Delta\varphi_o$, measured at f_{rf}, provides a cavity exciting current of

$$\tilde{I} = j\, I_o\, \Delta\, \varphi_0\, f_{cb} / f_{rf} \qquad (1)$$

where f_{rf} is the frequency of the accelerating voltage, f_{cb} is a synchrotron-sideband frequency for the mode, and I_o is the average current. This current will excite voltage $V_\parallel = \tilde{I}\, R_\parallel$ in a resonator that has shunt impedance $R_\parallel$ at the frequency f_{cb}. Similarly for the transverse case we have

$$V_\perp = I_o\, k_{cb}\, x\, R_\perp \qquad (2)$$

where $V_\perp$ is the transverse voltage impulse from a resonator with transverse shunt impedance $R_\perp$ ($R_\perp = R_\parallel/(k_{cb}a)^2$, e.g. as given by URMEL) when excited by a c.b. mode with amplitude x. k_{cb} is the wave number $2\pi f_{cb}/c$.

From these driving excitations, we find the growth rate for a given c.b. mode:

$$1/\tau_\parallel = \frac{I_o\, f_o\, \eta}{2 f_s\, \beta^2\, E/e} \sum f_{cb}\, \mathcal{R}e\, R_\parallel$$

$$\text{or} \quad \frac{1}{\tau_\perp} = \frac{I_o\, f_o}{2\beta\, E/e} \sum \beta_\perp\, k_{cb}\, \mathcal{R}e\, R_\perp \qquad (3)$$

where the summation is of the real impedances of all resonators at all + and - frequencies of the c.b. mode.

To damp the mode, we must reduce $1/\tau$ to below the radiation damping rate by some combination of (1) reducing the shunt impedances, (2) tuning to avoid overlap of mode frequencies and resonator frequencies, or (3) active feedback to oppose $V_\parallel$ or $V_\perp$.

The strongest resonators in the storage ring are usually the higher order modes (HOM) of the accelerating cavities. Example spectra of longitudinal resonances for accelerating cavities are shown in Fig. 1. The frequencies of c.b. modes are separated by about one half the orbital frequency f_o, so that if the ring is of small radius they are spaced sufficiently apart that it may be practical to tune to avoid coincidences between c.b. modes and HOMs. For large colliders or synchrotron radiation sources this is not practical and one must reduce impedances of the HOMs or use active feedback, or both.

II. REDUCTION OF EXCITING IMPEDANCES

Considering the cost and complexity of components of a strong active feedback system, particularly the kickers and power amplifiers, the reduction of the shunt impedances of resonators is of great advantage. Moreover, it can be a necessity as a means of reducing the growth rates to the order of the bunch frequencies (f_s or f_β) to avoid great sophistication if not infeasibility in the feedback design.

With the assumption that resistive damping can be provided for the HOMs, it is the values of R/Q of those modes in the basic cavity shape that is of importance. For cavities made of normal-conducting (NC) metal, such as copper, economy of rf power calls for a large value of R for the fundamental, accelerating mode; then one seeks a favorable ratio

*This work was supported by the Director, Office of Energy Research, Office of High Energy Physics, Advanced Energy Projects Division, of the U. S. Dept. of Energy under Contract No. DE-AC03-76SF00098.

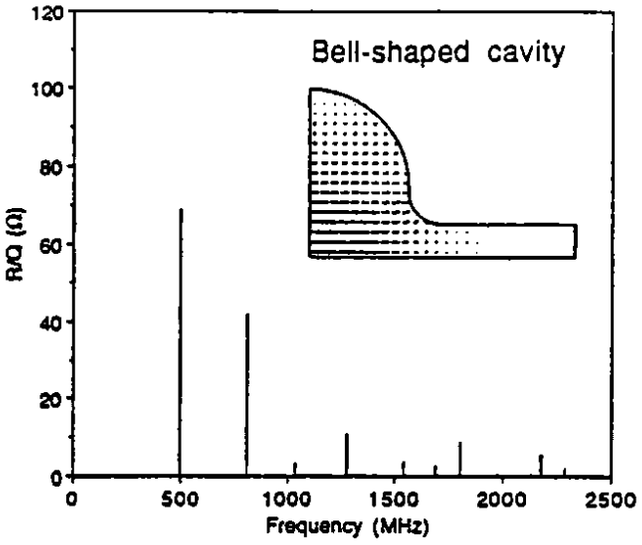

Fig. 1a.

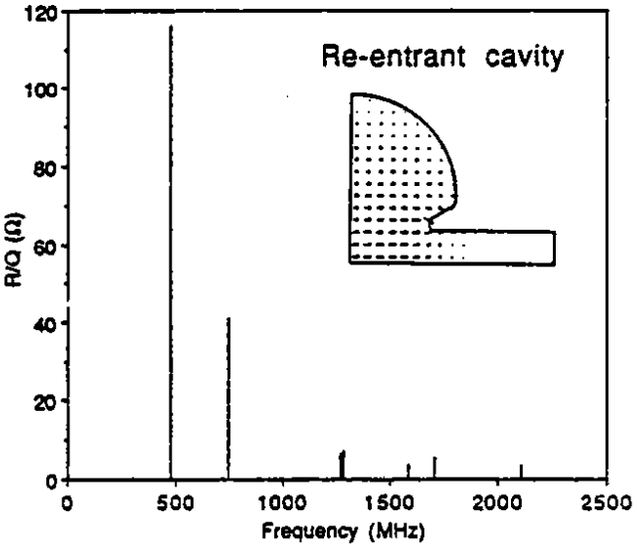

Fig. 1b.

Fig. 1 R/Q of resonances of two cavity shapes

of this to the R/Q's of HOMs. Fig. 1 compares the spectra of R/Q for cavities of closed or open configuration. We see that for the same bore diameter, as shown, the usual shape having nose cones is more favorable. This shape is chosen for the Advanced Light Source and the design of the SLAC/LBL/LLL B-Factory [1,2]. With larger bore, the number and strengths of the HOMs decrease but the power-efficiency of the cavity at the fundamental becomes uneconomically low. If the cavities are superconducting (SC), power cost is less important and the open shape is more suitable for other reasons. A large bore is the best choice for low R/Q of HOMs and best as a port for damping those modes. The value of R/Q may be as low as a few ohm. The open cavity is chosen for the design of a B-factory at Cornell [3].

A waveguide attached to the cavity can couple to the HOMs and carry power to a terminating load. For damping of all HOMs, the cutoff frequency of the waveguide should be between the fundamental and the lowest HOM. For calculating the performance of this method, Slater's analysis [4] has been used as adapted for e.m. field calculations by Kroll and Yu [5]. Fig. 2 shows a NC cavity with three attached waveguides. Computations for the first 4 modes yield Q-values in the range 12 to 64. This represents a reduction of > 1000 over the undamped shunt impedances [1] and brings the c.b. growth rates well within the range of feasible and affordable feedback systems. The loss of impedance at the fundamental is about 10%. This arrangement of dampers has been modeled on a test pillbox and Q-values of < 37 were measured [6] compared with 25 - 55 predicted. For the damping of SC cavities for a B-Factory [2], the scheme of Fig. 3 is proposed. The waveguide in this case is the enlarged bore tube with fluted walls leading to a resistive-surface load. Longitudinal Q-values of < 70 are calculated. With this damping and the relatively strong radiation-damping from a 120 meter radius, the need for active damping would be greatly reduced or zero.

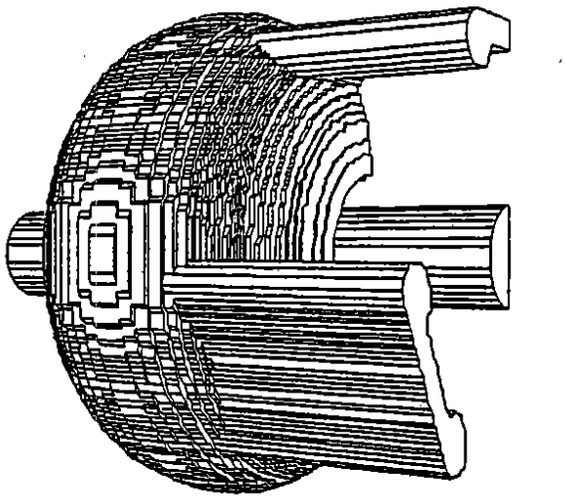

Fig. 2 One half of cavity with three damping waveguides

In a large ring with NC cavities, the low orbital frequency may bring the frequencies of longitudinal c.b. modes with low mode numbers within the response width of the fundamental cavity resonance. For the zeroth (phase oscillatron) mode this is always true and has commonly been stabilized by detuning the cavity so as to provide net (Robinson) damping by the shunt impedances at the mode frequencies $f_{rf} \pm f_s$. Other modes, at frequencies $f_{rf} \pm mf_o \pm f_s$, as shown in Fig. 4 are either damped or driven depending upon their positions on the rf resonance curve. Not only can this net driving impedance be greater than that from the typical HOM, but as part of the fundamental cavity resonance, it must not be resistively damped. However, the shunt impedance seen by the beam can

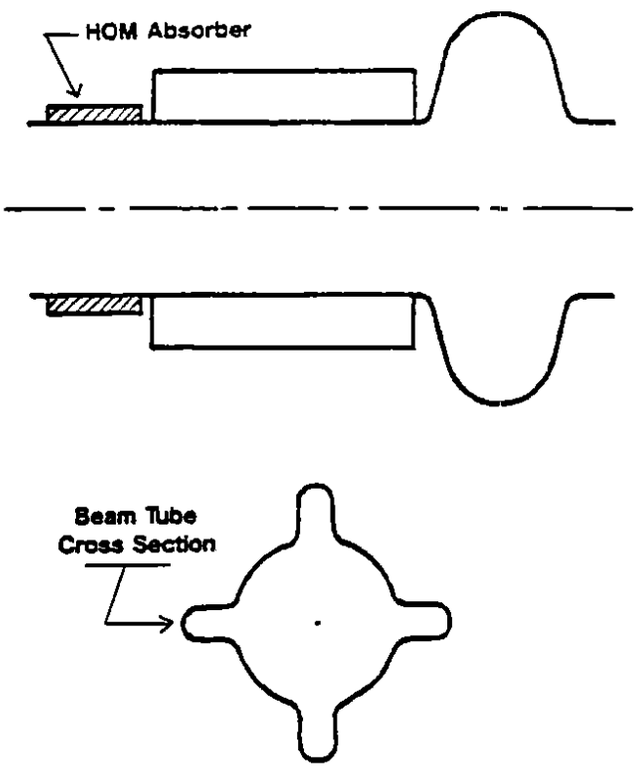

Fig. 3 Superconducting cavity with damping through beam tube

be reduced by active feedback of the rf around the cavity and power amplifier [7]. The degree of impedance reduction available from such a technique is limited by the unavoidable time delay of elements in the feedback loop, notably the power amplifier, which may amount to hundreds of nanoseconds. Feedback stability analysis of such a circuit for the B-Factory rf system has predicted a possible reduction of $R_{||}$ of a factor 10. A comb filter added in the rf loop allows greater loop gain at the harmonics of f_o; studies indicate that this scheme may further reduce the impedance, at least to the point where the net excitation is comparable to that of a damped HOM [8].

III. FEEDBACK OF COUPLED-BUNCH MOTION

Cancellation of the residual c.b. excitation after reduction of the driving impedances is done by active feedback that provides voltage kicks to cancel the resonator voltages $\tilde{I}R$. This view suggests the use of narrow-band feedback at the mode frequency, i.e. mode-to-voltage kick. But we note that stable and unstable mode frequencies arise closely spaced at the sides of harmonics of f_o and therefore narrow filters are needed to avoid positive feedback. Nevertheless, this mode-by-mode feedback has been the method of choice for those cases where only a few identifiable c.b. modes are growing. The narrow-band feedback in this case permits the use of efficient narrow bandwidth electronics and kickers and hence, minimum cost.

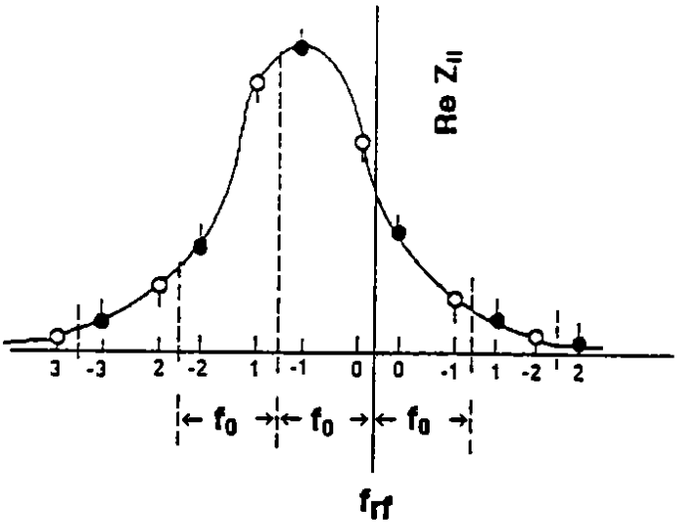

Fig. 4 Coupled-bunch modes within detuned resonance curve of fundamental

In the case of a large, high current ring, many modes may grow and the economics of a few narrow band channels is not available. A single HOM that has been broadened by damping can drive about 100 c.b. modes. The alternative to hundreds of circuits tuned to c.b. modes is the bunch-by-bunch system in which signals from individual bunch motions are kept separate in time and feed back to those same bunches after one or more turns delay. To address in this way M bunches circulating at rate f_o requires a bandwidth of at least $1/2\ Mf_o$. (Note that this same bandwidth would be required of the output stage of a mode-by-mode system that could feed back signals from a substantial fraction of the possible M modes.) It is the sensible and economic design of the single-bunch detection system, processing circuits, and output stages that is the challenge.

The gain that is required is straight forward to define for a given, expected shunt impedance R. One calculates the mode current $\tilde{I}$ for a given mode amplitude and provides a kick $V \geq \tilde{I}R$. And in the absence of noise, gain is no problem to provide. In contrast, the output kicker power is costly and depends upon the initial mode amplitude one needs to overcome. The kicker power is

$$P = V^2/2\ R_k = \tilde{I}^2 R^2/2\ R_k$$

where R_k is the combined shunt impedance of the kicker or array of kickers to be powered.

For perspective, we can estimate the power and its cost for some sample parameters. A typical single longitudinal kicker has $R_k \Delta f/f \approx 100$ ohm and for specific example parameters we may choose for a large ring with NC cavities:

$R_{||}$	=	20 kΩ for one HOM in 10 cavities at 2 kΩ each.
f_{cb}/f_{rf}	≈	2 at the HOM (~1000 MHz)
$\Delta\phi_o$	=	10 psec at 500 MHz = 0.03 radian c.b. amplitude
I_o	=	1 ampere average current
$\Delta f/f$	=	1/2 at ~f_{rf}

Then

$$\bar{I} = (1)(0.03)(2) = 0.06A$$

$$P = 1/2\ (0.06)^2\ (20{,}000)^2/200 = 3.6\ kW$$

At $150 per watt the power amplifier costs 0.5 M$. These numbers point out the importance of the initial amplitude that must be suppressed and the driving shunt impedance.

In operation, once the feedback has suppressed the c. b. motions, power demands should be very low. It is the oscillations of the injected beam and possible transients that are the most demanding. If the full ring current were injected in a time short compared to the c. b. damping rate with feedback, very large power could be demanded. Therefore it is worthwhile to damp beam as it is injected over many damping periods. Even then, a few bunches that have large excursions can readily call for large power from a broadband system. Here we note that perhaps only one tenth of the c. b. modes are unstable and hence not every frequency component in a few-bunch disturbance must be strongly damped. In the bunch-by-bunch scheme, tolerance for large local oscillations is provided by a design for controlled limiting of the output beyond a specified maximum. This non-linear behavior is most convincingly studied by numerical simulation; this has been carried out in the case of the B-Factory.

The components and parameters for longitudinal damping in the B-Factory at SLAC illustrate a bunch-by-bunch system. Transverse feedback is similar and usually less difficult and less costly.

Table 1 Parameters of B-Factory at SLAC

E	=	9.0 GeV electron energy
I_o	=	1.48 ampere average current
M	=	1746 (less 5% gap = 1658 bunches)
f_{rf}	=	476 MHz = 2x bunch rate
f_o	=	136 KHz orbital frequency
f_s	=	7 KHz synchrotron frequency
f_{cb}	=	750 MHz for strongest HOM (TM011)
$R_{\|\|}$	=	27 MΩ without dampers
	=	57 KΩ after damping to Q = 70
τ	=	18.5 msec from radiation damping
	=	0.04 msec growth time with full $R_{\|\|}$
	=	5.1 msec growth time with reduced $R_{\|\|}$
$\Delta\varphi$	=	0.44 radian error in 1/5 bunch injected at 60 Hz rate
$\Delta\varphi_o$	=	0.03 radian maximum amplitude of controllable c. b. osc.

The pickup electrode produces an 8-cycle burst at 2856 MHz from each passing bunch. This signal is the combined pulses from an array of 8 short pickups. A phase detector has been built that at this frequency can measure the phase of each bunch with ≤ 0.5 degree resolution at 476 MHz.[9] These signals are processed, delayed, and amplified by the power amplifier to drive the kicker structures.

Four kickers are used, each consisting of four drift tubes connected in series by half-wave delay lines. This provides a combined shunt impedance of $R_k = 4 \times 1600 = 6400$ ohm and a bandwidth of 200 MHz at 1.07 GHz. Installed kicker power is 2KW, 1.25 of which is nominally needed to provide kicks that are limited at 4 KV/turn. Although each injected charge is small, its error would, if response were linear, call for 12 KV per turn. The performance of the amplitude-limited feedback at injection as calculated by a simulation program [10] is shown in Fig. 5.

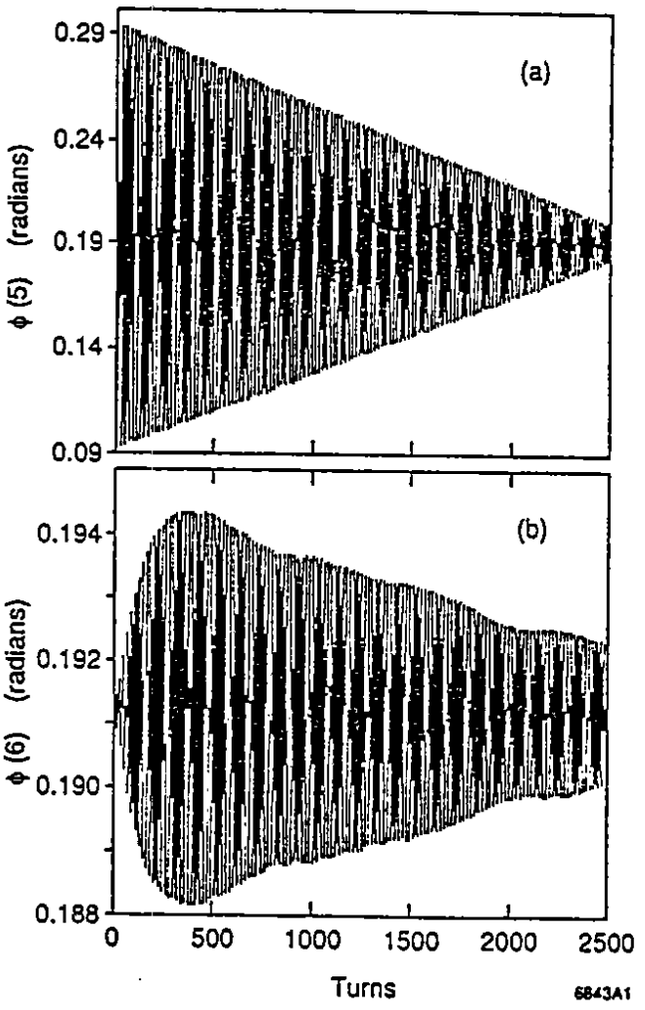

Fig. 5. Calculated phases of (a) a bunch injected with 0.1 radian effect and (b) the next following bunch (expanded scale) with damping by an amplitude-limited feedback

IV. SUMMARY

The damping of HOMS of accelerating cavities is necessary as part of systems to stabilize c. b. oscillations in new electron storage rings. Methods for this damping have been demonstrated in low-power cavities. Fast bunch-by-bunch feedback is possible and well suited for rings with many unstable c. b. modes. In that application it can damp disturbances from injection, noises, and beam-beam interactions as well as suppressing c. b. motion.

V. REFERENCES

[1] R. Rimmer, F. Voelker, G. Lambertson, M. Allen, J. Hodgeson, K. Ko, R. Pendleton, H. Schwarz, and N. Kroll, "An RF Cavity for the B-Factory," Proc. IEEE 1991 Particle Accel. Conf., San Francisco, May 1991, LBL-30624.

[2] "An Asymmetric B-Factory Based on PEP", Feb. 1991, LBL PUB-5303, SLAC-372, CALT-68-1715, UCRL--ID-106426, UC-IIRPA-91-01.

[3] "CESR-B, Conceptual Design for a B-Factory Based on CESR," Feb. 1991, CLNS 91-1050.

[4] J. C. Slater, Microwave Electronics, D. Van Nostrand Co, 1950, p. 84f.

[5] N. Kroll and D. Yu, "Computer Determination of the External Q and Resonant Frequency of Waveguide Loaded Cavities," SLAC-PUB-5171.

[6] F. Voelker, G. Lambertson, and R. Rimmer, "Higher Order Mode Damping in a Pill Box Cavity," Proc. IEEE 1991 Particle Accel. Conf., San Francisco, May 1991, LBL-30625.

[7] D. Boussard, "Control of Cavities with High Beam Loading," IEEE Trans. on Nuclear Science, NS-32, No. 5, October 1985, p. 1852.

[8] F. Voelker and G. Lambertson, "Calculations on RF Feedback Using a Simple Analytic Model," BECON-94, ABC-27, 1991.

[9] D. Briggs, P. Corredoura, J. D. Fox, A. Gioumousis, W. Hosseini, L. Klaisner, J.-L. Pellegrin, K. A. Thompson, and G. Lambertson, "Prompt Bunch by Bunch Synchrotron Oscillation Detection via Fast Phase Measurement," Proc. IEEE 1991 Particle Accel. Conf., San Francisco, May 1991.

[10] D. Briggs, J. D. Fox, W. Hosseini, L. Klaisner, P. Morton, J.-L. Pellegrin, K. A. Thompson, and G. Lambertson, "Computer Modeling of Bunch-by-Bunch Feedback for the SLAC B-Factory Design," Proc. IEEE 1991 Particle Accel. Conf., San Francisco, May 1991.

An RF Cavity for the B-Factory*

R. Rimmer, F. Voelker, G. Lambertson, LBL,#
M. Allen, J. Hodgeson, K. Ko, R. Pendleton, H. Schwarz, SLAC‡,
N. Kroll, UCSD†/SLAC

Abstract

The paper describes the proposed design for the 476 MHz accelerating cavity for the SLAC/LBL/LLNL B-Factory. This machine will require a high power throughput to the beam because of the large synchrotron radiation losses, and very low impedances for the higher order modes because of the high current proposed. Use of conventional construction in copper means that careful consideration has to be paid to the problem of cooling. The need for a high shunt impedance for the accelerating mode dictated the use of a re-entrant shape. This maximized the impedance of the fundamental mode with respect to the troublesome longitudinal and deflecting higher order modes, when compared to open or "bell shaped" designs. A specialized damping scheme was employed to reduce the higher order mode impedances while sacrificing as little of the fundamental mode power as possible. This was required to suppress the growth of coupled bunch beam instabilities and minimize the workload of the feedback system needed to control them. A window design capable of handling the high power was also required.

I. INTRODUCTION

The B-Factory RF system is required to meet the demands of a high luminosity, and therefore high current, while operating in a reliable manner befitting the "factory" philosophy of the project [1]. Choices of the parameters of the RF cavity are intended to be conservative and reasonable extrapolations from existing technology. The chosen frequency of 476MHz is a subharmonic of the SLAC linac frequency, to allow for stable injection. Commercial 1MW Klystron designs can be made to work at this frequency The very large beam currents, 1.48A in the High Energy Ring (HER) and 2.14A in the Low Energy Ring (LER), require up to 10MW and 5MW respectively to replace the energy lost to synchrotron radiation, cavity wall heating, and other effects. The need for short bunches (σ_l =1cm), requires a voltage of 18.5MV for the HER, 9.5MV for the LER. Unfortunately the number of cavities over which the power can be distributed must be kept to a minimum because, with such large currents, the impedances of higher order modes (HOMs) will cause very large longitudinal and transverse coupled-bunch instablility growth rates. Even so it is necessary to provide damping of these modes in the cavities and an active bunch-by-bunch feedback system in each ring to control this. Since most of the power goes into the beam, the saving in RF power from using superconducting cavities would not be large, and has to be weighed against the increased complexity associated with the cryogenic system. Also the technology for coupling such large drive and HOM power to and from a superconducting cavity is not yet mature. For these reasons and because expertise in the project team is primarily with room temperature structures, conventional copper construction was preferred. Single cell cavities of a re-entrant design were chosen to maximize the shunt impedance of the fundamental mode with respect to HOMs. It was decided to limit power to 500kW in each cavity (and window), of which up to 150kW is dissipated in the walls, yielding 20 cavities in the HER and 10 in the LER. This gives a gap voltage in the cavities of less than 1MV and an average field of about 4.3MV/m. The high wall dissipation requires careful attention to be paid to the cooling system, especially around structures such as the damping waveguides, which may have localized concentrations of current

* Work supported by the Director, Office of Energy Research, Office of High Energy Physics, Advanced Energy Projects Division of the U.S. Department of Energy.
# Lawrence Berkeley Lab.,DOE contract DE-AC03-76SF00098
‡ Stanford Linear Accelerator Center, DE-AC03-76SF00515
† U.C.San Diego, DOE contract DE-AC03-89ER80726

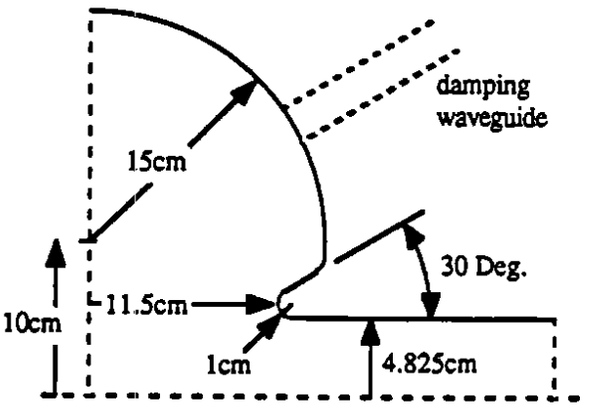

Fig.1: Basic B-Factory cavity shape

II. CHOICES FOR CAVITY PARAMETERS

Cavity designs and commercial 1MW CW klystrons are available at around 350MHz and 500MHz. PEP, LEP and APS use 350MHz, while Daresbury (SRS), KEK and ALS operate at 500MHz. A frequency in the higher region was chosen because less overvoltage is required in the cavity to achieve the short bunch length and more bunches can be circulated.

The type and shape of the cavities is determined by the need to maximize the fundamental mode shunt impedance with respect to HOMs. This is best achieved with a re-entrant or "nose-cone" shape. With conventional copper construction, an open or bell shape, as often used in superconducting cavities, does not work as well in this respect. The shape chosen (fig.1)

is similar to those used in the SRS, KEK and ALS, with a beam pipe internal radius of 4.825cm, (coming from the internal dimensions of a standard sized 10cm OD pipe used for the vacuum chamber in the RF straight). Analysis of the basic shape was done using the 2D URMEL code [2] Single cells were chosen to keep the number of HOMs to a minimum, in multi-cell structures the coupling between cells results in more modes.

URMEL calculates the transit time corrected shunt impedance R_s ($=V^2/2P$) for the basic shape to be about 5.3MΩ with a Q of 45,000 and R/Q of 116Ω. In a real cavity this impedance is degraded by the addition of ports and damping waveguides and by the effect of wall temperature on the conductivity of the copper. Experience with other designs suggests about 10% will be lost with the addition of the tuner, drive and other ports. Using MAFIA [3] and ARGUS [4] to study the 3D shape shows a loss of 10% or less in the fundamental mode R_s and Q when the damping waveguides are added (R/Q stays about the same). Based on extrapolation from existing cavities and thermal studies using ANSYS [5], loss of efficiency due to surface temperature rise may be as high as 14% with 150kW dissipated in the cavity. Thus a practical shunt impedance of 3.5MΩ with a Q of about 30,000 should be achievable, (table 1).

To get the required match at the nominal operating currents requires a coupling factor β of about 3.7. Loop and aperture couplers were considered, the loop has the advantage that the coupling factor can be adjusted by rotating it, but it must be well cooled because of the very high surface current densities. An aperture has the advantages of simplicity and lower surface currents but may need a larger opening in the cavity and requires a sliding short circuit in the waveguide to adjust the match which may be a problem because of limited space in the tunnel. A loop is favored because of the compactness and adjustability and because of the experience of the SLAC team with this type of coupler.

Either type of coupler requires the use of a vacuum window at some point. Existing designs using a ceramic window in the aperture or as part of the loop structure are not well suited to such high power levels. It was decided to locate the window well away from the harmful cavity standing wave fields, which may evanesce some distance into the waveguide, using a simple waveguide window. Designs are being developed commercially for 500kW CW operation. The location of the window in these designs requires that part of the waveguide be evacuated which may increase conditioning time. Anti-multipactor coatings will be applied to the windows and may be used on other surfaces if any problems are encountered with excessive multipactor during conditioning.

Active tuning of the cavities is proposed to be done by motorized plungers of the type used in PEP. These have carbon brushes to prevent HOM power from getting into the bellows. An interesting alternative is to distort the cavity slightly by external pressure to change its frequency. This has the advantage that no hole needs to be cut in the cavity wall. Both of these methods will be investigated in more detail.

Table 1: RF Parameters for the high and low energy rings.

Parameter	HER	LER
RF frequency (MHz)	476	
Beam current (A)	1.48	2.14
Number of cavities	20	10
Shunt Impedance R_s* (MΩ)	3.5	
Gap Voltage (MV)	0.93	0.94
Accelerating gradient (MV/m)	4.2	4.3
Wall loss/cavity (kW)	122	130
Coupling factor without beam (β)	3.7	3.8
Unloaded Q of cavity	30000	

* $R_s = V^2/2P$

The high beam currents have the potential for very high coupled-bunch instability growth rates, requiring special attention to be paid to the HOM impedances of the cavities. Existing damping techniques using externally applied tuned couplers have not proved effective enough to meet the B-Factory requirements, and reduce the growth rates to a level where an economically feasible feedback system could take control. For this application damping waveguides were included in the design of the cavity right from the start. These waveguides are designed to propagate at the HOM frequencies and are positioned to couple most strongly to the most troublesome modes while avoiding the field nulls of all the other modes (so that no modes, however innocuous, remain trapped). The waveguides are below cutoff at the fundamental mode frequency and result in only a small perturbation of the accelerating field. The effect of the size, shape and location of the damping waveguides has been studied experimentally on a simple pillbox cavity [6] and calculated using MAFIA and ARGUS, for the pillbox case and realistic B-Factory cavity shapes. Neither MAFIA nor ARGUS is currently capable of solving the complex eigenvalue problem created by lossy materials in the damping waveguides so the method of Kroll and Yu [7,8] was used to calculate the mode frequencies and Q's of the loaded structures. Three waveguides are used, spaced 120 degrees apart around the cavity azimuth so that all HOMs up to sextupole (m=3), and many higer orders, can be damped. This maintains symmetry, avoiding introducing low order (m=1,2) multipole components into the fundamental mode .

Experiments on the pillbox cavity showed that strong damping of HOMs can be achieved, and the measured Q's agreed well with those calculated by MAFIA/Kroll-Yu. Initially it was intended to get the Q's down to below 100 for the worst modes, on the pillbox this was achieved with only a 8% (calculated) loss in fundamental mode. Loaded Q for the longitudinal (m=0) TM011 mode was calculated to be between 15 and 35, measured to be 31. The dipole (m=1) TM110 mode was calculated to have a Q of 55, measured to be 37.

The first attempt to calculate the damping of the B-Factory cavity used a model having three rectangular waveguides with a cut-off frequency of about 600MHz. These waveguides were too broad to join directly to the cavity wall so an iris was used. Results for this geometry show strong

damping of the worst HOMs, with a Q of about 30 for the TM011 mode, with about 12% loss of the fundamental mode Q (table 2). It may be possible to reduce this degradation of the fundamental mode by smoothing out the sharp corners in the iris. In an attempt to dispense with the iris altogether a scheme was developed using smooth ridged waveguides which can be made small enough to open directly into the cavity. Using this scheme the Q of the TM011 mode is reduced to less than 26 (possibly as low as 12 - there is some uncertainty due to the limited number of data points used in the Kroll-Yu method), while the fundamental mode Q is lowered by only 7%. The ridged waveguides have a slightly larger area, which may account for the stronger damping, while the smoothing of the corners and the lack of iris could explain the reduced perturbation of the fundamental mode. Other HOMs are reduced to Q's in the range 30-50, except for the TM020 which was accidentally missed by the placement of the ridged waveguide. (When the waveguide shape was changed the effective center of the waveguide moved slightly, onto a null of the TM020 magnetic field).

Table 2: Damping of prototype cavity by waveguides.

	No Waveguides			Rect wg+iris		Ridged wg	
mode	freq (MHz)	Q_0	RT^2 (MΩ)	Freq (MHz)	Q_L	Freq (MHz)	Q_L
TM010	480	40003	4.71	475	35248	473	37344
TM011	750	33270	1.35	745	30	738	12- 26
TM020	993	38700	0.009 Trans.* (MΩ/m)	997	>1000	992	>5600
TE 111	685	54844	0.191	680	~65	678	30- 47
TM110	794	57762	18.3	795	~73	793	31- 64
TM111	1068	51836	33.2	1040	>50	1038	>49

* $R/k(r)^2$ (where r is the beam pipe radius=0.04825m)

Work is continuing on the optimization of the shape and position of the damping waveguides to get the lowest Q's for the most significant modes and to check all the higher order modes to make sure none are missed. Additional damping may be achieved by using higher order mode filters in the drive waveguide as there will be significant transmission through the power coupler for many HOMs. As a last resort any single mode which still has a significant impedance may be tackled by a tuned antenna inserted through a service port.

The high power dissipation and multiple apertures in the B-Factory cavity require careful attention to the problem of cooling. It is proposed to use a construction similar to that of the Daresbury and ALS cavities where the cooling water is channeled between two shells forming the inner and outer surfaces of the cavity. Particular care must be taken to ensure adequate cooling of the nose-cones and the damping waveguide apertures. The surface power dissipation is available from the numerical codes and this information can be transferred to a finite element program to perform thermal and, ultimately, stress analyses of the proposed designs. Early investigation suggested there might be strong local heating in the nose-cone region and around the rectangular waveguide iris. Current work is taking account of these results and the present design iteration is including a wider nose-cone angle (30 degrees) which allows easier access for the cooling water, and will feature a smoothed iris or rounded ridged waveguide.

Field enhancement on the small radius of the cavity nose-cone, as calculated by URMEL, leads to local surface electric fields about 5.9 times the average accelerating field in the cavity. At about 25MV/m this is comparable to the Kilpatrick number at this frequency, 20.9MV/m, so sparking should not be a problem after conditioning.

III. DEVELOPMENT PROGRAM

The current design effort is targeted on optimization of the RF performance of the cavity shape and the damping scheme, while keeping in mind the problems of cooling and mechanical construction. The first test of the design will be the construction of a low power test model to measure the effectiveness of the damping scheme and confirm the calculated mode spectrum. An automatic bead-puller is being constructed to allow detailed investigation of the HOM impedances. This model may also be used to test the RF control loops, using a low power amplifier instead of the klystron. At the same time programs will be under way to evaluate high power window and coupler designs, leading ultimately to their verification in a high power test stand at SLAC. Any lessons learned from the low power tests will be included in the next design iteration of the cavity which will concentrate on the engineering of a high power prototype.

IV. REFERENCES

[1] "An Asymmetric B-Factory based on PEP," Conceptual Design Report, LBL PUB-5303, SLAC 372

[2] U. Laustroer, U. van Rienen, T. Weiland, "URMEL and URMEL-T Userguide," DESY M-87-03, Feb 1987.

[3] "Reports at the 1986 Stanford Linac Conference., Stanford, USA, June 2-6 1986," DESY M-86-07, June 86

[4] A.Mondelli, eLal. "Application of the ARGUS Code to Accelerator Design Calculations," Proc. 1989 PAC, Chicago IL, March 20th-23rd, 1989.

[5] From Swanson Analysis Systems Inc., Johnson Road, P.O.Box 65, Houston, PA, 15342-0065.

[6] F. Voelker, G. Lambertson, R. Rimmer, "Higher Order Mode Damping in a Pill Box Cavity," Proc. 1991 PAC, San Francisco, May 6-9th. 1991. LBL-30625, BECON-92

[7] N. Kroll, D. Yu, "Computer Determination of the External Q and Resonant Frequency of Waveguide Loaded Cavities," SLAC-PUB-5171.

[8] N. Kroll, R. Rimmer, "Computer Determination of HOM Damping for a prototype JLC Accelerator Cavity and a prototype B-Factory Cavity," Proc. 1991 PAC, San Francisco, May 6th-9th. 1991.

BECON-92
LBL-30625

High Order Mode Damping in a Pill Box Cavity

F. Voelker, G. Lambertson and R. Rimmer
Lawrence Berkeley Laboratory,
University of California
Berkeley, CA 94720

April 1991

* Work supported by the Director, Office of Energy Research, Office of High Energy Physics, Advanced Energy Projects Division, of the U.S. Department of Energy under Contract No. DE-AC03-76SF00098.

HIGHER ORDER MODE DAMPING IN A PILL BOX CAVITY

F. Voelker, G. Lambertson, and R. Rimmer
Lawrence BerkeleyLaboratory
University of California
Berkeley, CA

ABSTRACT

We have substantially damped the higher order modes (HOM's) in a pill box cavity with attached beam pipe, while reducing the Q of the principal mode by less that 10%. This was accomplished by cutting slots in the cavity end wall at a radius at which the magnetic field of the lowest frequency HOM's is large. The slots couple energy from the cavity into waveguides which are below cut off for the principal mode, but which propagate energy at the HOM frequencies. Three slots 120 degrees apart couple HOM energy to three waveguides. We are concerned primarily with accelerating and deflecting modes: i.e. the TM_{mnp} modes of order m=0 and m=1. For the strongest damping, only three m=0 and m=1 modes were detectable. These were the principal TM_{010} mode, the TM_{011} longitudinal mode, and the TM_{110} deflecting mode. In addition the HOM Q's and the reduction of Q for the principal mode were determined by computer calculation. The principal mode Q for an actual rf cavity could not be measured because the bolted joints used in the construction of the cavity were not sufficiently good to support Q's above 6000. The measured Q of the first longitudinal mode was 31 and of the first transverse mode 37. Our maximum damping was limited by how well we could terminated the waveguides, and indeed, the computer calculations for the TM_{011} and TM_{110} modes give values in the range we measured.

I. INTRODUCTION

A large number of modes can be excited in an rf cavity by a bunched beam. Energy at frequencies below the cut off of the beam pipe will be trapped in the cavity, and interact with successive beam bunches. The voltage induced in the cavity at these higher order mode (HOM) frequencies is proportional to the shunt impedance of the mode. Shunt impedance is the product of a geometrical factor (R/Q) and the Q of the cavity; reducing the Q by damping the mode reduces the voltage excited at that frequency.

We are presenting a method to damp the HOM's without excessive damping of the principal mode. This has been demonstrated in a pill box cavity with three slots coupled to waveguides that carry HOM energy to terminating loads.

* Work supported by the Director, Office of Energy Research, Office of High Energy Physics, Advanced Energy Projects Division, U.S. Department of Energy. Contract DE-AC03-76SF00098.

HOM Damping

Imagine a typical rf cavity as a globe with the beam passing through the poles. The magnetic field of the principal mode at the wall is a maximum at the equator, and falls off toward a pole. On the other hand, most of the HOM's have zero H field at the equator, and the H field on the wall is a maximum at some distance away from the equator. The HOM's have broad maximums, and it is feasible to find a position where a slot couples strongly to most of them. The coupling is strongly dependent on the length of the slot, and less on height of the slot. A narrow aspect slot couples adequately, and it perturbs the fundamental mode less than a square aperture. Care must be taken not to place the slots on a zero of one of the HOM's.

The width of the waveguides is greater than the length of the slot, and was chosen to propagate the lowest troublesome HOM, but not the fundamental mode. The evanescent fields of the fundamental mode will reach a short distance into the waveguides, and the terminating loads must be far enough away in the guide to not damp the principal mode. The slots cause additional loss at the fundamental frequency because the wall currents are concentrated at the edges of the slots. Nevertheless, it is possible to have adequate coupling for the HOM's and still lower the fundamental Q less than 10 percent.

Experimental Setup

A pill box cavity with a 38.3 cm diameter and a 25 cm height was available from another mode damping experiment, and it was modified by adding 16.5 cm (inside diameter) beam pipes to each side. See figure 1. The beam pipes were terminated in 20.3 cm long crossed-wedges of 1 cm thick Eccosorb AN-73 material. Three 2.54 cm x 19 cm rectangular waveguides are attached to one end wall at a 14 cm radius and spaced at 120 degree intervals. The waveguides are coupled to the cavity through 2.54 cm x 15.24 cm rectangular slots, and are terminated by lossy elements at the far end. In an r.f. accelerator cavity the TM_{011} longitudinal mode is excited very strongly because it has a large R/Q. Because it is usually lower than the beam pipe cut-off frequency, it is trapped, and also has a high Q. We targeted our slot geometry to couple strongly to this mode, and the damping-waveguide cut-off frequency was chosen to be well below its frequency.

To sense beam coupling to the longitudinal modes, we need an antenna that couples to the E_z fields on the axis of the cavity. On the other hand, we don't want to perturb the fields on the axis with a metal coaxial line. Our solution

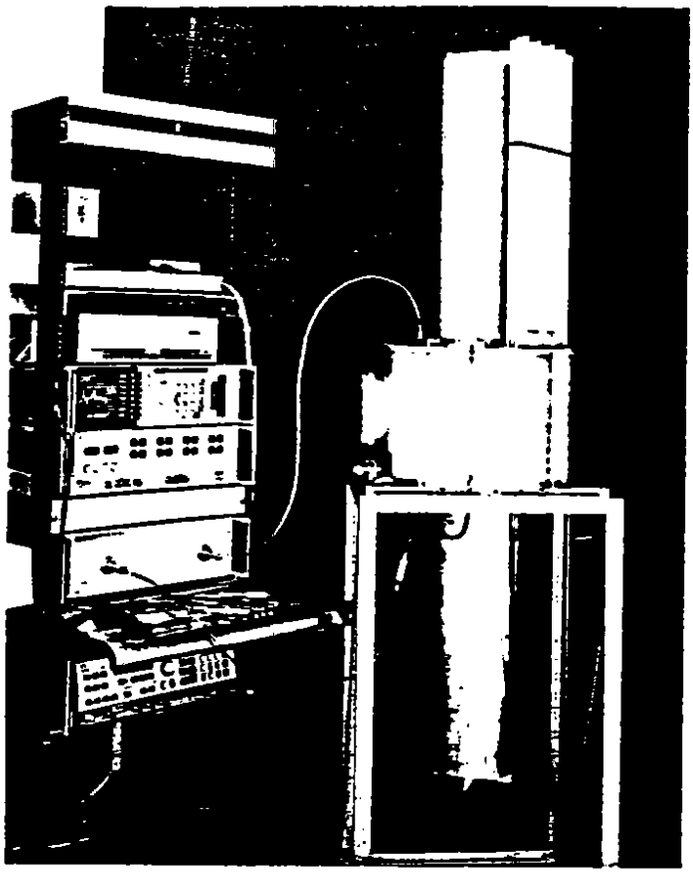

Fig. 1. Pillbox Cavity with One Damping Waveguide

was to use four 5 mm long electric-probes in the end walls as close to the beam pipe as mechanically feasible. These were spaced 90 degrees apart. Making them alike reduces coupling to modes with m=1, 2, or 3. The signals from these four probes are combined and become one port of the cavity. A similar electric-probe was placed on the opposite end wall and becomes the other port.

The probes are purposefully very short to simplify the Q measurements. The signals from the each pair of adjacent probes were combined in separate 180 degree hybrids. The sum signals from these hybrids are combined in another 180 degree hybrid, and for longitudinal modes the sum output is used as the port to the cavity. To measure transverse modes, i.e. m=1 modes, the difference signal is used as the cavity port. For both cases S_{21} was measured using an HP 8510B Network Analyzer. With the dampers in use, the signals for some modes were very weak, and the readings were enhanced by averaging 128 readings and smoothing the data slightly. We later lengthened the fifth probe to 9 mm to improve the signal-to-noise on some of the readings.

Measured Results

We started our measurements by covering the slots with metal tape to enable us to identify the basic cavity modes, and to allow us to determine the undamped Q's. Modes up to 2 GHz were identified by comparing with calculated frequencies from URMEL code. We also saw some quadrupole and sextupole modes, because the probes were not exactly symmetrical. These should not couple to the beam.

Our initial goal was to damp the HOM's sufficiently to reduce the Q's to less than 100. Our first waveguide terminations consisted of four 18 cm long wedges of Eccosorb material across the 2.54 cm dimension of each guide.

The damping greatly reduced the amplitude of most modes, and it was necessary to average the signals from the weakest signals to reduce the noise background. Even so, many modes disappeared into the noise background completely.

Waveguide Terminations

Preliminary measurements were made with a single waveguide, and a variable length slot. We observed that as the slot length was increased, the TM_{011} mode became smaller in amplitude to a point where it split into two frequencies. Further damping resulted in a greater separation in frequency, but no further reduction in Q.

For the final measurements using three slots, most of the HOM Q's were below 100, but the TM_{011} mode was split in two parts, one with a Q of 50.5 and the other a Q of 105. After some experimentation, we found that the mode splitting was caused by reflection from the waveguide termination. Reflections between the slot and the termination cause the waveguides to act like resonant cavities over-coupled to the main cavity.

The wedges were removed, and terminations made of Eccosorb NZ-51 (.5 cm x 3 cm x 6 cm) tiles inserted into the corner of each waveguide. The character of the split mode was observed as the number of tiles was increased. As tiles were added, the split mode coalesced and a final Q of 31 was reached. With these improvised terminations, the first tiles reached into the evanescent field of the principal mode and lowered its Q. However a longer waveguide with ferrite loading could be designed to give a sufficiently good match and without increasing the principal mode loss.

Calculated Values:

Using the MAFIA code together with a computational method developed by Kroll [1], the shunt impedance and Q of the pillbox cavity was calculated with three damping waveguides. Figure 2 shows the three dimensional model used to calculate these parameters. The cut-off frequency of the damping waveguides is 787 MHz, and the TM_{010} mode at 841 MHz is well damped. There is a TE_{111} mode in the cavity at 708 MHz that is not damped. We expected the symmetry of the probes to reject it, but it was quite visible as an undamped mode: For a typical accelerating rf cavity shape this mode occurs at higher frequency with respect to the fundamental, and it would also to be well damped even though we expect TE modes to couple only weakly to the beam.

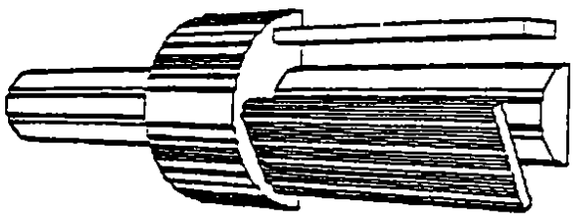

Fig. 2. Three Dimensional Model Used for MAFIA Calculations

The table below summarizes the results of both the calculations and the measurements. The frequencies of the damped modes were perturbed very little by the dampers, and there was no difficulty in identifying them.
Calculated Q values indicated that the principal mode was perturbed a minimal amount; the Q was reduced by only 8 percent. The first longitudinal mode (TM011) and the first transverse mode (TM111) were reduced to Q's of less than 40, and agreed closely with the calculated values. None of the other longitudinal or transverse modes were strong enough to see, but there was one quadrupole mode with a Q of 152. (We don't expect the beam to couple to quadrupole modes.)

	Calculated			Measured	
mode	freq	Q	ΔQ	freq	Q
TM010	611	33400	-8%	609.5	649*
TM011	840	15-35		836.2	31
TE111	708	39300	-7%	704.2	667*
TM110	907	56		898.8	37
TM111	1021	31		**	**
TE211	957	55		**	**
TM211	-	-	-	1366	152

* Waveguide load sees evanescent field.
** Not visible.

REFERENCES

[1] Conciauro, G. and P. Arcioni, 1990. "A New HOM-free Accelerating Resonator," in Proceedings of the 2nd European Particle Accelerator Conference, Nice., June 12-16, 1990.

[2] Arne F. Jacob, Glen R. Lambertson, Walter Barry, "Higher Order Mode Damping in an ALS Test Cavity," Proceedings of the 2nd European Particle Accelerator Conference, p 928-930, Nice, June 12-16, 1990.

COMPUTER DETERMINATION OF HOM DAMPING for a PROTOTYPE JLC ACCELERATOR CAVITY and a PROTOTYPE B FACTORY CAVITY*

Norman M. Kroll†
University of California,San Diego,
Department of Physics- 0319 La Jolla, CA 92093-0319
and
Stanford Linear Accelerator Center, Stanford University, Stanford, CA. 94309

Robert Rimmer#
Lawrence Berkeley Laboratory,
UCB, Berkeley, CA. 94720

Abstract

In this paper we describe the determination of the properties of the above referenced cavities with particular emphasis on the damping of the higher order modes (HOM). Because mode frequency spectra were determined for a large number of shorted waveguide lengths, rather complete analyses are possible. Phase frequency plots have proved to be an invaluable aid in sorting out overlapping resonances and separating cavity resonances from waveguide resonances. Algorithms for the determination of the parameters of several resonances simultaneously have been developed. Determinations of Q from multiresonance analyses are compared to those from single resonance analyses, and the changes are typically found to be small.

I. INTRODUCTION

The damping of higher order modes in accelerator cavities has been a subject of extensive study for many years. The primary technique employed has been to couple the energy out through wave guides to be terminated in matched loads. Computer programs such as MAFIA (as in this paper) have been extensively employed to assist in the design of such structures. To obtain values of the Q_{ext} and the shifted resonant frequencies due to the wave guide loading, it has been necessary to develop special analysis techniques to be applied to the results obtained from a program such as MAFIA. The methods of Kroll-Yu[1] (KY) and Kroll-Lin[2] (KL, or KYL when referring to them collectively) are examples of such techniques and will be employed for the two problems which we discuss in this paper. The thrust of KYL was aimed towards minimizing the number of computer runs needed. The two examples discussed here are, however, considerably more complex than those discussed in those papers, and the rather large number used here have permitted a more complete overall analysis of the mode spectrum. Also, since we are still acquiring experience with these methods, the larger "data sample" is very useful for providing validation.

A problem which we have experienced in applying KYL has been the separation of waveguide resonances from cavity resonances. One deals here with the spectrum of a lossless coupled cavity waveguide system, and any run at a particular waveguide length will produce a series of resonances, some cavity associated, some waveguide associated, and some, when the two occur at neighboring frequencies, strongly coupled. When the waveguide coupling is not too strong, these cases can be readily distinguished by inspection of field plots. Current interest, however, centers about the strongly coupled case where this method has not always been convincing. We have found phase-frequency plots to be of great assistance in sorting out this problem.

The phase of a given computer determined mode at a particular waveguide length is given by

$$\varphi = 2\pi L/\lambda_g$$

As the length is varied each mode traces out a section of a phase-frequency curve. As pointed out by KY each such section is displaced by a multiple of π from a single universal curve that applies to all of the modes. The designation "phase-frequency plot" is intended to refer to that single universal curve. An example is provided by Fig. 1. It is based on data reported by Higo et. al at the LINAC 90 conference[3]. We were provided with a list of the lowest seven modes arising from MAFIA runs at twelve different waveguide lengths. The quantity $n\pi$ was subtracted from the phase of the n'th mode at each length and the entire set of 84 points plotted. As is apparent from Fig. 1, the points do indeed trace out a smooth curve. The high density of points in the low frequency portion of the curve results from the high degree of overlap which results from the $n\pi$ shifts. The smallness of the scatter is an indication of the high quality of the computer output. The cavity resonances are associated with the steeper portions of the curve, and as we shall discuss later, the low frequency portion is indicative of overlapping resonances. The presence of these overlapping resonances has been the motivation for the development of multiresonance fitting procedures. Both single mode propagation and a unique symmetry relation between the fields in the two outputs has been assumed in the above discussion. These were assured by the boundary conditions applied in the MAFIA calculations.

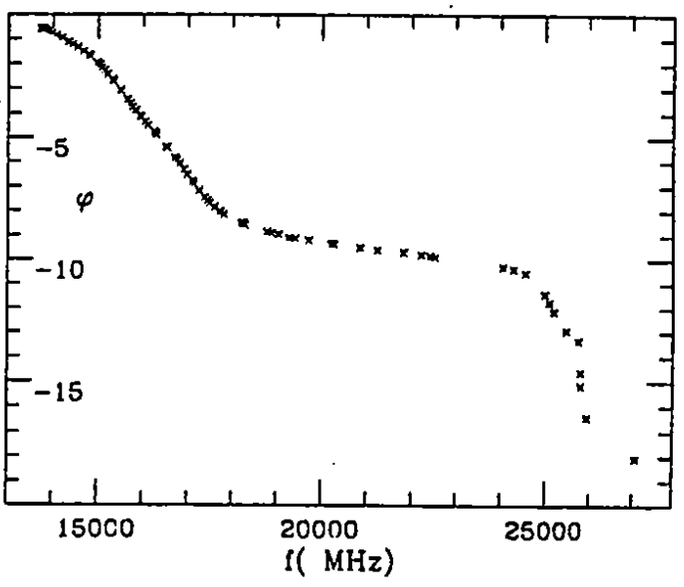

Fig. 1 Phase frequency plot for JLC prototype cavity.

2. THE JLC CAVITY

The KYL methods are based upon the following representation of the phase-frequency relation:

$$\varphi(\omega) = \sum_t \arctan\left(\frac{v_t}{\omega - u_t}\right) - \chi(\omega)$$

$$\chi(\omega) = \chi_0 + \omega\chi'$$

For each mode, u/2v is the Q value and u the resonant frequency. The branches of the arctangents are to be chosen so as to obtain a smooth curve. The function χ is intended to represent the effect of resonances not taken into account explicitly. If one ignores χ, it is apparent that as the frequency passes through a resonance the phase decreases by π. If all resonances occurring within a given

*Works supported by Department of Energy contracts AS03-89ER40527†, AC03-76SF00515†, and AC03-76SF00098#.

frequency interval are recognized and included explicitly in eq. (1), then χ may be presumed to be due to resonances outside the interval and therefore to vary by substantially less then π over the same interval. Thus we do not consider a "feature" in the phase-frequency plot to correspond to a resonance unless a phase change of π is involved, and strongly overlapping resonances produce phase changes which are multiples of π.

Applying these considerations to Fig. 1, we conclude that the region below 18000 MHz contains three overlapping resonances, the region 18000-24000 MHz is resonance free, and the region 24000-26000 MHz contains two resonances. The isolated point above 26000 suggests an additional resonance, but because of inadequate supporting information we ignore it in our analysis. We determined resonance parameters for the three low frequency and two high frequency parameters separately. To obtain parameters for the low frequency resonances we chose eight more or less evenly spaced data points between 15340 and 18236 MHz, and determined the six resonance parameters and two χ parameters so that the theoretical curve passed through the eight selected points. The results of this procedure are shown in Fig. 2. The resultant fit is seen to be excellent, and the theoretical curve fits the data accurately until the high frequency resonances are approached. Attempts to fit the data with only two resonances failed and showed clearly that the

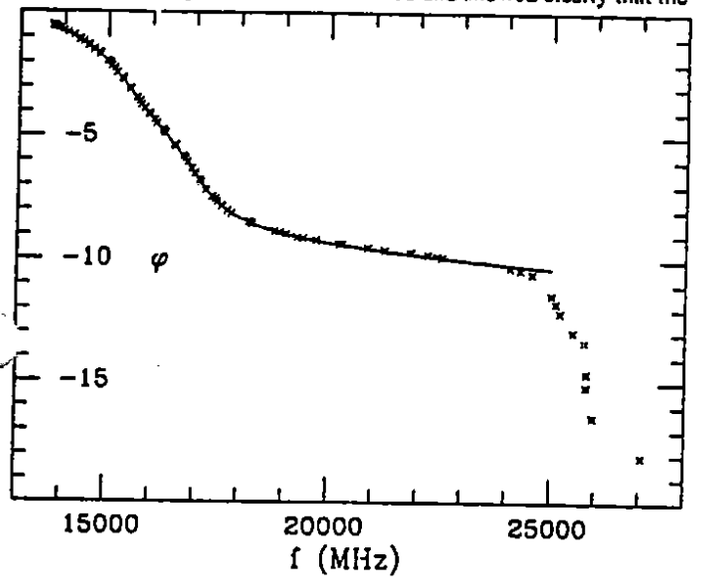

Fig. 2 Three resonance eight point fit for the low frequency resonances.

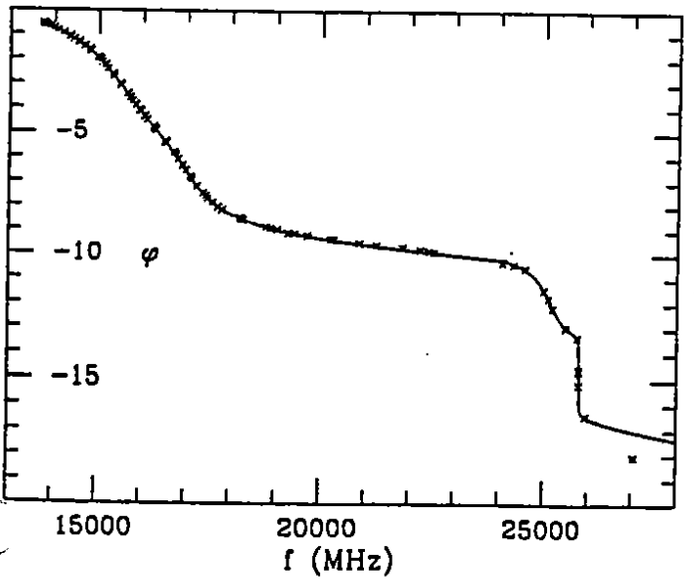

Fig. 3 Composite plot of the low frequency fit of Fig. 2 with a two resonance six point fit to the high frequency resonances. The break point is at 24100 MHz.

phase span in the resonance region combined with the slope of the resonance free region is inconsistent with the assumption that only two resonances are involved. For the high frequency resonances we selected six points in the range 25006 to 25956 MHz and determined four resonance parameters and two χ parameters so that the theoretical curve passed through the six selected points. A composite curve containing both fits is shown in Fig. 3. The break between the two representations occurs at ~ 24100 MHz where the two curves cross. Frequencies and Q values that yielded Fig. 3 are shown in Table I. The figures in parentheses are those obtained from single resonance four parameter fits carried out with data points selected from the neighborhood of the resonance as determined by visual inspection of Fig. 1. Mode 2 is not discernible in this way and attempts to find it with the four point method after its position had been determined were not successful. Nevertheless the results show that the four point method can give quite reliable results even in the presence of severe overlap. It appears that the free slope parameter does a quite effective job of taking account of the effect of omitted resonances on the Q values.

Table I. Frequencies and Q's for the JLC Cavity

Mode Number	Frequency (MHz)	Q
1	15375 (15552)	10.9 (12.0)
2	16077	7.1
3	17048 (16927)	14.8 (13.5)
4	25121 (25138)	43.1 (42.0)
5	25814 (25814)	~1000 (~1000)

We have not identified the modes because we have not seen the associated field plots. Fig. 1 of ref. 3 plus the symmetry imposed in the MAFIA calculations suggest TM_{110}-π for mode 1 and TE_{111}-0 for mode 2 or 3. We suspect that the other of these two modes is associated with the radial slot in the disk.

3. THE PROTOTYPE B FACTORY CAVITY

The cavity referred to in the heading above consists of a pill box with three waveguides mounted symmetrically on one end, emerging perpendicular to the end, and with the wide dimension perpendicular to the radius. In addition it includes a cylindrical section of smaller radius intended to represent the beam pipe, symmetrically disposed on the two ends and terminated with a short. A computer simulation of half the cavity is shown in Fig. 4. It is a *B* factory prototype only in the context of a study of higher order mode damping.

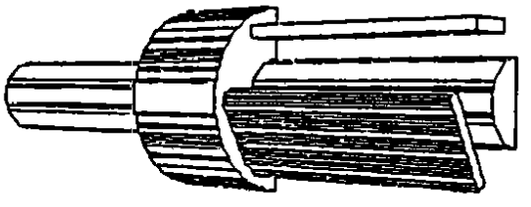

Fig. 4 MAFIA simulation of the prototype B factory cavity used for the MAFIA computations.

Because the cavity is symmetric under 120° rotation about the beam axis, its modes can be characterized by an $m=-1$, $m=0$, or $m=1$ symmetry index corresponding to the lowest fourier component in the azimuthal fourier expansion of the fields. The $m=+-1$ modes are degenerate, but because only half the cavity is modeled only a single linear combination of this pair appears. Thus we can analyze the $m=0$ and $m=1$ modes separately.

MAFIA calculations were carried out for 14 different lengths of waveguide, beginning with zero. The results of the calculation are summarized in Fig. 5. Connecting lines have been drawn which preserve the mode order of $m=1$ and $m=0$ modes separately. Identification was based upon the fact that fields at the end of the waveguide should be equal for the $m=0$ case and in the ratio -1 to 2 for the $m=1$ case (the -1 refers to the amplitude in the full width waveguide). Because the computer mesh does not accurately reflect

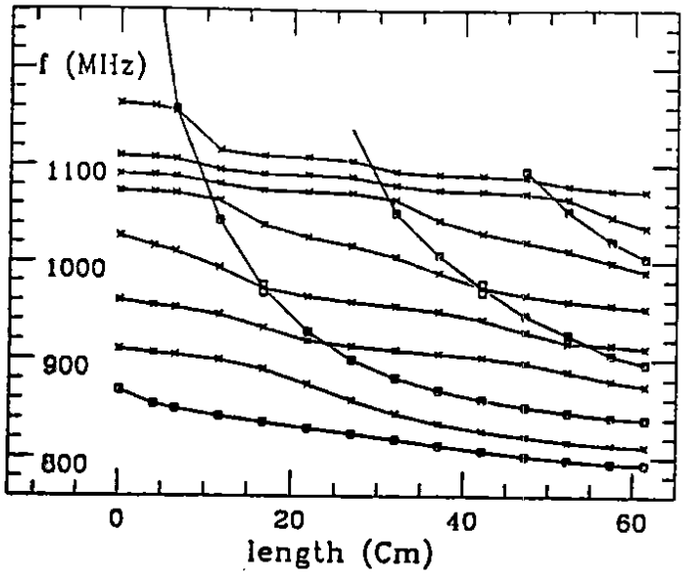

Fig. 5 MAFIA computed mode spectra of the Prototype B factory cavity shown as a function of the length of the shorted waveguides. Connecting lines join points belonging to the same symmetry class. m=0 square points. m=1 x points.

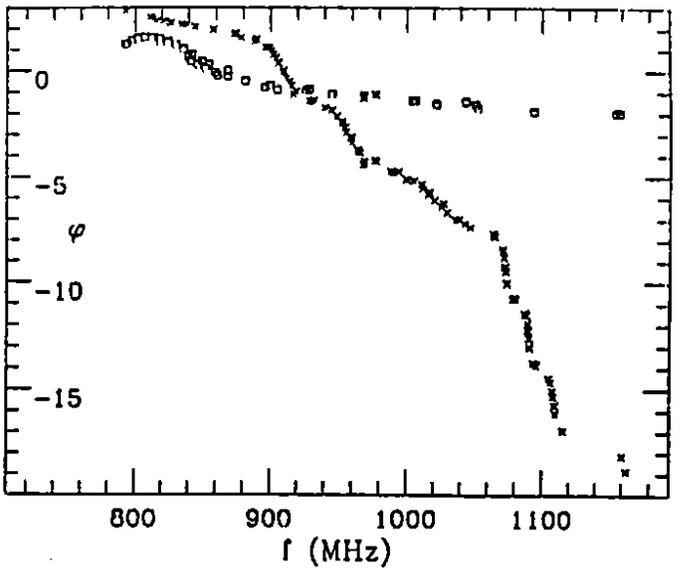

Fig. 6 Phase-frequency plot for the prototype B factory cavity. m=0 square points. m=1 x points. ambiguous (plotted twice) star points.

the symmetry of the physical structure, these relations are satisfied only approximately, and large deviation occurs at the crossing points. The $n\pi$ displacement procedure is applied to the $m=0$ and $m=1$ sequences separately, and the phase-frequency curves illustrated in Fig. 6 emerge. The squares mark $m=0$ and the x's $m=1$. The four "star" points are from the crossing regions and have ambiguous symmetry. Both points appear on each curve. These points were avoided in carrying out frequency-Q determinations. The figure also contains points from a calculation carried out at length 61.29cm with a magnetic boundary condition imposed at the waveguide ends. These fall on the universal curves if their phase is displaced by an extra $\pi/2$.

The $m=0$ curve exhibits a maximum at the low frequency end instead of the usual monotonic decrease. This is due to a mode trapping phenomenon which has plagued the application of waveguide damping. The mode involved here is the TM_{011}. It has a frequency of 868.36 MHz for the closed cavity, well above the waveguide cutoff of 786.86. As the waveguides emerge from the cavity end and lengthen, the frequency of the mode is pulled down and eventually falls below the guide cutoff frequency. When this happens the phase-frequency plot is guaranteed to exhibit a maximum as a function of frequency. (The reality of this phenomenon has been confirmed with an analytically solvable model.) The mode did not actually fall below cutoff at the largest length (61.29cm). However, the appearance of the maximum is considered to be the indication that it will eventually do so. Replacing the electric boundary condition with a magnetic one at the waveguide end has an effect similar to increasing the length, and such a calculation was performed to see whether it would exhibit an extra trapped mode. Indeed such a mode was found at 773.87 MHz, which we take to be a confirmation of the above. Apart from the trapped mode, the $m=0$ curve shows only one resonance, a detrapped and low Q counterpart of the trapped TM_{011} mode. The determination of the resonance parameters of this mode is degraded by the fact that the KY phase-frequency formula does not include the trapping phenomenon, so that the Q determination appears to be uncertain up to a factor two or so.

The $m=1$ phase-frequency curve is of the expected form and clearly shows the seven lowest waveguide damped $m=1$ modes. Four parameter single resonance fits have been carried out using both the KY and, where adequate data was available, the KL method. The phase-frequency plot identifies appropriate regions for the selection of data points for fitting and enables one to avoid the study of waveguide resonances. The two methods are found to be in excellent agreement except for the low Q TM_{011} mode. As mentioned before, we consider this to be due to the fact that the phase-frequency formula does not include the trapping phenomenon. These results are summarized in Table II. The waveguide loaded frequencies F_L for the trapped modes are taken directly from the MAFIA results.

Table II. Frequencies and Q's for the Prototype B Factory Cavity

Mode type	F_0 (MHz)	F_L(KY) (MHz)	F_L(KL) (MHz)	Q(KY)	Q(KL)
TM_{010}	617.17	610.94		trapped	
TE_{111}	711.61	708.00		trapped	
TM_{011}	868.36	<773.87		trapped	
TM_{011}		841-842	840-845	15-17	24-35
TM_{110}	909.58	906.7	906.7	55	56
TE_{210}	959.92	956.9	956.6	56	55
TM_{111}	1027.22	1021.3	1021.4	32	31
TM_{112}	1073.44	1073.0	1073.7	338	336
TM_{113}	1090.53	1090.0	1090.0	401	411
TM_{114}	1109.39	1108.6	1107.5	300	318
unknown (m=1)	1163.15	1162.0		333	

The TM_{11n} modes above 1070 MHz are associated with the sudden opening of the beam pipe to propagation in the TE_{11} waveguide mode (cutoff at 1064 MHz). The bulk of the stored energy as well as the extra nodes are in the beam pipe for all three. An experimental investigation of this cavity has been carried out by Voelker et al[4]. Absorbers were placed in the beam pipe so that agreement with computed Q's of the "beam pipe" modes is not expected. Otherwise reasonable agreement was obtained.

We thank T. Higo and M. Takao for providing as with the MAFIA generated data for the JLC cavity, and X-T. Lin for assistance with the graphics.

REFERENCES

1. N. Kroll and D. YU, Part. Acc. 34 p. 231 (1990)
2. N. Kroll and X. Lin, Proc. 1990 Linac Conf. Albuquerque, NM, June 10-14 (1990) p. 238
3. T. Higo, M. Takao, M. Suetake, K. Kubo, and K. Takata, Proc. 1990 Linac Conf. Albuquerque, NM, June 10-14 (1990) p. 147. We undertook the analysis of this cavity at the request of T. Higo.
4. F. Voelker, G. Lambertson, and R. Rimmer; IEEE Part. Acc. Conf., San Francisco, CA. May 6-9 (1991) Abs. IIRA22.

DAMPING OF HIGHER-ORDER MODES IN A THREEFOLD SYMMETRY ACCELERATING STRUCTURE

D. Yu*
DULY Consultants, Rancho Palos Verdes, CA 90732
N. Kroll†
University of California, San Diego and SLAC

Abstract

We investigate a waveguide-coupled damping structure with threefold symmetry using the 2-D and 3-D MAFIA codes. Within the frequency range considered, all higher order modes except the TM011 and TE111 modes are heavily damped. Possible ways to detrap these by using asymmetric waveguides offset with respect to the accelerating cavity in the direction of the beam are studied. External Qs and resonant frequencies are calculated using recently developed computer methods.

INTRODUCTION

Much work has been done since the first workshop on Future Linear Collider held in SLAC in 1988 on the design of damped accelerating structures using various waveguide loaded cavities. Accelerating structures in which higher order modes (HOM) are damped by coupling to waveguides via radial and circumferential slots have been proposed by R. Palmer[1]. We have studied several of these damped cavities with radial or circumferential couplers and have calculated, in each instance, the external Qs and resonant frequencies of the damped structure using a theory developed by Kroll and Yu[2], based on frequencies and phase shifts for shorted waveguides. A useful extension and variation of this theory has been recently developed[3] and is also used in our evaluation.

We begin by recapitulating some results for cavities with twofold-symmetry radial or circumferential slots which have been reported previously[4]. The calculated Q for the principal transverse mode of the radially slotted cavities is between 8.7 to 13.2, depending on the waveguide cutoff frequency. Results for the Q values using the Kroll-Yu method are highly accurate and convincing, and compare favorably with those obtained with other methods[5]. In addition, the Kroll-Yu method determines the resonance frequencies accurately. A problem with the radial slot cavity is the existence of a slot mode which persistently has a lower frequency than the accelerating mode. Because it has a different symmetry from the accelerating mode, however, it can be strongly coupled out by use of a double ridge waveguide[2] having a lower cutoff frequency than the fundamental mode, without significantly damping the latter.

An advantage of circumferentially coupled cavities is the absence of any slot modes. Not restricted by clearance considerations, use of smaller irises in these cavities also helps preserve accelerating field structure and depress HOM longitudinal coupling. A potential problem of these cavities is that the lowest transverse frequency is very near the waveguide cutoff. It is important to design the structure with extreme care in order to avoid trapped transverse modes. The possibility exists that a transverse mode is trapped even when its frequency, in the absence of damping waveguides, is above the waveguide cutoff. Ideally, the waveguide cutoff frequency should be far enough below the HOM to avoid trapping, and yet be sufficiently high above the fundamental, so that the accelerating mode is well preserved[5].

Recently, Arcioni and Conciauro[6] (AC) proposed a threefold symmetric, circumferentially coupled, waveguide loaded cavity. They showed that the shunt impedance and the Q of the accelerating mode are degraded by 20% and 12%, respectively, from those of a closed cavity, while most of the HOMs were effectively damped. In this research we applied our computer method to further analyze this S-band cavity. The resonance frequencies and external Qs of the HOM for this structure were calculated. Then we studied a similar X-band waveguide loaded accelerating structure with a threefold symmetry, and showed that in the frequency range considered, two HOMs (TM011 and TE111) remain trapped. Finally, we studied methods to detrap these modes.

3-FOLD SYMMETRY CAVITY

The AC cavity shown in Figure 1 has a radius (r) of 3.0 cm and a height of 3.5 cm. The cylindrical cavity is coupled to three square waveguides, 120° apart, each having a width of 3.5 cm. We calculated the frequencies of

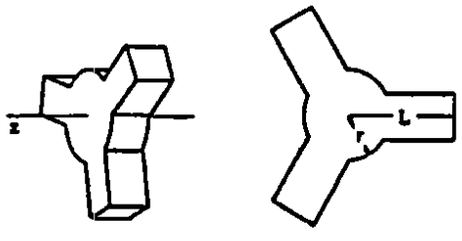

Fig. 1 A threefold symmetry cavity (ref. 6)

the TM and TE modes of this structure with URMEL-T for waveguide lengths (L) of 7.3, 7.9, 8.5, 9.1 and 18.0 cm. For ease of mode identification, only half of the structure was

modeled with reflection symmetry imposed on the half plane. A 32000-point mesh is used for the half model with the longest guide length. The number of mesh points for shorter guide lengths was reduced to maintain compatible mesh fineness. The beam pipe was not included in the 2-D model as its effect on the external Q was judged to be negligible. Table 1 lists the frequencies of the TM modes, with principal electric fields along the axis of the resonator, shorted at various guide lengths:

Table 1 Modal frequencies vs guide lengths for AC cavity

Mode	7.3 cm	7.9 cm	8.5 cm	9.1 cm	18.0 cm
TM010	3354.30	3360.94	3352.05	3356.40	3341.75
TM110	4637.98	4603.07	4556.38	4526.22	4335.70
TM020	5104.74	4989.96	4865.69	4785.28	4376.92
TM120	5699.26	5529.12	5374.89	5252.20	4553.26
TM030	6682.62	6367.92	6101.79	5883.56	4664.38
TM130	6955.29	6730.32	6498.38	6292.62	4893.36
TM210	7956.85	7683.32	7448.07	7255.65	
TM040	8371.52	7927.96	7545.96	7203.79	5101.62
TM140				8161.31	5340.50
TM050				8542.02	5640.47
TM150					5865.92

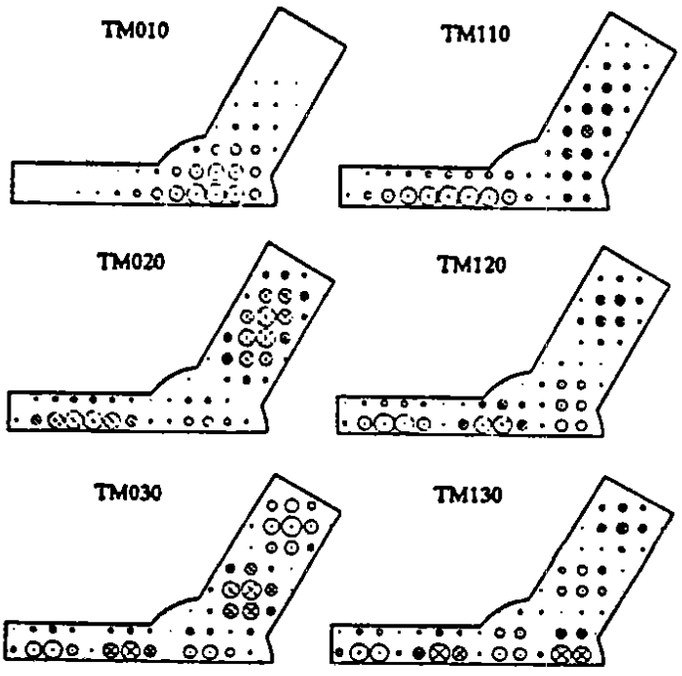

Fig. 2 Electric field plots from URMELT-T

A typical set of axial electric field plots is shown in Figure 2 for the L=9.1 cm case. The phase shifts, defined as:

$$\varphi = \frac{L_g}{c}\sqrt{\omega^2-\omega_c^2} + m\pi$$

are plotted in Figure 3 for both the monopole (TM0n) and dipole (TM1n) modes as a function of frequency. In the above expression, ω is the angular frequency for a given mode, ω_c is the waveguide cutoff, L_g is equal to L-r, and c is the speed of light. The integer m depends upon the branch on which the mode appears. When properly chosen all the points for a specific symmetry fall on a single curve. This is illustrated in Figure 3, which includes all data from four guide lengths (excluding the longest length). The phase shifts for the monopole modes (represented by data points on the upper curve) undergo a change less than π in the frequency range considered. The data were fitted to a single-resonance 4-point formula[2] with a frequency of 9309 MHz and a Q of 2.3. The data for the dipole modes (lower curve) clearly show that there are two resonances in the same frequency range. The phase shifts in this frequency range undergo a change of 2π. The lower curve on Figure 3 is a theoretical fit obtained with a two-resonance formula[2] for the phase shifts:

$$\varphi(\omega) = \tan^{-1}\left(\frac{v_1}{\omega-u_1}\right)+\tan^{-1}\left(\frac{v_2}{\omega-u_2}\right)-\chi(\omega)+m\pi$$

$$\chi(\omega) = \chi_0 + \chi_1\omega$$

The resonance frequencies of 4459 MHz and 7350 Mhz, and their corresponding Q of 2.7 and 6.3 were obtained from the six parameters u_1, u_2, v_1, v_2, χ_0 and χ_1 fitted to the data. A high degree of consistency for these results is evident by selecting data points from different crossed branches. We also used the data points from a *single* run with the longest guide length to calculate the dipole resonance frequency and Q. We obtained, using the four-point formula of reference 2, a resonance at 4311 MHz with Q=2.6, or 4385 MHz with Q=2.9, depending on the selection of the four points. These were consistent with the results for the lower resonance obtained from Figure 3 using data from four different runs. Data for the monopole modes using only the longest guide length were insufficient to yield a four-point solution. The extremely low Q values for the single monopole and two dipole resonances lead us to conclude that principal TM mode resonances in the AC cavity are indeed highly damped.

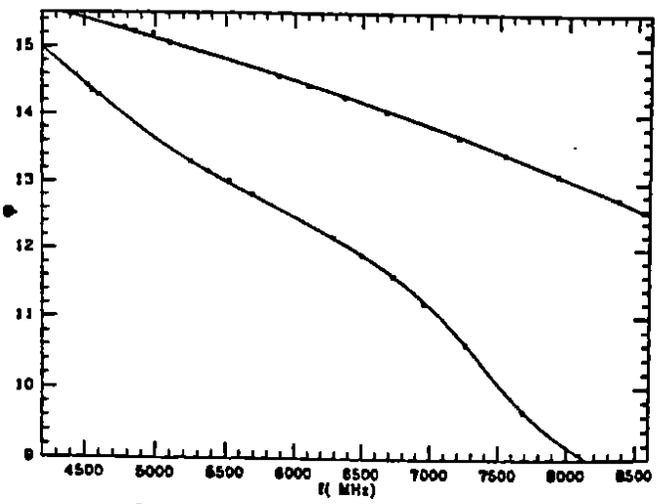

Fig. 3 Phase shift vs frequency Plot

TRAPPED MODES AND DETRAPPING

A review of the AC cavity URMEL-T plots of the electric fields in the plane perpendicular to the axis of the resonator shows that there are two possible trapped modes. These are shown in Figure 4, identified as (a) a TE111 mode, and (b) a TM011 mode in the cavity. To assess possible impact of these trapped modes on the accelerating cavity, we considered a π-mode, X-band accelerating structure with a threefold waveguide symmetry, similar to the AC cavity, using 3-D MAFIA models with up to 460000 mesh points. The 3-D models included long waveguide lengths (up to five times the cavity radius) and a finite cavity and waveguide height ($\approx\lambda$, where λ is the fundamental wavelength). The waveguide width was chosen so that the cutoff frequency is above the fundamental and below the HOM. The MAFIA models confirm that the TE111 and TM011 modes are in fact trapped in the cavity. The TE111 mode may not require damping because its impedance arises only from the probably very small TM contamination. On the other hand, damping is required for the TM011 mode. In order to minimize emittance growth of electron bunches over a very long distance, as in a linear collider, it was desirable to eliminate as much strayed

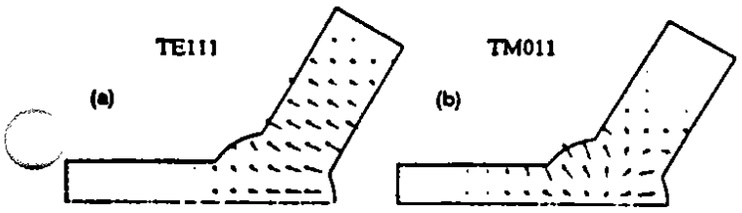

Fig. 4 Trapped modes in the AC cavity

fields in the structure as possible. We therefore considered methods to detrap the TE111 and TM011 modes. In a first unsuccessful attempt we tried to shift each of the three waveguides by a small offset (about 1/10 of the cavity height) with respect to the cavity along the beam direction. This proved insufficient to detrap the modes. In a second attempt, we tried to break the symmetry of the waveguide with respect to the cavity by reducing half of its height. This detrapped the TM011 mode (though not the TE111 mode), but it also distorted the accelerating mode[7]. In a third attempt we increased the waveguide height by 50% in an unsymmetrical way with respect to the cavity. The results of this calculation are shown in Figures 5a and 5b, showing two views of the detrapped TE111 and the TM011 mode, respectively. By making two MAFIA runs at different guide lengths, we were able to use the derivative method[3] to calculate the loaded Q. The TE111 mode is effectively detrapped with a Q of 10.9. The Q of the TM011 mode is substantially reduced, but still over 100. Oversized waveguides preclude installation on adjoining cavities. But damping waveguides may not be needed in every cavity if they are used in combination with other methods[8] of wakefield suppression.

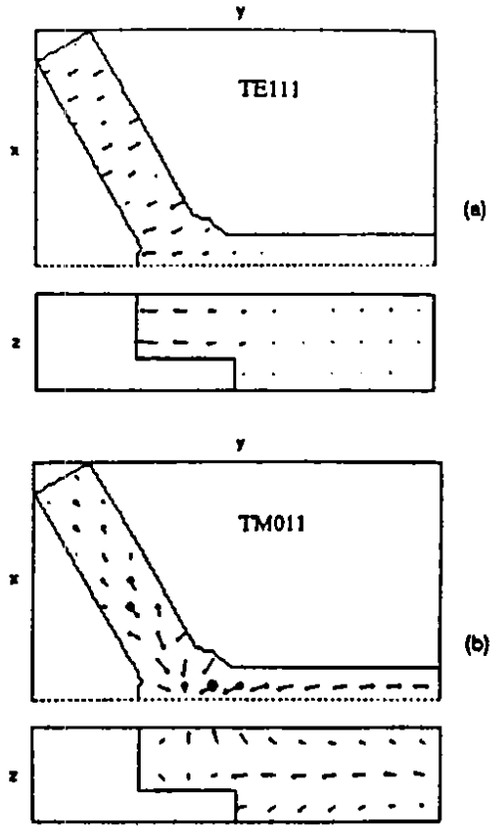

Fig. 5 Detrapped TE111 and TM011 modes

CONCLUSIONS

The problems of trapped modes which have persisted in previous damped structure designs have been partially solved with a threefold symmetry. Some progress has been made in detrapping the newly found trapped TM011 and TE111 modes unique to this geometry.

*Supported by DOE SBIR Grant No. DE-FG03-90ER81080.
†Supported by DOE Contracts DE-AC03-89ER40527 and DE-AC03-76SF00815.

[1] R.B. Palmer, High Energy Physics in the 90's, Snowmass Conference Proceedings, p. 638 (1989).
[2] N. Kroll and D. Yu, Particle Accelerators, 34, 231 (1990).
[3] N. Kroll and X.T. Lin, Proc. 1990 Linac Conf., Albuquerque, NM, June 10-14 (1990) p. 238.
[4] D. Yu and Kroll, poster paper in Linear Accelerator Codes Conf., Los Alamos, NM, January 22-25 (1990); H. Deruyter, et al., Proc. 1990 Linac Conf., Albuquerque, NM, June 10-14 (1990) p. 132.
[5] Y. Goren and D. Yu, Proc. 1989 IEEE Part. Acce. Conf., Chicago, IL, March 20-23 (1989) p. 189.
[6] G. Conciauro and P. Arcioni, European Particle Accelerator Conference, Nice, France (1990).
[7] K. Ko has provided us with ARGUS computations for a similar model considered for this case, with an asymmetric step which reduces the waveguide height by 38%. Using the derivative method of reference 3, we calculate a Q of 74 for the TM011 mode. The TM110 continues to exhibit extremely low Q's.
[8] D. Yu and J.S. Kim, "Wakefield Suppression Using Beatwave Cavities", this conference.

SLAC-PUB-5525
LBL-30604
May 1991
(A/I)

Prompt Bunch by Bunch Synchrotron Oscillation Detection via a Fast Phase Measurement*

D. Briggs, P. Corredoura, J. D. Fox, A. Gioumousis
W. Hosseini, L. Klaisner, J.-L. Pellegrin, K. A. Thompson
Stanford Linear Accelerator Center, Stanford University, Stanford, CA 94309 USA
and
G. Lambertson
Lawrence Berkeley Laboratory, University of California, Berkeley, CA 94720 USA

Abstract: An electronic system is presented which detects synchrotron oscillations of individual bunches with 4 ns separation. The system design and performance are motivated by the requirements of the proposed B Factory facility at SLAC.

Laboratory results are presented which show that the prototype is capable of measuring individual bunch phases with better than 0.5 degree resolution at the 476 MHz RF frequency.

Introduction

Many accelerator facilities have incorporated feedback systems to suppress the growth of coupled-bunch oscillations [1-5] . The proposed SLAC-LBL-LLNL B Factory design presents several challenges in the design of transverse and longitudinal feedback systems. To achieve a design luminosity of 3*10**33, the B Factory will contain 1658 bunches per ring (total current 1.5 A for the high energy ring, 2.1 A for the low energy ring), spaced every other RF bucket at the 476 MHz RF frequency. This large number of bunches, plus the short (4.2 ns) inter-bunch period, forces difficult constraints on the detection, processing and energy correction stages of the feedback system. Our proposed feedback design uses a bunch by bunch (time domain) strategy that treats each bunch as an independent oscillator . [6-11] This approach has the additional advantage that it damps not only coupled bunch oscillations, but any disturbance, such as injection timing errors, that may induce energy oscillations.

Principle of Operation

Figure 1 presents a system constructed to test and evaluate various signal detection schemes for the longitudinal feedback system. In this laboratory prototype we have implemented a two bunch system with a time structure similar to the planned accelerator. The master oscillator of this model uses a 102 MHz oscillator that is harmonically multiplied by a factor of 28 to generate a phase synchronous 2856 MHz reference. The 102 MHz oscillator provides the excitation for two step recovery diodes which generate 60 ps FWHM impulses to simulate beam bunches. Two analog phase shifters are used to adjust the spacing of the bunches relative to the 102 MHz master oscillator, and these phase shifters allow simulated synchrotron oscillations to be impressed on the 60 ps impulses. We space

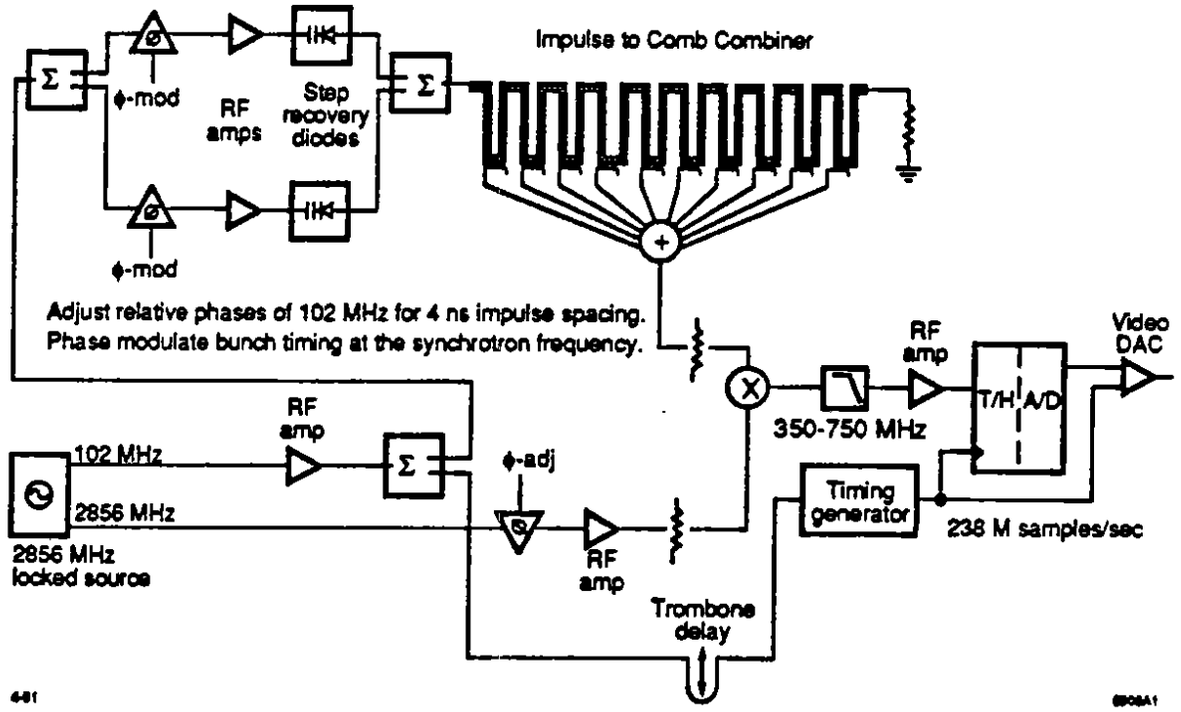

Figure 1. Block diagram of the prototype front end circuitry. This system converts a beam signal impulse into a 2856 MHz 8-cycle tone burst, and compares the phase of the burst against a reference oscillator. A 250 MHz A/D digitizes the phase each bunch crossing. The proposed B Factory design has 1658 bunches with a 4.2 ns bunch interval. The laboratory prototype uses 2 step recovery diodes and phase shifters to simulate bunches with independent synchrotron oscillations.

* Work supported by Department of Energy contract DE-AC03-76SF00515.

Contributed to the IEEE Particle Accelerator Conference, San Francisco, CA, May 6-9, 1991

the nominal positions of the bunches with a 4.2 ns interval which corresponds to the B Factory ring design, however in our test there is an extra 2 ns gap following the second bunch, after which the sequence repeats. With this system we can simulate independent synchrotron oscillations of the two bunches at frequencies up to 100 kHz, and study the performance of the detection system.

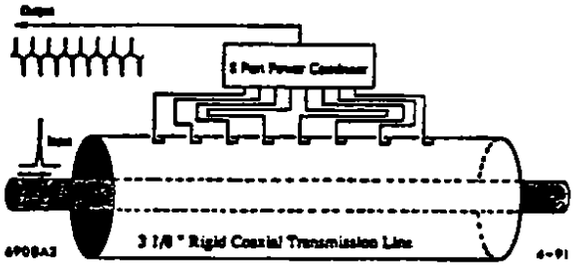

Figure 2. The eight quarter wave couplers are aligned 10 cm apart along the transmission line. Their outputs are connected to the power combiner with semi-rigid cables of equal length.

Figure 1 also shows the detection circuitry. A periodic coupler is used to generate a short eight cycle tone burst from each bunch. The phase of each burst is compared against the 2856 MHz reference oscillator in the double balanced mixer. The output of the phase detector is filtered with a 750 MHz low pass filter to remove the second harmonic and to limit the bandwidth for noise reduction. A fast analog to digital converter (with an internal track and hold) digitizes the phase error signal at a 238 MHz rate [12]. This process provides a unique error signal for each bunch crossing. In a complete feedback system this digital data stream would undergo further digital processing, but in our laboratory model we reconstruct the digitized values with a fast digital to analog converter which allows us to use traditional lab instruments to study the system performance [13]. A digital timing system, constructed with 100 K ECL logic, is clocked by the 102 MHz master oscillator and provides the timing for the A/D and D/A stages. This system allows us to measure the resolution, noise, and inter-bunch isolation of the bunch phase measurements.

Results

The beam pick-up generates a short (less than 4 ns) tone burst at the 2856 MHz frequency. We use a periodic coupler, rather than a tuned resonant structure, to avoid coupling between adjacent bunches. We have studied two possible configurations. We have constructed a comb generator in a coaxial geometry, using an array of quarter wave couplers aligned 10 cm apart along a coaxial transmission line. All the coupler outputs are then combined coherently in a power combiner as shown in Fig. 2. As an alternative, we have also fabricated and measured a structure constructed of periodically coupled stripline circuits. This latter approach minimizes the number of RF connections, and in the case of a beam coupled structure, would also minimize the number of vacuum feedthroughs.

The measured response of the coaxial generator is shown in Fig. 4. We see the signature of the time of arrival of each bunch as an eight cycle tone burst. There is a small amount of residual ringing (approximately 5-10%) evident in the time domain measurements. In comparison, the stripline fabricated generator produced fewer reflections, but due to its larger design coupling value and skin effect losses displayed less amplitude uniformity during the output burst.

Lab Measurements of Combined System

This periodic coupler output has been used to study the performance of the electronic system. Fig. 4 presents the analog output signal of the mixer for the two bunch system; also shown in the figure is the reconstructed analog output of the D/A converter. We can see that the bunch spacing alternates between 4 and 6 ns, as produced by our beam simulator. The response shows the bandwidth required for independent measurements on bunches with the 4.2 ns spacing.

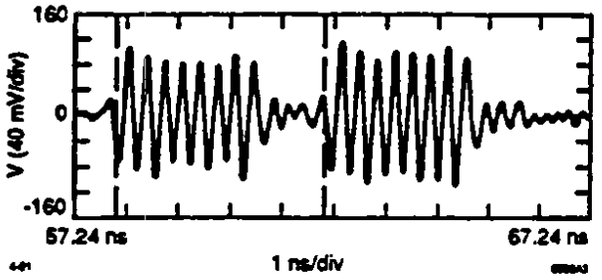

Figure 3. Measured response of the coaxial comb generator for two simulated beam signals with 4 ns bunch spacing.

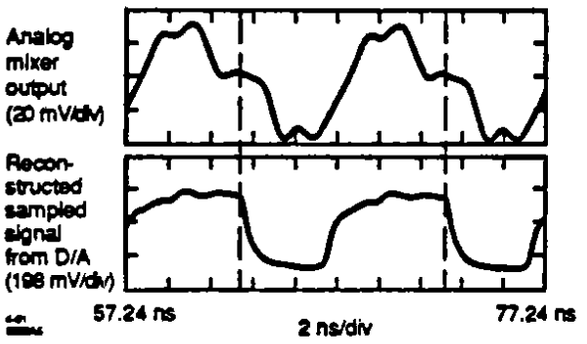

Figure 4. Measured response of the mixer (phase detector) for two bunches nearly 180 degrees apart. Also shown is the digitized phase signal after reconstruction in the D/A.

Figure 5 shows the system response for six independent DC phase offsets of the bunches. The top traces show the analog mixer response for 3 distinct DC phases of bunch A, with bunch B left undisturbed. Similarly, the lower pair of traces show three DC phases of bunch B, with bunch A left undisturbed. Again, the lowest traces are the reconstructed D/A output showing excellent isolation of the bunches.

Figure 6 is an oscilloscope photograph which shows the AC response of the system. In these measurements a 10 KHz AC sine wave is impressed on the control signal of the step recovery diode of a selected bunch. The AC modulation exactly simulates a synchrotron oscillation. In the figure bunch A is modulated with an amplitude corresponding to 0.7 degrees p/p (+/-0.006 radians) at the 476 MHz ring RF frequency. We note the prompt in-phase detection of this oscillation, which corresponds to a +/- 2ps time displacement of the bunch. The rms noise floor in this measurement is found to be better than 0.1 degrees at the 476 MHz RF frequency within the 10 kHz oscillation bandwidth.

The bunch to bunch coupling in our system is measured using a variant of the technique used in Fig. 6. By driving bunch A with a large oscillation, and detecting the bunch B output signal at the modulation frequency we can measure the coupling from A to B.

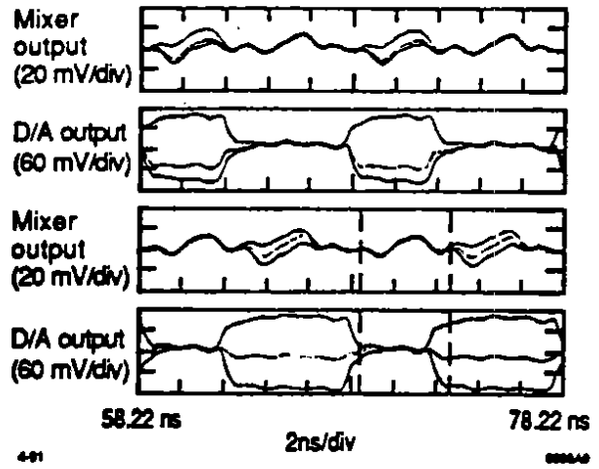

Figure 5. The upper trace shows the analog output signal of the phase detector (mixer) for three phase offsets of Bunch "A", while the next trace shows the digitized and reconstructed waveform of the upper trace. The lower traces are the same measurement of three phase offsets of bunch "B" with bunch "A" undisturbed.

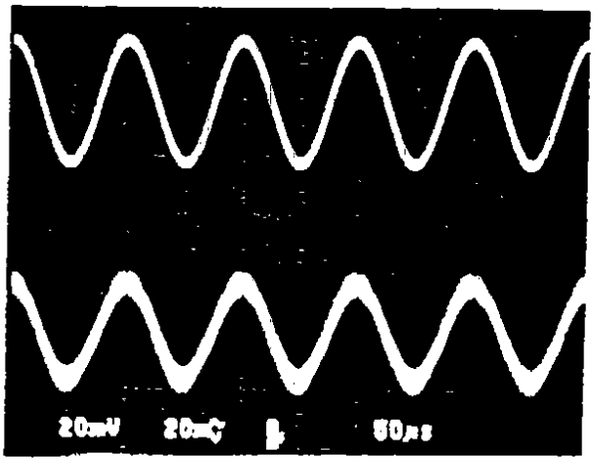

Figure 6. The upper trace shows the signal applied to a step recovery diode phase shifter, and represents a synchrotron oscillation amplitude of 0.7 degrees (+/- 0.006 radians) at the 476 MHz RF frequency. The lower trace shows the reconstructed D/A output.

Table 1 presents a summary of the measured performance of our various system components for the configuration of Fig. 1. We see that the performance of the two comb generators is similar. We also note that the coupling between the bunches for the A to B and B to A cases is very similar, notwithstanding the extra 2 ns present for the B to A case. The noise performance of the system is consistent with the eight bit quantization of the digitizer, and suggest that a system using this technique could easily achieve measurement resolutions of better than 0.5 degrees at the 476 MHz RF frequency.

Summary and Conclusions

We have demonstrated a signal processing system designed to detect longitudinal oscillations of stored bunches in a B Factory like storage ring. Our prototype system has been shown to be capable of measuring the phase of individual bunches separated by 4.2 ns with better than 0.5 degree resolution (at 476 MHZ). We have shown that the periodic coupler is capable of generating isolated tone bursts from the simulated bunches, and that the detection of individual bunch phases for a large number of bunches (1658) with a 4.2 ns interval is feasible.

Table 1
Isolation, Resolution, and Noise Measurements

Comb Generator	Configuration	Isolation
Coaxial	A to B	25.9 dB
Coaxial	B to A	28.5 dB
Microstrip	A to B	26.7 dB
Microstrip	B to A	29.4 dB
Phase Detector Range		±15° at 476 MHz
Phase Detector Resolution		1.3 mRad at 476 MHz
	or	0.08° at 476 MHz
Phase Detector Noise		1.55 mRad rms at 476 MHz
	or	0.09° rms at 476 MHz

Acknowledgments

The authors would like to thank J. Dorfan, A. Hutton, and M. Zisman for their encouragement and support for this project, and H. Schwarz and J. Judkins for the loan of specialized laboratory equipment.

References

[1] D. Heins, R. D. Kohaupt et al., "Wideband Multibunch Feedback Systems for PETRA," DESY 89-157, 1989.

[2] P.L. Corredoura, J.-L. Pellegrin, H.D. Schwarz and J.C. Sheppard, "An Active Feedback System to Control Synchrotron Oscillations in the SLC Damping Rings," in Proc. Particle Accelerator Conf., 1989, vol. 3, p. 1879.

[3] Toshio Kasuga, Masami Hasumoto, Toshio Kinoshita and Hiroto Yonehara, "Longitudinal Active Damping System for UVSOR Storage Ring," Japanese Jour. Applied Physics, vol. 27, no. 1, 1988, p. 100.

[4] M. A. Allen, M. Cornacchia, and A. Millich, "A Longitudinal Feedback System for PEP," in IEEE Trans. Nucl. Sci. NS-26, 1979, no. 3, p. 3287.

[5] E. Higgins, "Beam Signal Processing for the Fermilab Longitudinal and Transverse Beam Damping System," in IEEE Trans. Nucl. Sci. NS-22, 1975, no. 3., p. 1581.

[6] "An Asymmetric B Factory based on PEP," Conceptual Design Report, SLAC 372, 1991.

[7] K. A. Thompson, "Simulation of Longitudinal Coupled-Bunch Instabilities," B Factory Note ABC-24, 1991, SLAC.

[8] B Factory Accelerator Task Force, S. Kurokawa, K. Satoh and E. Kikutani, Eds., "Accelerator Design of the KEK B Factory," KEK Report 90-24, 1991.

[9] C. Pellegrini and M. Sands, "Coupled Bunch Longitudinal Instabilities," SLAC Technical Note PEP-258, 1977.

[10] R. F. Stiening and J. E. Griffin, "Longitudinal Instabilities in the Fermilab 400 GeV Main Accelerator," IEEE Trans. Nucl. Sci. (1975), NS-22, no. 3, p. 1859.

[11] D. Briggs et al., "Computer Modelling of Bunch by Bunch Feedback for the SLAC B Factory Design," Proc. Particle Accelerator Conference, 1991.

[12] Tektronix Corporation, TKADC-20C 250 MSample/Sec Hybrid Analog to Digital Converter.

[13] Brooktree Corporation, BT108BC Digital to Analog Converter.

SLAC-PUB-5466
LBL-30772
May 1991
(A)

Computer modelling of bunch-by-bunch feedback for the SLAC B-factory design*

D. Briggs, J. D. Fox, W. Hosseini, L. Klaisner,
P. Morton, J.-L. Pellegrin, K. A. Thompson
Stanford Linear Accelerator Center, Stanford University, Stanford, CA 94309 USA

and

G. Lambertson
Lawrence Berkeley Laboratory, University of California, Berkeley, CA 94720

Abstract

The SLAC B-factory design, with over 1600 high current bunches circulating in each ring, will require a feedback system to avoid coupled-bunch instabilities. A computer model of the storage ring, including the RF system, wake fields, synchrotron radiation loss, and the bunch-by-bunch feedback system is presented. The feedback system model represents the performance of a fast phase detector front end (including system noise and imperfections), a digital filter used to generate a correction voltage, and a power amplifier and beam kicker system.

The combined ring-feedback system model is used to study the feedback system performance required to suppress instabilities and to quantify the dynamics of the system. Results are presented which show the time development of coupled bunch instabilities and the damping action of the feedback system.

I. INTRODUCTION

The large average current in the SLAC B-factory design is distributed into many bunches of sufficiently small charge to minimize the beam-beam interaction and single-bunch instabilities. Although the cavity higher-order-modes (HOMs) will be strongly damped ($Q < 70$), there will still be significant coupling of the longitudinal and transverse motion of adjacent bunches via wakefields. Furthermore, the high-Q accelerating mode can also strongly couple the bunches longitudinally. The resulting instabilities will be controlled via wideband, bunch-by-bunch feedback. Such a feedback system can handle disturbances to the bunch motion arising from any source, including but not limited to wakefields and injection errors.

The feedback systems to control the longitudinal and transverse coupled-bunch instabilities will be similar in architecture. Since the signal detection and kicker requirements are more stringent for the longitudinal system and for the high energy ring (HER), we shall concentrate our discussion on this case. Basic longitudinal-feedback system specifications are shown in Table 1. The proposed system implementation, its block diagram and description, and hardware tests are discussed elsewhere [1].

Table 1: Basic feedback system specifications

RF freq.	476 MHz
Max. mode amplitude	10 ps = 0.03 rad
Injection scheme	1/5 bunch at 60 pps
$\frac{\delta E}{E}$ injection error	0.002
δt injection error	100 ps

* Work supported by Department of Energy contract DE-AC03-76SF00515.

II. SIMULATION MODEL

The simulation model (see Fig. 1) consists of a model of the feedback system electronics, combined with a model of the dynamics of the bunches in the ring.

The feedback system model simulates the transfer function of the feedback system and includes: (1) the electronic properties of the phase detector, mixer, low-pass filter, and A/D converter, (2) input noise, gain and offset errors, bandwidth limitations, and dynamic range of the analog components, and (3) the algorithm running in the set of digital signal processors (DSP farm), that takes as input the digitized bunch phases and calculates the longitudinal kick.

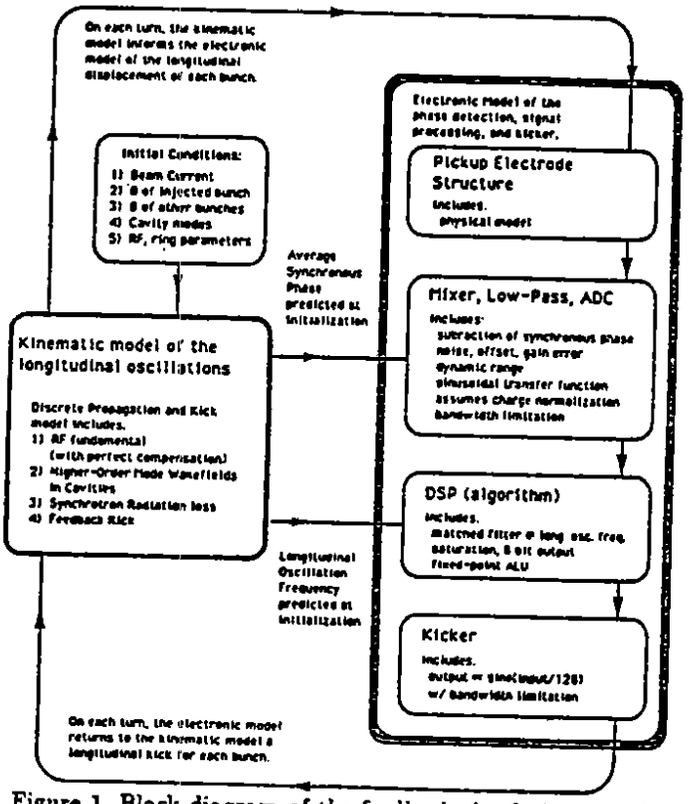

Figure 1. Block diagram of the feedback simulation model.

The model of the DSP farm emulates a 20-tap finite impulse response (FIR) matched filter. The coefficients ξ_j of the taps comprise a sinusoid with the synchrotron period of 19.3 turns, that is,

$$\xi_j = A_{DSP} \sin\left(2\pi \frac{j-1}{19.3}\right) \quad , \qquad (1)$$

where $j \in 1, \ldots, n_{samples}$, and we take $n_{samples} = 20$. Given measures $\tilde{\varphi}_i(k) \equiv \varphi_i(k) - \varphi_s$ (where φ_s is the synchronous phase) of the phase of bunch i on successive turns k as input, the result of the DSP algorithm is the output:

Presented at the IEEE Particle Accelerator Conference, San Francisco, CA, May 6–9, 1991

$$y_i(k) = \sum_{j=1}^{n_{samples}} \xi_j \bar{\varphi}_i(k-j) \quad . \tag{2}$$

This result is clipped to an 8-bit signed integer and used to set the phase of the kicker oscillator for that bunch on that turn. The kicker model is implemented as a phase-modulated RF kicker with a nominal 4 keV maximum output amplitude.

The measurement of the phase of a bunch is assumed independent of its charge, i.e., it is assumed that a separate measurement of bunch charge is available for normalization. A propagation delay of at least one turn (7.33 μs) is enforced in the feedback transfer function.

In the ring simulation model, a discrete kick is given to each bunch at a single point in the ring; that is, the system is modelled as though there were a discrete change in energy at a single point on each turn. This simplification is justified since the synchrotron frequency is small compared to the revolution frequency. The kick given to bunch i is comprised of several components: (1) the RF cavity voltage $\hat{V}_g \sin\varphi_i + V^{cav.fbk.}$, where $\hat{V}_g$ is the peak generator voltage, φ_i is the phase of bunch i with respect to the zero crossing of the RF, and $V^{cav.fbk.}$ is the RF cavity feedback needed to control beam loading in the fundamental mode, (2) the wake field voltage V^{wake} (including both the accelerating mode and the HOM's) accumulated in the cavity up to the present moment, (3) the synchrotron radiation loss per turn, and (4) the voltage V_i^{fdbk} applied to bunch i by the bunch-by-bunch feedback system. Thus, the equation for the total kick is

$$\Delta\dot{\varphi}_i = -\frac{\alpha\omega_{rf}}{E_0/e}\left[\hat{V}_g \sin\varphi_i + V^{cav.fbk.} - U_0/e + V^{wake} + V_i^{fdbk}\right] - \frac{2T_0}{\tau_E}\dot{\varphi}_i \quad , \tag{3}$$

where α is the momentum compaction factor, ω_{rf} is the RF frequency, and τ_E is the longitudinal radiation damping time; E_0 is the ring energy, T_0 the revolution period, and U_0 the synchrotron radiation loss per turn, for a particle on the design orbit. In the present simulations it is assumed that the cavity feedback is perfect, so that the part of V^{wake} due to the fundamental mode is exactly cancelled by $V^{cav.fbk.}$. More realistic models, including the cavity phase, amplitude, and tuning loops, and modification of the impedance at coupled-bunch frequencies that fall within the bandwidth of the fundamental mode [2] are under study [3].

III. SIMULATION RESULTS

Parameters used in the simulations are shown in Table 2. The harmonic number of the HER is 3492, with every other bucket filled except for a 5% gap; the total current is 1.48 A. The initial conditions used were $\varphi_5 = 0.2915$ rad, that is, bunch 5 starts at an 0.1 rad offset from the remaining bunches i, which were started at the synchronous phase $\varphi_i = 0.1915$ rad. The feedback gain in the examples described here was set so that a 5 mrad sinusoid on the input (at the synchrotron oscillation frequency) corresponds to a 4 keV sinusoid on the kicker output.

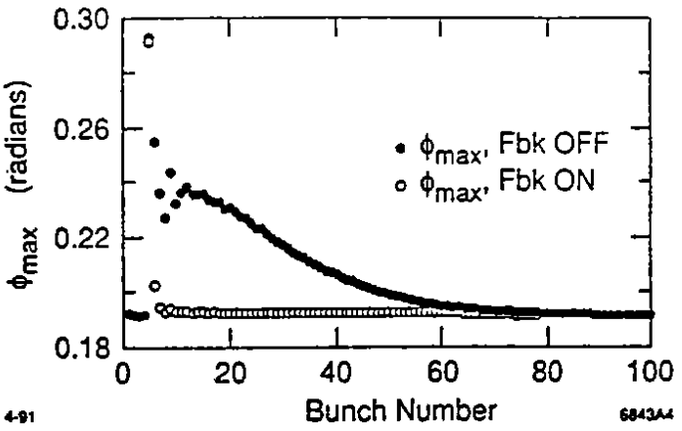

Figure 2. Plot of the maximum bunch offset reached in 3000 turns for the first 100 bunches after the gap, with and without feedback.

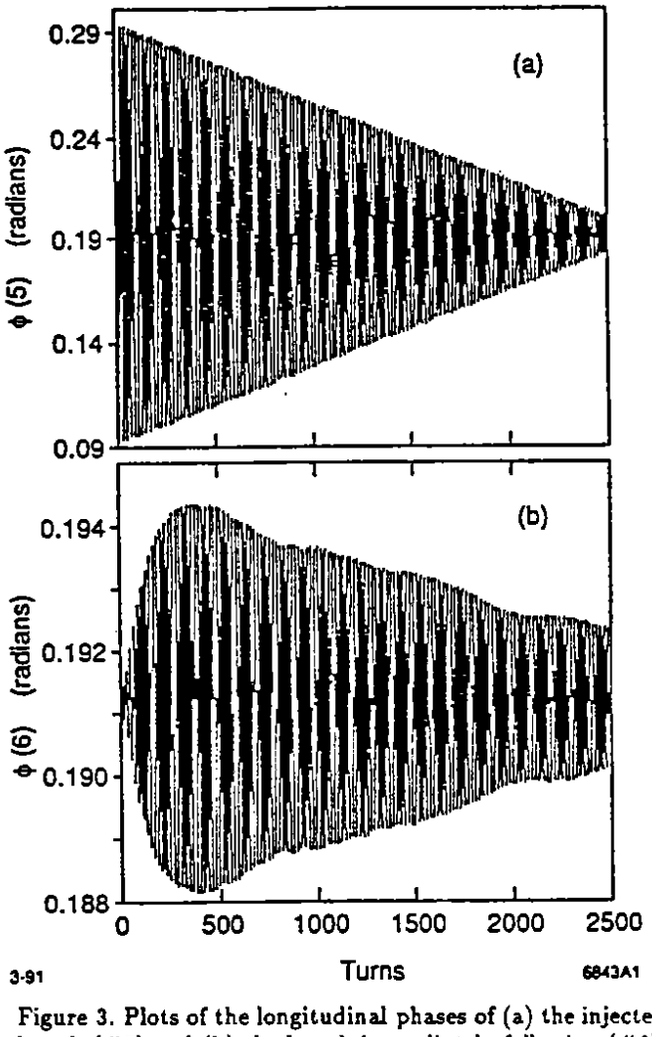

Figure 3. Plots of the longitudinal phases of (a) the injected bunch (#5) and (b) the bunch immediately following (#6), vs turn number, in the presence of feedback. Note the expanded vertical scale in (b).

In Fig. 2, we show a plot of maximum bunch offsets reached after 3000 turns, with and without feedback. Note that the time between injection pulses is 1/60 second, which is about 2300 turns. In the absence of feedback, the disturbance shown would grow even larger and propagat further back in the bunch train. With the feedback systen

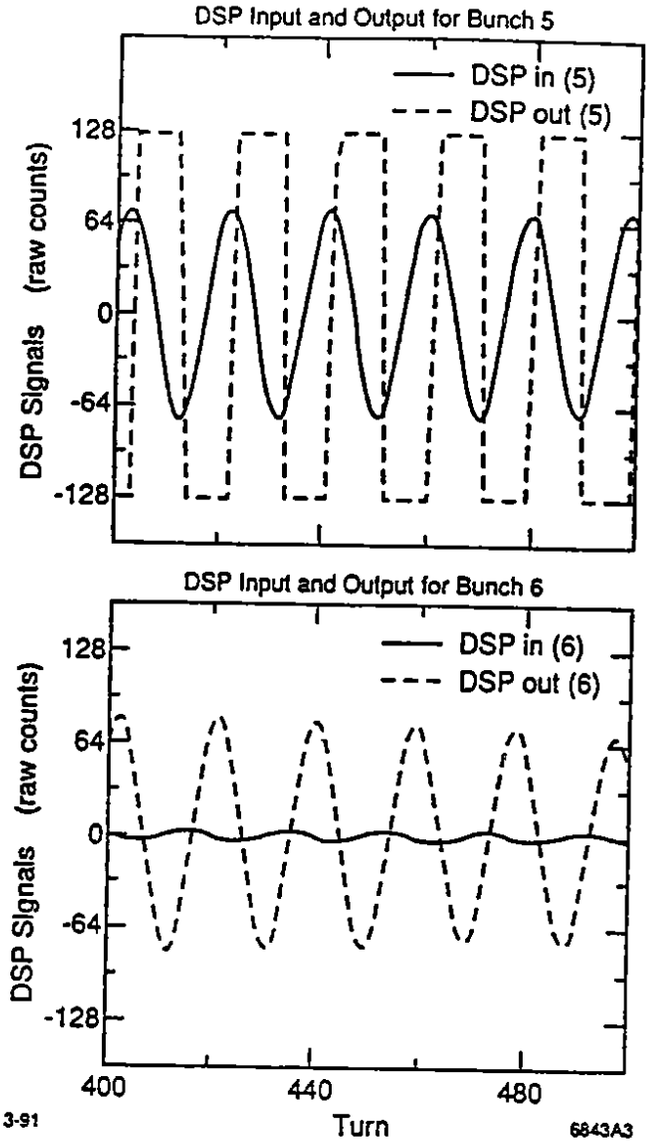

Figure 4. Plots of the input and output of the DSP model for (a) bunch #5, and (b) bunch #6, shortly after the injection of bunch #5.

Table 2: Simulation parameters for HER

Bunch charge	4×10^{10}
Number of bunches	1658
Bunch interval	4.2 ns
Number of cavities	20
Freq. of strongest HOM	750 MHz
Q of HOM	70
R/Q of HOM (per cav.)	33 Ω
$\hat{V}_g$	18.5 MV
α	0.00241
U_0	3.52 MeV/turn

turned on, the coupled bunch excitation does not extend beyond a very few bunches.

Fig. 3 shows the phases of the injected bunch (#5) and the immediately following bunch, vs turn number. The envelope of the phase of the injected bunch damps linearly, reflecting the fact that the kicker saturates, and the phase of the following bunch grows quickly to a maximum and then slowly damps. The excitation of subsequent bunches is strongly suppressed.

Fig. 4 shows the input and output of the DSP model for bunches #5 and #6 shortly after injection. The DSP output saturates for bunch #5, but maintains the proper 90° phase lag. Such benign saturation behavior is difficult to realize with conventional analog approaches.

Fig. 5 compares the amplitude of the injected bunch #5 and following bunches, first without (Fig. 5a) and then with (Fig. 5b) a 10% bunch-to-bunch coupling in the front-end electronics and a 3% coupling in the kicker. With coupling, bunch #6 suffers a greater disturbance, but still damps, while subsequent bunches suffer only slightly. Thus the system is tolerant of a reasonable amount of bunch to bunch coupling in the analog components.

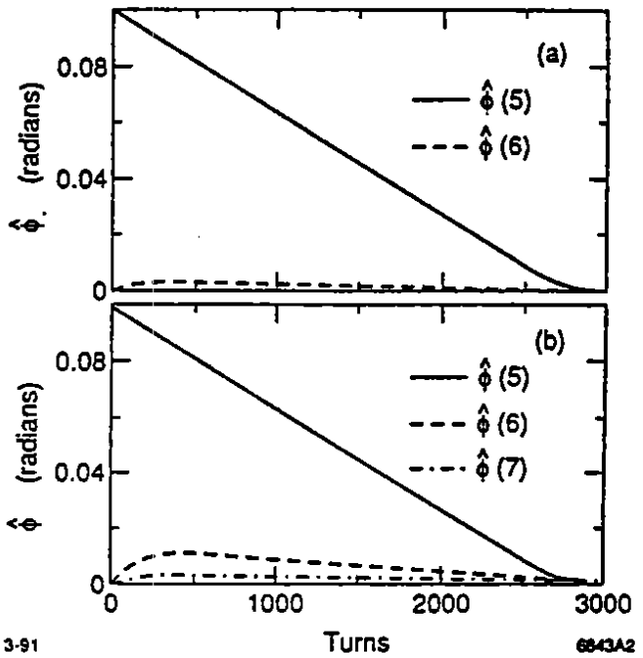

Figure 5. Plots of the phase-space error amplitude for the injected bunch (#5)and following bunch(es), (a) with no coupling, and (b) with 10% bunch-to-bunch coupling in the front-end electronics and 3% coupling in the kicker.

In conclusion, our simulations indicate that the present conceptual approach to bunch-by-bunch feedback is satisfactory. Simulations to support the detailed design effort are in progress.

We thank D. Boussard, J. Galayda, Q. Kerns, F. Pedersen, and P. Wilson for reviewing this work, and J. Dorfan, A. Hutton, and M. Zisman for their interest and encouragement.

REFERENCES

[1] D. Briggs, et.al., "Prompt Bunch-by-Bunch Synchrotron Oscillation Feedback via Fast Phase Measurement", these proceedings.

[2] D. Boussard and G. Lambert, IEEE Trans. Nucl. Sci, NS-30, (1983), p. 2239.

[3] P. Corradoura and F. Volker, private communications.

UCRL- JC-105593
PREPRINT

MODELING PHOTO-DESORPTION IN HIGH CURRENT STORAGE RINGS

William A. Barletta

This paper was prepared for submittal to the
1991 IEEE Particle Accelerator Conference
Accelerator Science and Technology
San Francisco, California
May 6-9, 1991

April 9, 1991

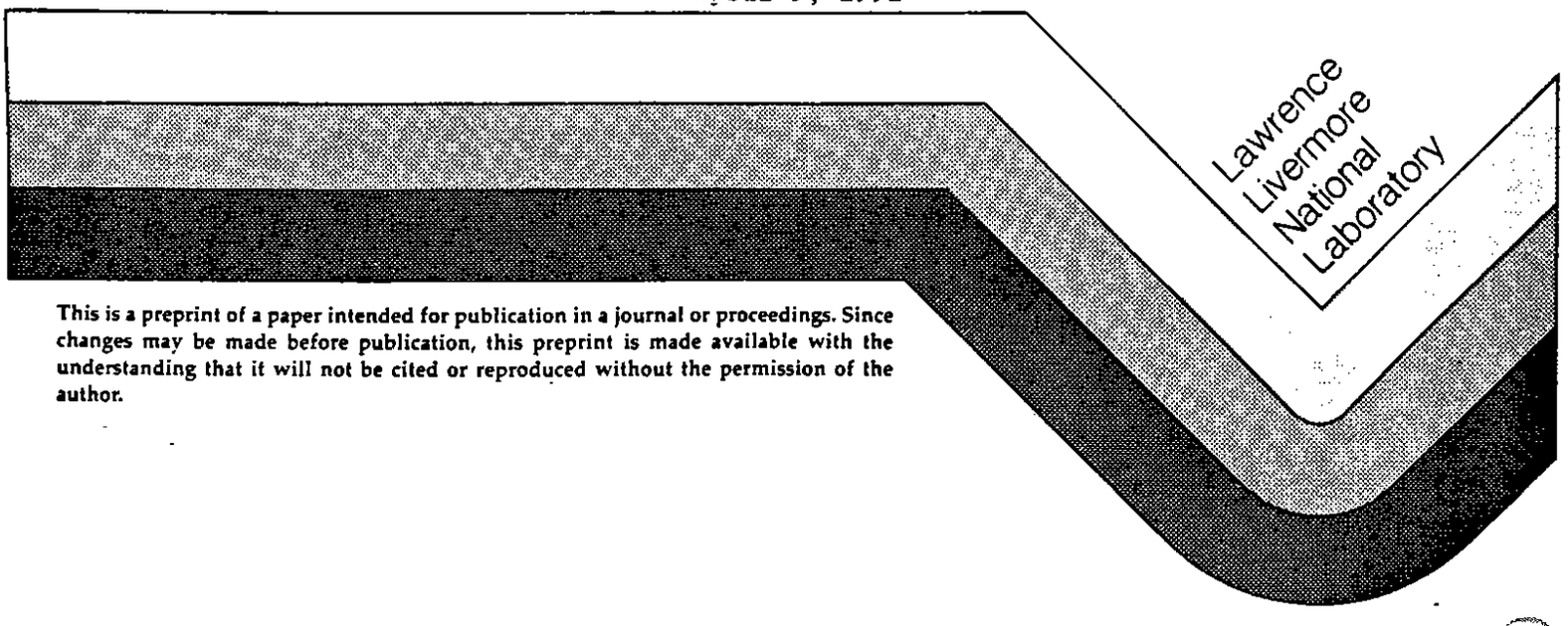

MODELING PHOTO-DESORPTION IN HIGH CURRENT STORAGE RINGS

William A. Barletta
Lawrence Livermore National Laboratory, P. O. Box 808, L-630, Livermore, CA 94551
and
Dept.of Phys., University of California, Los Angeles, 405 Hilgard Avenue, Los Angeles, CA 90024-1547

ABSTRACT

We present a simple phenomenological model of photo-desorption that includes effects of dose dependence and diffuse photon reflection to compute the leveling of gas loads in beamlines of high current storage rings that typify heavy flavor factories. This model is also used to estimate chamber commissioning times.

I. INTRODUCTION

High luminosity flavor factories are characterized by high fluxes of synchrotron radiation that lead to thermal management difficulties. The associated photo-desorption from the vacuum chamber walls presents an additional design challenge, providing a vacuum system suitable for maintaining acceptable beam-gas lifetimes and low background levels of scattered radiation in the detector. Achieving acceptable operating pressures (1 – 10 nTorr) with practical pumping schemes requires the use of materials with low photo-desorption efficiency operating in a radiation environment beyond that of existing storage rings. Extrapolating the existing photo-desorption data base to the design requirements of high luminosity colliders requires a physical model of the differential cleaning in the vacuum chamber. We present a phenomenological model, including dose dependence of desorption and diffuse photon reflection, to compute the leveling of gas loads due to non-uniformities of radiation absorption in realistic beamlines. The model also allows one to estimate collider commissioning times.

II. WALL HEATING AND DYNAMIC GAS LOAD

To scale the vacuum system charcteristics as a function of collider performance one writes the thermal and photon loads on the chamber walls in terms of the luminosity, L;

$$L = \frac{N_- N_+ f_c}{4\pi \sigma_x \sigma_y} , \qquad (1)$$

where f_c is the collision frequency, N_- and N_+ are the charges in the electron and positron bunches, and σ_x and σ_y are the horizontal and vertical beam sizes respectively. For beam-beam tune shifts, $\xi_x = \xi_y = \xi$, L scales with the beam current, I, and the β^*_y at the interaction point as

$$L = 2.7\times 10^{32}\left(\frac{\xi(E)}{0.05}\right)\left(\frac{I}{1\,A}\right)\times \left(\frac{4\,cm}{\beta^*_y}\right)\left(\frac{E}{1\,GeV}\right)(1+r)\,cm^{-2}\,s^{-1}, \qquad (2)$$

where r is the ratio of vertical to horizontal beam sizes.

The synchrotron radiation, P_{sr}, generated per beam is

$$P_{sr} = 88.5\ Watts\ E^4_{GeV}\, I_{mA}/\rho_m , \qquad (3)$$

where ρ_m is the bending radius in the ring. In terms of the dipole field strength, B_T, one can rewrite (3) as

$$P_{sr} = 26.5\ kW\ E^3_{GeV}\, I_A\, B_T . \qquad (4)$$

If the radiation is generated over $2\pi\,\rho_m$, the linear power density generated by each beam, P_L, is

$$P_L = 1.26\ kW/m\ E^2_{GeV}\, I_A\, B^2_T . \qquad (5)$$

Combining Eq. (1) and (5) yields the scaling law,

$$P_L = 12\,\frac{kW}{m}\left(\frac{L}{10^{34}}\right)\left(\frac{\beta^*_y}{1\,cm}\right)\left(\frac{0.05}{\xi}\right)\frac{B_T^2\, E_{GeV}}{1+r} . \qquad (6)$$

In high current electron storage rings the dynamic gas load due to photo-desorption is generally much larger than the static thermal outgassing of the chamber. The number of photons[1] incident on the chamber is

$$\dot{N}_\gamma = 8.08\times 10^{17}\, E_{GeV}\, I_{mA}\ photons/sec, \qquad (7)$$

A fraction, η_F, of the photons cause a gas molecule to be desorbed to produce a dynamic gas load (for an ideal gas) of

$$Q_{gas} = 2.4\times 10^{-2}\, E_{GeV}\, I_{mA}\eta_F\,\frac{Torr\cdot l}{s} . \qquad (8)$$

Combining Eq. (8) with Eq. (2) yields the scaling law for the pumping needed to maintain an operating pressure, P,

$$S = 6.7\times 10^5\,\frac{l}{sec}\left(\frac{5\,nTorr}{P}\right)\left(\frac{\eta_F}{1.5\times 10^{-5}}\right)\times \left(\frac{L}{10^{34}}\right)\left(\frac{\beta^*_y}{1\,cm}\right)\left(\frac{0.05}{\xi}\right)\frac{1}{1+r} \qquad (9)$$

The scaling laws show that large thermal and gas loads are the price of high luminosity; however, they are only estimates useful to scope the size of the gas and thermal management tasks. To locate and size the pumps one must account for localization of the gas load due the actual distribution of radiation deposited along the chamber walls. Naively, one might apply Eq. (7) and (8) directly using the radiation deposition profile with the adopted design value of η_F to compute the distributed gas load. Doing so, however, neglects the strong variation of η_F with dose.

III. PHENOMENOLOGICAL MODEL OF DESORPTION

The desorption coefficient is a property of the chamber which depends on several factors: 1) the chamber material, 2) the fabrication and preparation procedures, 3) the cumulative prior radiation dose, 4) the photon angle of incidence, 5) the photon energy. Given these complexities, rather than considering η_F to be a fundamental material property, one should regard it as an effective engineering characteristic that accounts for the differential illumination of the chamber walls both by direct (i.e., beam-produced) photons and by secondary, diffusely scattered and florescence photons. Using a single value of η_F in Eq. (8) predicts a gas load which is valid only to the extent that the desorption coefficient is constant along the beamline. Ignoring the non-uniformities can lead to a significant underestimate of the pumping required.

Recent experimental measurements[2, 3, 4] of η_F for samples of Al, stainless steel, and oxygen free Cu indicate minimum values of η_F ranging from $< 2 \times 10^{-6}$ for Cu and stainless steel to 2×10^{-5} for Al. From a typical set of data[3] in which effects of secondary photons are minimal one observes that for large exposures, η_F tends to follow a power law dependance on dose (photons/cm^2); i. e.,

$$\eta \propto (It + t_o)^{-p} \qquad (10)$$

where t is the exposure time and $0.4 < p < 0.7$ (depending on material and preparation). Assuming that $p = 0.6$ for copper, one can compute a local value of $\eta_F(s)$ along the beamline. Then the gas load at a position, s, is

$$Q_{gas}(s) = \eta_F(s)\,\dot{N}_\gamma(s)\,. \qquad (11)$$

In the literature most workers present desorption data as a function of photons per cm or merely of Amp-hours. To compare data or to apply the data to a chamber conditioning scenario one must convert the dose to photons/cm^2.

As an example, consider the arcs of the 9 GeV ring of the asymmetric B factory based on PEP[5] (APIARY). The maximum allowed current is 3 A and the bending radius is 165 m. From Eq. (5) the maximum power is 102 W/cm with a distribution as illustrated by the dark curve in Fig. 1. By assuming that η_F assumes its design value where P_{SR} assumes its maximum value, one compute the relative gas load along a half-cell of the arc. This figure becomes a system specification for the vacuum engineer. The effect of the non-uniform exposure of the chamber is to level the gas load along the beamline and thus to require substantially more pumping capacity than would be needed if Q_{gas} were a constant multiple of the synchrotron power. For convenience this effect is termed "eta-leveling."

To extend the analysis one notes that although the synchrotron radiation fan cleans a thin band of height, H, around the mid-plane of the chamber, a large number of photons, from 20 - 50% of the number of primaries, are re-radiated or diffusely scattered. These secondary photons due to the effective albedo, R, illuminate rather uniformly the remainder of the chamber cross section of perimeter, P, as shown schematically in Fig. 2.

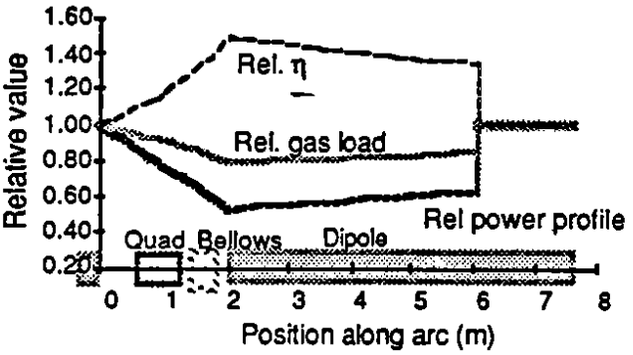

Figure 1. Relative distribution of synchrotron radiation, η, and gas load in arcs of 9 GeV APIARY ring.

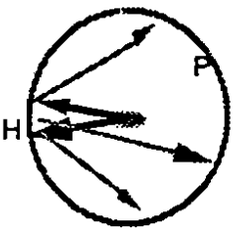

Figure 2. A cross section of the vacuum chamber in a bend

Though secondary photons have a much softer spectrum than the primaries, their photo-desorption efficiency is similar for energies exceeding a few tens of eV. Thus the remainder of the chamber perimeter is an important source of photo-desorbed gas, albeit one illuminated much more weakly, i. e., by a factor RH/P. With time, the effective desorption probability at a given location will vary as

$$\eta \propto (It + t_o)^{-p} + R\,(It\frac{RH}{P} + t_o)^{-p} \qquad (12)$$

As illustrated in Fig. 3, the effects of albedo and chamber geometry delay significantly the time at which the chamber attains a very low effective η_F. As the original power law behavior is eventually recovered for exposures >10 Amp-hr, the implications of the simple "eta-leveling" of the gas load remain accurate with respect to the pumping required with a well conditioned chamber.

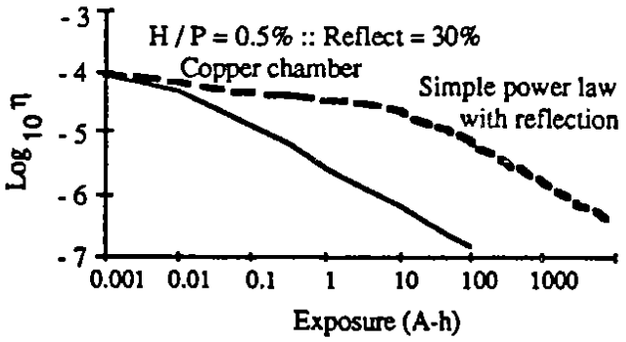

Figure 3. The effect of scattered photons on the dose dependence of the effective photo-desorption for a copper vacuum chamber.

The predictions of the phenomenological, eta-leveling model have been compared to the recent data of Ueda, et al.[4], which unlike exposures of Ref. 3 are dominated by secondary photons. Figure 4 compares data for lightly etched Cu, compared with a calculation with Eq. (12); the fit is very good for $0.5<p<0.6$. For $p = 0.62$ Fig. 5 shows the effect of chamber albedo on the effective η. The data are for an etched stainless steel chamber of which only 0.1% is directly illuminated. The authors estimate the albedo to be ≈50%. The model again displays good agreement. Note that if R< 50% for the storage ring, basing the vacuum design on the data of Ref. 4 represents a conservative choice.

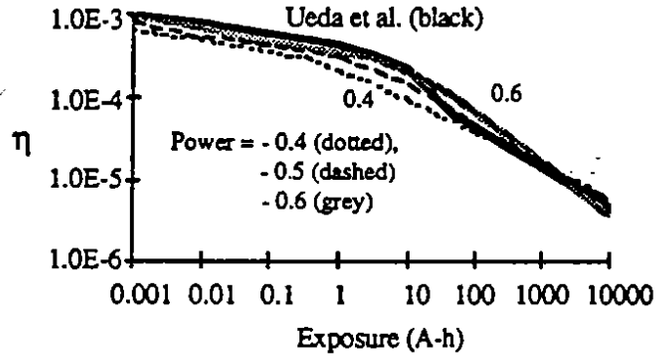

Figure 4. Comparison of the eta-leveling model with data from an etched copper test chamber

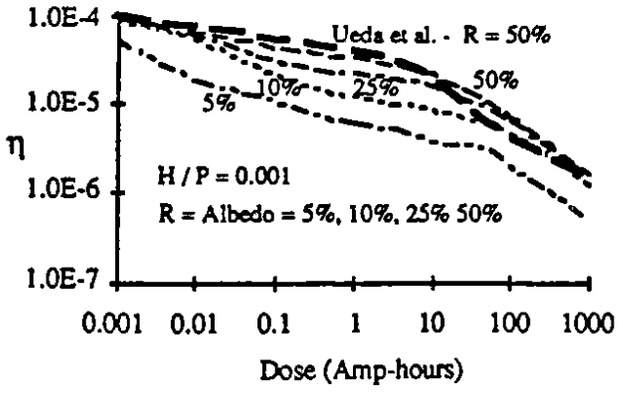

Figure 5. The dependence of η on chamber albedo

One use of the model is to specify a commissioning scenario for a high current storage ring. For a given the installed pumping the ring initially will be unable to maintain high current for a long lifetime. For the scattering lifetime to exceed ≈1 hour, one will be forced initially to store very low currents until η becomes sufficiently small that raising the current does not increase the operating pressure. Eventually, the chamber will be cleaned sufficiently by the radiation to allow operation at the full design current. A calculation for the high energy ring of APIARY, Fig. 6, shows that the design current (1.5 A) can be stored for >3 hours after ≈200 hours of operation.

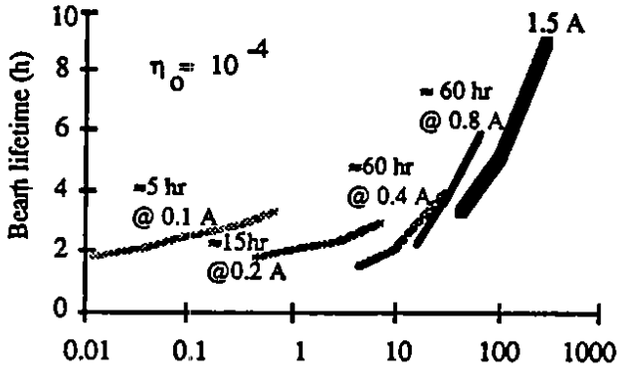

Figure 6. Commissioning scenario for the APIARY ring with an etched Cu vacuum chamber

In summary, a phenomenological model of the evolution of the effective photo-desorption coefficient, η_F, in high current storage rings is both a useful and necessary design tool. Without an adequate appreciation of the evolution of η_F, one is likely to underestimate the required pumping by as much as a factor of two and misjudge the commissioning time by an order of magnitude or more.

The author thanks Manuel Calderon (LLNL), Jonathan Dorfan and Andrew Hutton (SLAC), Henry Halama (BNL), Oswald Gröbner and Alastair Mathewson (CERN), and Michael Zisman (LBL) for their critical comments. This work was partially supported by Lawrence Livermore National Laboratory for the U. S. Dept. of Energy under contract W-7405-eng-48.

IV. References

[1] O. Gröbner, et al., Vacuum 33, 397 (1983).

[2] C. Foerster, H. Halama, C. Lanni, *J. Vac. Sci. Technol.* A8, (3) 2856, 1990.

[3] A. Mathewson, et al., "Comparison of Synchrotron Radiation Induced Gas Desorption from Al, Stainless Steel, and Cu Chambers", Proceedings of the Symposium on Vacuum Systems for Synchrotron Radiation Sources, ANL, Nov., 1990.

[4] Ueda, et al., "Photo-desorption from stainless steel, aluminum alloy and oxygen free copper test chambers", Proceedings of the Symposium on Vacuum Systems for Synchrotron Radiation Sources, ANL, Nov., 1990.

[5] "An Asymmetric B Factory based on PEP - Conceptual Design Report", LBL PUB-5263, February, 1991.

UCRL- JC-105594
PREPRINT

VACUUM DESIGN FOR A SUPERCONDUCTING MINI-COLLIDER

William A. Barletta
Sergio Monteiro

This paper was prepared for submittal to the
1991 IEEE Particle Accelerator Conference
Accelerator Science and Technology
San Francisco, California
May 6-9, 1991

April 9, 1991

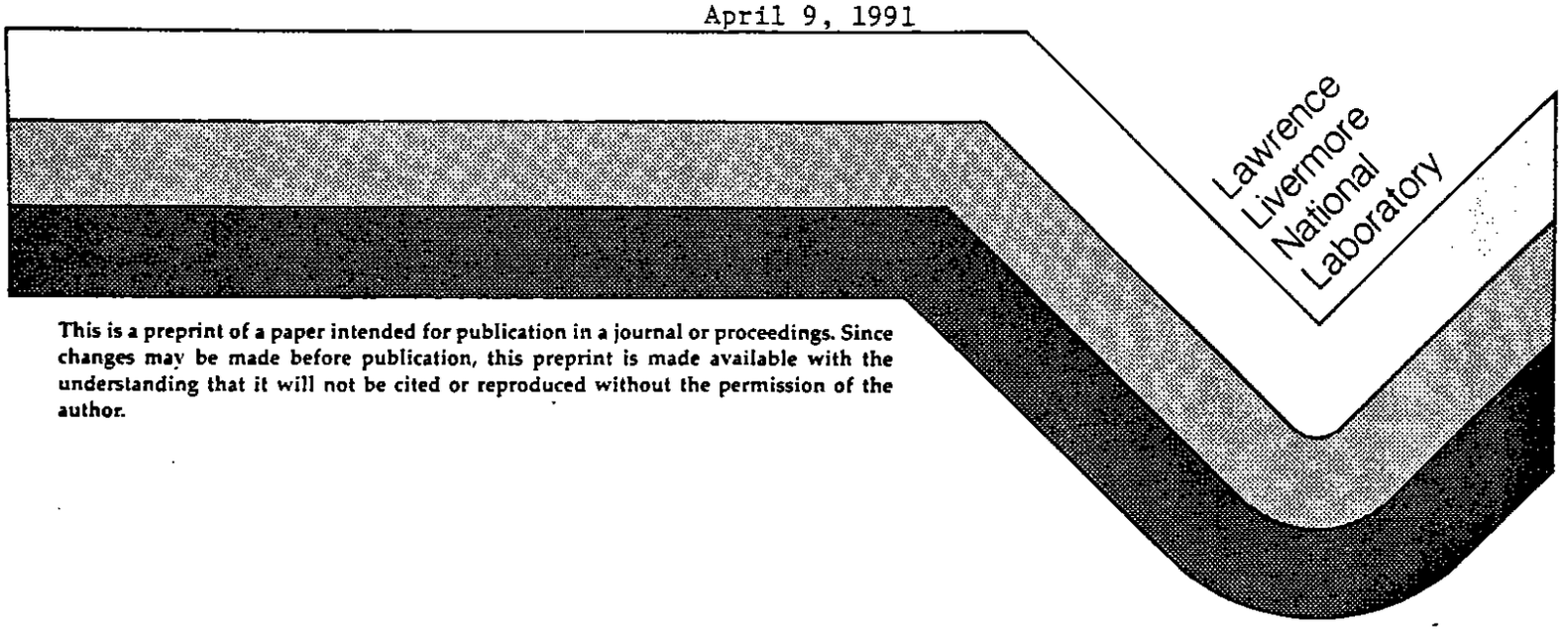

VACUUM DESIGN FOR A SUPERCONDUCTING MINI-COLLIDER

William A. Barletta
Lawrence Livermore National Laboratory, P. O. Box 808, L-630, Livermore, CA 94551;
Dept. of Phys., University of California, Los Angeles, 405 Hilgard Avenue, Los Angeles, CA 90024-1547
and
Sergio Monteiro
Moorpark College, Moorpark, CA 93021

ABSTRACT

The phi factory (Superconducting Mini-Collider or SMC) proposed for construction at UCLA is a single storage ring with circulating currents of 2 A each of electrons and positrons. The small circumference exacerbates the difficulties of handling the gas load due to photo-desorption from the chamber walls. We analyze the vacuum system for the phi factory to specify design choices.

I. INTRODUCTION

To limit gas scattering that can limit collider performance one must maintain a low pressure in the vacuum chamber despite the copious synchrotron radiation generated by the high current beams. The heart of a sound vacuum system is a well designed vacuum chamber. The chamber must 1) withstand large thermal loads, 2) present a tolerable gas load to the pumps, 3) remain within the electromagnetic impedance budget. The designer of the vacuum system is faced with several options. The chamber may be of conventional "elliptical" shape or it may have an antechamber. The chamber material may be Al, stainless steel, or a Cu alloy as in HERA at DESY and as proposed for B factories by CERN, SLAC/LBL/LLNL (APIARY)[1] and Cornell (CESR-B). Each material allows alternate fabrication techniques.

II. THERMAL LOADS AND DESORPTION

Each beam generates a synchrotron radiation power, P_{sr},

$$P_{sr} = 88.5 \text{ Watts } E^4_{GeV} I_{mA} / \rho_m , \qquad (1)$$

where ρ_m is the bending radius in the ring. In terms of the dipole field strength, B_T, one can rewrite (1) as

$$P_{sr} = 26.5 \text{ kW } E^3_{GeV} I_A B_T . \qquad (2)$$

If the radiation is deposited over $2\pi \rho_m$, the linear power density deposited by each beam on the walls, P_L, is

$$P_L = 1.26 \text{ kW/m } E^2_{GeV} I_A B^2_T . \qquad (3)$$

For SMC[2], E = 0.51, B_T = 4 T, and I = 2 A. The thermal load per beam is ≈ 10 kW/m. As both beams circulate in the same ring, the radiation fans overlap at the center of the bends yielding a local thermal load of ≈20 kW/m for an conventional elliptical vacuum chamber.

The power per unit area incident on the chamber wall depends on the height of the radiation fan at the wall. The height is a function of both the vertical angular spread, θ, of radiation from the beam electrons (or positrons) and on the distance, d, from the beam orbit to the wall. The angular spread from a electron of energy, E, is

$$\theta \approx \frac{m c^2}{E} = \gamma^{-1} . \qquad (4)$$

The half-height, h, of the radiation fan on the walls is related to the rms beam height, σ_y, the vertical emittance, ε_y, and the distance from the beam to the wall, d, by

$$h = \pm \left[\sigma_y^2 + d^2 \left(\left(\frac{\varepsilon}{\sigma} \right)^2_y + \theta^2 \right) \right]^{1/2} . \qquad (5)$$

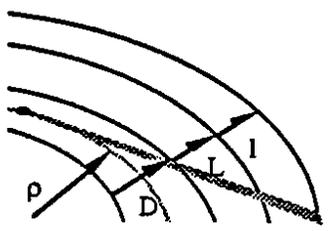

Figure 1. Geometry of chamber and radiation fan.

With the geometry of Fig. 1, which describes a beam chamber of width D, connected via a thin duct of length, L, to an antechamber of width, l, and using ρ = 0.42 m, D = 0.27 m, L = 0.2 m, and l = 0.14 m, we find d = 0.79 m. Thus, from Eq. (5) h = ±5 mm in the central dipole of the arcs and ± 2 mm elsewhere. These values are dominated by the heights of the electron and positron beams, which are 4.7 mm in the central dipole and 1.6 mm in the remainder of the collider. For the SMC, the P_{sr} ≈ 60 kW; thus, the maximum power density is 280 W/cm^2, one third the design value for the PEP ring at Stanford. In contrast the P_L for the 9 GeV ring of APIARY is ≈10 kW/m. For Cu alloys linear power densities ≈20 kW/m and areal densities ≈2 kW/cm^2 can be cooled with conventional techniques. Stainless steel, with its poor thermal conductivity, must be thin and backed by a OFHC Cu cooling bar. Forced water circulating in multiple channels keeps the vacuum chamber at a low enough temperature (<120° C) to cause negligible thermal desorption of gas into the system.

As the synchrotron radiation is not deposited uniformly, due to the alternation of bends and drifts in the ring, Eq. (6) represents the maximum P_L on the chamber. Applying an analytical formulation[3] for computing the distribution of radiation to the lattice of the SMC yields Fig. 2. The distribution is symmetric about the center of the detector (z = 0); the position of the detector and the superconducting dipoles are shown as boxes.

Following Gröbner, et al.[4], we compute gas load from the number of photons incident on the chamber:

$$\dot{N}_\gamma = 8.08 \times 10^{17} E_{GeV} I_{mA} \text{ photons / sec}, \qquad (6)$$

of which, a fraction, η_F, cause a molecule to be desorbed from the wall. For an ideal gas,

$$Q_{gas} = 2.4\times10^{-2}\, E_{GeV}\, I_{mA}\eta_F \frac{\text{Torr - l}}{\text{s}}. \qquad (7)$$

The desorption coefficient decreases with the cumulative exposure of the material to synchrotron radiation. Several groups[5] have measured the photo-desorption from Al, Cu, and stainless steel, for conditions similar to the ones expected for the vacuum chamber of the SMC. As η_F depends only weakly on photon energy, our estimate of gas loading based on these data should be conservative.

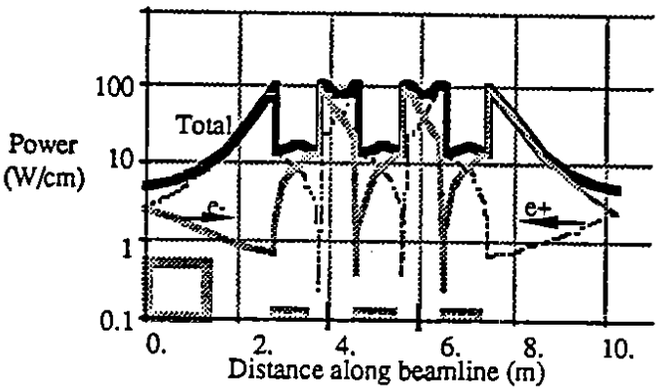

Figure 2. Distribution of radiation in the antechamber.

For the SMC, the dynamic gas load in an Al chamber with $\eta_F = 1.5 \times 10^{-5}$ is 7.2×10^{-4} Torr-l/s. To obtain a pressure of 5 nTorr requires 145,000 l/s or ≈20,000 l/s/m of pumping. These values are impractically high. In contrast, the use of an elliptical stainless steel chamber with $\eta_F = 2 \times 10^{-6}$ reduces the gas load to ≈ 10^{-4} Torr-l/s. The total required pumping would be ≈ 20,000 l/s or roughly 2,500 l/s/m of pumping distributed along the arcs. Therefore, we choose stainless steel as the chamber material. A more conservative alternative to stainless steel is copper which has excellent thermal conductivity and photo-desorption properties similar to stainless steel. Using Cu does require a considerably more difficult fabrication .

Even for an elliptical chamber of copper 2500 l/s/m is impractically large for either sputter ion pumps or non-evaporable getters (NEG). To lower the distributed pumping further we adopt an antechamber design in which the synchrotron radiation escapes from the beam chamber via a thin slot in the wall of the beam tube though a thin channel to an antechamber where it impinges on the wall. As the antechamber extends beyond the dipoles, large pumps can easily be located where the gas loads are produced. With the two chambered system of Fig. 3, the pumping speed can be reduced by a factor of ≈ 5.

The pressure in the inner chamber depends on the conductance[6], C, of the duct between two chambers. As the circumference is much larger than the duct height, we can approximate the slot as a thin, rectangular duct using the circumference as the width to obtain C = 900 l/s. To obtain pressure in a stainless steel outer chamber of 25 nTorr, the required pumping speed is 3.8×10^3 l/s. In that case the gas load in the inner chamber, where the beam is circulating is:

$$q = C\,(P_{out} - P_{in}) . \qquad (8)$$

The gas load in the beam tube is ≈1.8×10^{-5} Torr-l/s with an antechamber. The required pumping for an ultimate pressure of 5 nTorr in the beam tube is 3.6×10^3 l/s.

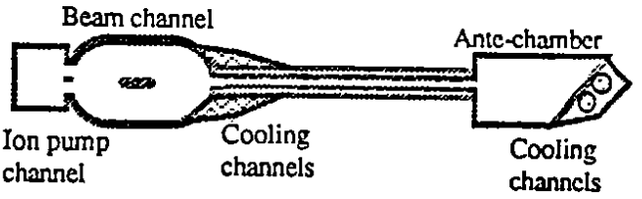

Figure 3. Ante-chamber cross section for the phi factory.

With a stainless steel chamber the combined pumping is 7,300 l/s or ≈600 l/s/m in the arcs, of which 400 l/s/m must be pumped from the beam tube. Although 400 l/s/m is well within the capability of NEG pumps, our estimate of the time between regeneration of the NEG is ≈100 hours, an unacceptably short interval. Even the difficulty of pumping the inner chamber may be surmounted. If we raise the pressure in the beam tube to 10 nTorr and lower the pressure in the outer chamber to 20 nTorr, the pumping requireed in the beam chamber falls to 90 l/sm well within the current practice in storage rings such as PEP which use distributed ion pumps requiring no regeneration.

The preceding discussion does not account for the variation of photo-desorption coefficient due to the non-uniformity of illumination of the walls of the chamber. The desorption efficiency decreases with long exposures, It, (in Amp-hours) approximately following $\eta_F \propto (It)^{-p}$ where $0.4 < p < 0.7$. Applying this variation increases the gas load ("eta leveling[7]") vis á vis a value simply proportional to P_L. The resulting gas load shown in Fig. 4.

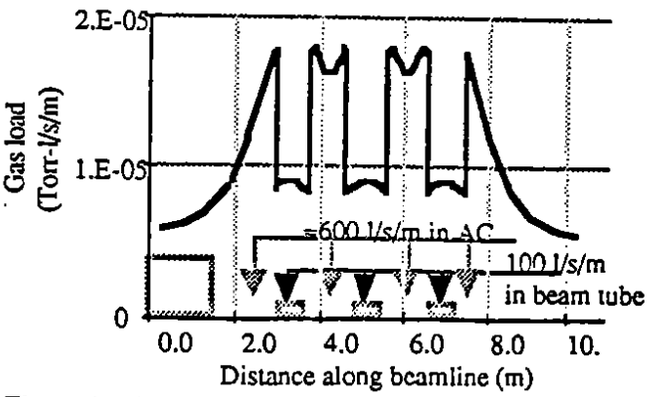

Figure 4. Distribution of gas load and pumping in SMC.

The antechamber is pumped with 600 l/s/m by either turbo-molecular, cryo-, or Ti sublimation pumps. The beam tube requires 100 l/s/m of pumping by a combination of turbo-molecular and distributed ion pumps. The pumping for the antechamber can be localized between the dipoles where the gas load is the highest. With our pumping scheme, the pressure

Such low values of η_F have been measured in pure Cu. Confirming the practicality of our design choice for η_F is a key part of an experimental validation program.

To pump this gas load, we have selected an all sputter ion pump design. We show the inventory of pumping capacities for each pumping element in a typical cell in Table 2. At 1.5 A the desired average pressure (5 nTorr) is maintained with distributed pumping of 125 l/s/m. To achieve these speeds the distributed ion pumping in the dipoles of PEP has been redesigned to operate in a 0.18 T field. The anode was increased to 1.8 cm diameter, and one more row was added, increasing the number of anodes by 33% with a packing factor of about 90%. Distributed ion pumping (DIPs) has been added at the quadrupoles in stainless steel housings to one side of the beam tube and below but none on the top to preclude particles dropping into the beam chamber. As the available space is restrictive, the anodes have been reduced in size. The calculated pumping speed in the beam tube will be about 75 l/s/m from each of the steel housings. However, the total pumping speed for the defocusing and focussing quadrupoles are different owing to their different lengths. To augment the DIPs we have added 60 l/s lumped ion pumps in each of the quadrupole spaces of the cells. Given the low conductance of the beam pipe, larger pumps would not improve system performance. Moreover, the ports are designed to accommodate additional pumps if needed.

Table 2. Pumping inventory of HER arc cell

2 Dipole DIPs	800 l/s
1 Quad DIP	110 l/s
1 Quad DIP	80 l/s
1 Lumped ion pumps	60 l/s
Total distributed pumping	125 l/s/m

VI. STRAIGHT SECTIONS & SPECIAL COMPONENTS

To keep the contribution of the ports to the machine impedance negligible the ports are shielded with perforated screens with longitudinal slots 10 cm long by about 0.2 cm wide. The pumping slots in the septum between the pump channel and beam tube have been calculated as rows of slots 9 cm long by about 0.2 cm wide at a pitch of 10 cm, similar to HERA, giving a conductance of about 500 l/s/m. These slots contribute a negligible amount to machine impedance.

Each bend cell contains a beam position monitor (BPM) located at and anchored to the defocusing quadrupole. The BPM for APIARY follows the HERA design with minor modifications. The housing will be accurately machined from a solid Cu block having recesses on its end faces to index the ends of the beam tube for alignment during brazing. Cooling on both sides will preclude a temperature asymmetry between lateral sides.

Changes in cross section between the arcs of octogonal cross section and the straight sections of circular cross section are made with tapered transition elements. To keep the total contribution to the chamber impedance within the impedance budget, the taper angle is <10°.

A typical cell in the straight sections is 15.125 m in length. The vacuum conduit is a 10 cm diameter, stainless steel tube of circular section sized to clear the 100 mm bore of the magnets. To produce an average pressure <3 nTorr in the straight sections we will install lumped sputter ion pumps rated at 230 l/s spaced by ≈8 m. We have calculated the pump size and spacing assuming a thermal outgassing rate of 10^{-11} torr-l/cm^2/s and a pressure differential in the beam tube of 0.5 nTorr. In situ baking compatibility to 150° C is provided to reduce the initial outgassing and to allow for pressures in the 0.1 nTorr range if such low pressures are required.

To aid in the assembly both bend and straight cells contain bellows designed to permit 130°C of thermal expansion. In their extended position at room temperature, the bellows are 22.9 cm long. They can compress ≈4 cm to 18.9 cm at the maximum temperature (150° C) to which the ring can be baked in situ without disassembly. The inner bellows which carry the surface currents is fabricated as one piece with formed convolutions in the plane of the beam tube flats and has narrow slits at the intersecting corners to permit axial movement. A narrow slit permits synchrotron radiation to shine through to thick-wall, water cooled, Cu absorbers cantilevered from the flanges to carry away the thermal load.

A calculation of a commissioning scenario [2] shows that the time needed to store the design current for >2 hours varies with the initial value of η_F as determined by fabrication procedures. For $\eta_F(0) = 10^{-3}$, commissioning the Cu chamber requires ≈500 hr. For an appropriately cleaned chamber we expect $\eta_F(0) = 10^{-4}$, in which case the full design current can be stored after 150 hours (Fig. 3).

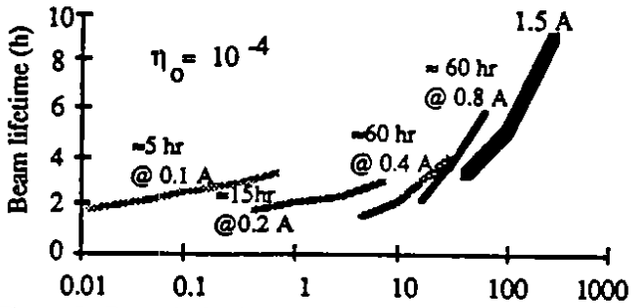

Figure 3. Commissioning scenario for an etched Cu chamber.

The authors thank William Davies-White, Andrew Hutton (SLAC), Henry Halama (BNL), Oswald Gröbner, Alastair Mathewson (CERN), and Michael Zisman (LBL) for their critical comments. Supported by U. S. Dept. of Energy at LLNL under contract W-7405-eng-48 and at SLAC under contract DE-AC03-76SF00515.

VII. References

[1] "An Asymmetric B Factory Based on PEP - Conceptual Design Report", LBL PUB-5263, February, 1991.

[2] W. A. Barletta, Modeling Photo-desorption in High Current Storage Rings, Proceedings, this conference.

[3] C. Foerster, H. Halama, C. Lanni, J. Vac. Sci. Technol. A8 (3)June, 1990, p. 2856.

[4] A. Mathewson et al., "Comparison of Synchrotron Radiation Induced Gas Desorption from Al, Stainless Steel, and Cu Chambers", Proceedings of the Symposium on Vacuum Systems for Synchrotron Radiation Sources, ANL, Nov., 1990.

[5] Ueda et al., "Photo-desorption from Stainless Steel, Aluminum Alloy and Oxygen free Copper Test Chambers", ibid.

distribution in the antechamber with 2 A per beam circulating is as shown in Fig. 5. The 100 l/s of distributed pumping in the beam tube reduces the pressure to less than 10 nTorr as required.

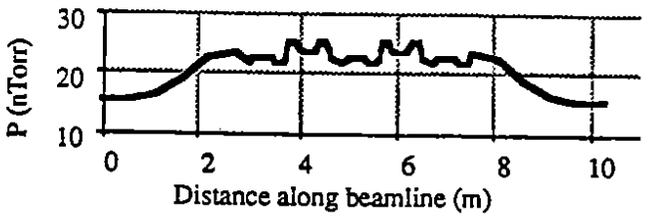

Figure 5. Pressure in the antechamber.

To assure an adequate quantum lifetime for the beams under all operating conditions, the vacuum chamber must be large enough to avoid depopulation of the wings of the beam. The physical aperture set equal to 12 times the beam size plus a closed orbit allowance and 5 mm for fabrication and alignment tolerances. For an elliptical chamber, one determines the horizontal and vertical radii from the maximum β_x and β_y, the maximum dispersion, ε_x and ε_y, and the closed orbit allowances. The most conservative assumption is to use the uncoupled ε_x and the fully coupled ε_y. Then, the radius of the beam stay clear is

$$\Sigma_i = 12\left[\varepsilon_i \beta_{i,\,max} + \eta^2_{max}\left(\frac{\Delta E}{E}\right)^2\right]^{0.5} + CO_i + 0.5\ \text{cm} \quad (9)$$

where i = x, y. Inserting the relevant lattice characteristics[2] of the phi factory (Table 1) into Eq. (12), we obtain chamber radii, Σ_x = 13.5 cm and Σ_y = 10.5 cm.

Table 1. Characteristics of phi factory optics

Uncoupled horizontal emittance	4 μm
Fully coupled vertical emittance	2 μm
Maximum horizontal beta	24 m
Maximum vertical beta	28 m
Maximum dispersion	0.8 m
Natural energy spread, ΔE/E	10^{-3}
Closed orbit, CO_x, CO_y	± 1, ± 0.5 cm

We have computed a conservative commissioning scenario for the SMC choosing an initial η_F of 10^{-3}, which is several times larger than achievable with good preparation techniques. Figure 6 shows that after ≈250 hours of operation the collider can be operated at the design current of 2 A with acceptable beam-gas scattering lifetime.

Engineers at LLNL have estimated the hardware cost of a stainless steel chamber with a copper cooling bar to be 175 KS plus 120 KS for the pumps, bellows and special hardware. Fabrication costs add an additional 130 KS. Use of copper for the entire design is likely to raise these costs by an additional 150KS. Hence, a stainless steel (copper) vacuum system for the SMC will cost ≈425 KS (575 KS). Engineering, design and inspection adds an additional 650 KS regardless of chamber material.

The SMC vacuum system, while more challenging than that of existing storage rings is within the bounds of sound engineering practices. The antechamber moves the gas load away from the beam thereby lowering the required distributed pumping. To minimize photo-desorption we have selected stainless steel backed by a Cu cooling bar for the chamber material. The x-ray opacity of stainless steel is sufficiently high over the entire range of photon energies that additional lead shielding is not needed to protect the superconducting magnets from the intense synchrotron radiation. Our design allows for chamber commissioning in ≈300 hours of ring operation. The cost per meter is relatively high, ≈50 KS/m, reflecting the considerable engineering effort required for this highly integrated and complex design.

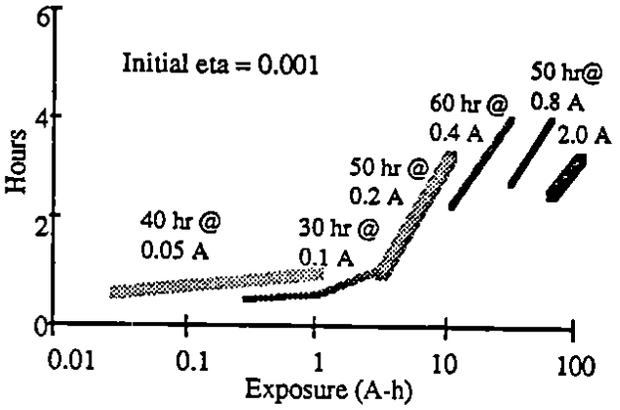

Figure 6. Beam lifetime during commisssioning.

We thank Howard Patton, Manuel Calderon, and Carl Anderson of LLNL, Michael Zisman of LBL and Henry Halama of BNL for several helpful conversations. Supported by U.S. Dept. of Energy at LLNL under contract W-7405-eng-48.

III. References

[1] *Investigation of an Asymmetric B Factory in the PEP Tunnel*, 1990. LBL PUB-5263, SLAC-359, CALT-68-1622

[2] William A. Barletta and Claudio Pellegrini, "Injection System for the UCLA Phi Factory" *Proceedings of the International Workshop on Phi factories and Related Physics Issues*, UCLA, April. 1990.

[3] A. Alexandrov, A. Hutton and, P. Legachev, *Synchrotron Radiation Power Calculations and Bending Radius Choice for the LER*, SLAC Internal Report ABC-13.

[4] O. Gröbner, et al., Vacuum 33, 397 (1983).

[5] See a) C. Foerster, H. Halama, C. Lanni, *J. Vac. Sci. Technol* A8 (3) 2856, 1990; b) A. Mathewson, et al., Comparison of Synchrotron Radiation Induced Gas Desorption from Al, Stainless Steel, and Cu Chambers, *Proceedings of the Symposium on Vacuum Systems for Synchrotron Radiation Sources*, Argonne National Laboratory, Nov., 1990 and c) Ueda, et al., Photo-desorption from Stainless Steel, Aluminum Alloy and Oxygen Free Copper Test Chambers, ibid.

[6] John F. O'Hanlon, *A User's Guide to Vacuum Technology*, John Wiley (1980).

[7] W. A. Barletta, Modeling Photo Desorption in High Current Storage Rings, This conference.

UCRL- JC-105595
PREPRINT

VACUUM SYSTEM OF THE HIGH ENERGY RING OF AN ASYMMETRIC B-FACTORY BASED ON PEP

W. A. Barletta
M. O. Calderon
R. L. Wong
T. M. Jenkins

This paper was prepared for submittal to the
1991 IEEE Particle Accelerator Conference
Accelerator Science and Technology
San Francisco, California
May 6-9, 1991

May 7, 1991

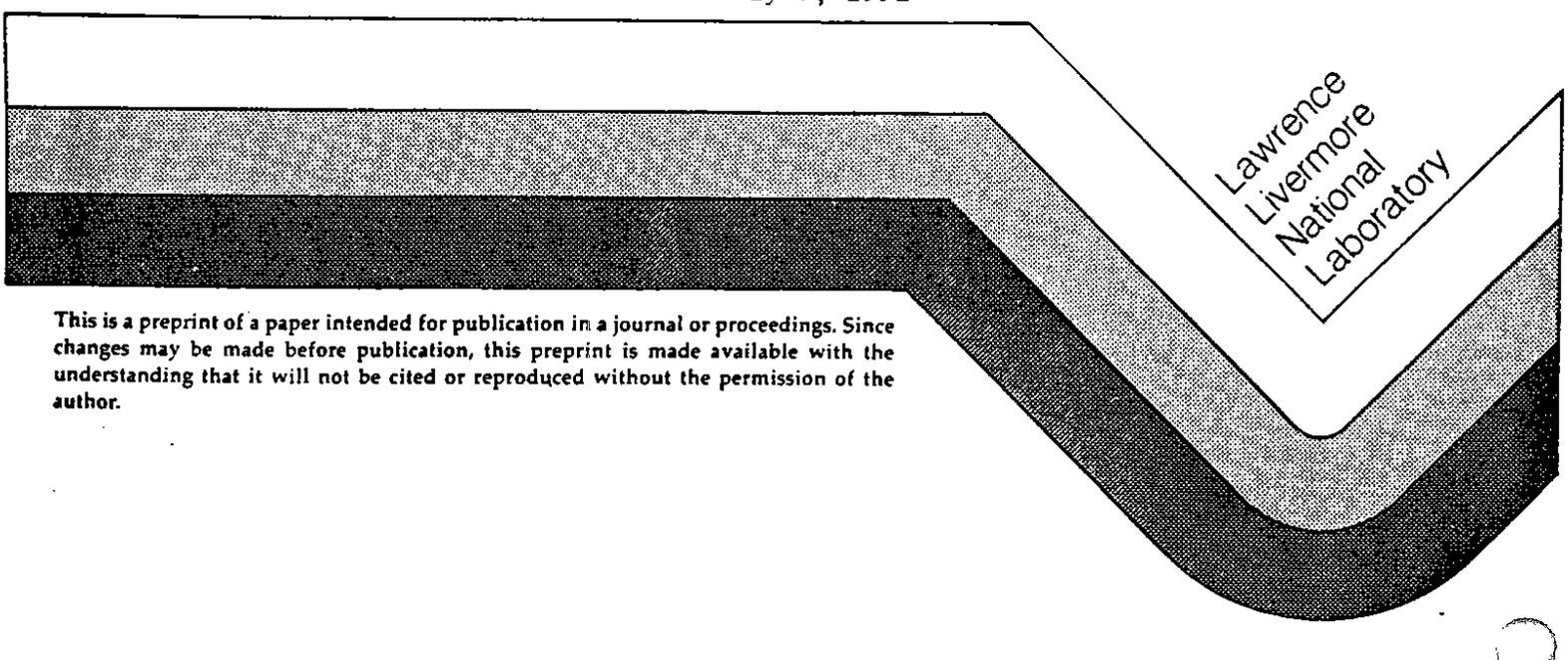

DESIGN OF THE VACUUM SYSTEM FOR THE HIGH ENERGY RING OF AN ASYMMETRIC B-FACTORY BASED ON PEP

William A. Barletta , Manuel Calderon, Robert Wong
Lawrence Livermore National Laboratory, P. O. Box 808, Livermore, CA 94551
and
Theodore Jenkins
Stanford Linear Accelerator Center, P. O. Box 4349, Stanford, CA 94309

ABSTRACT

The multi-ampere currents required for high luminosity operation of an asymmetric B factory leads to extremely stressing requirements on a vacuum system suitable for maintaining long beam-gas lifetimes and acceptable background levels in the detector. We present the design for a Cu alloy vacuum chamber and its associated pumping system for the 9 Gev electron storage ring of the proposed B factory based on PEP. The excellent thermal and photo-desorption properties of Cu allows handling the high photon flux in a conventional, single chamber design with distributed ion pumps. The x-ray opacity of the Cu is sufficiently high that no additional lead shielding is necessary to protect the dipoles from the intense synchrotron radiation generated by the beam. The design allows chamber commissioning in <500 hr of operation.

I. INTRODUCTION

The vacuum system of the asymmetric B-factory based on PEP [1] (APIARY) presents a technical challenge beyond that of any existing electron storage ring. Each technical sub-system must meet demanding design criteria to meet the overall system requirements. The sub-systems for the high energy (electron) ring (HER) are the beam chamber, the pumping sub-system, the cooling sub-system, and the special components.

The 9 GeV HER will have a circulating beam current of ≈1.5 A for a design luminosity of 3×10^{33} $cm^{-2}s^{-1}$. To allow for possible upgrades and to provide for luminosity "breathing room", we specify a maximum limiting current of 3 A. This value is an order of magnitude beyond that which typifies present colliders. As such it presents an appreciable challenge to the system designer. The system requirements specifying pressures during collider operation at a maximum limiting current of 3 A are as follows:

- ≤ 10 nTorr in the dipole arcs,
- ≈3 nTorr in the straight sections,
- ≈1 nTorr in the straight upstream of the detector,
- ≈ 0.1 nTorr base pressure with no beam.

The circulating electron beam subjects the walls of the vacuum chamber to copious synchrotron radiation. As the angular distribution of the radiation fan is narrow, the associated thermal flux is high enough to require considerable cooling of the chamber wall. The cooling sub-system is designed to remove the waste heat safely under the conditions of high radiation flux regardless of machine tune. As is common, cooling is accomplished by water flowing in channels exterior to the chamber. In addition to assuring the mechanical stability of the chamber under thermal loads as high as 10 MW in the HER maintaining the chamber wall at a relatively low temperature minimizes the gas load due to thermal desorption.

II. CHAMBER SIZE

The HER lattice outside the interaction region is composed of 48 standard straight cells, 72 standard arc cells and 24 dispersion suppressor cells. The chamber size in the arcs is determined by the beam's emittance, its energy spread, and the lattice functions. For adequate quantum lifetime regardless of tune, we designed the chamber to accommodate the uncoupled horizontal emittance and the fully coupled vertical emittance. The chamber cross section is kept constant throughout the bends to minimize the constribution to the impedance budget from the chamber. Hence, we use the maximum values of the optical functions to size the chamber. In the absence of extensive wigglers, the beam's energy spread should be close to its natural value, 6.1×10^{-4}. For conservatism, we assume a value of 10^{-3}. As the optics are similar to PEP, the closed orbit allowances should also be similar. The emittance and optical specifications for the HER are given in Table 1.

Table 1. Optical parameters for the HER

Max uncoupled ε_{xo}	100 nm
Fully coupled ε_{yo}	50 nm
Max. horiz. β in arcs, β_{xmax}	25.6 m
Max. vert. β in arcs, β_{ymax}	32.9 m
Max. dispersion, η_{max}	1.86 m
Horiz. closed orbit, CO_x	± 10 mm
Vert. closed orbit, CO_y	± 5 mm

The minimum horizontal and vertical sizes are given by

$$\sigma_{xtot} = 10\left\{\varepsilon_{xo}\,\beta_{xmax} + \eta_{max}^2\left(\frac{\sigma_E}{E}\right)^2\right\}^{1/2} + CO_x \qquad (1)$$

and

$$\sigma_{ytot} = 10\left\{\varepsilon_{yo}\,\beta_{ymax}\right\}^{1/2} + CO_y \qquad (2)$$

respectively. To include allowances for fabrication and mechanical positioning, we adopted the following chamber (inner) dimensions for the HER: $BCS_x \times BCS_y = \pm45$ mm × ± 25 mm. The corresponding conductance of a 1 m section of beam pipe is 35 l/s.

III. SYNCHROTRON RADIATION LOAD

Each cell of the HER arcs has a length of 15.2 m and is divided into two two halves, each containing a PEP dipole (0.182 T), a quadrupole and a bellows. Our estimate of the

thermal load from the synchrotron radiation generated in the dipole follows from the analysis of [2]. The relative power profile is displayed in Fig. 1. At the design current of 1.5 A maximum power deposited is 51 W/cm.

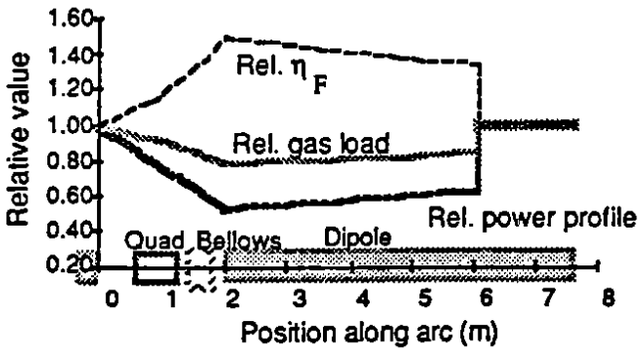

Fig. 1. Relative distribution of synchrotron radiation, η_F, and gas load in arcs of 9 GeV APIARY ring.

In the arcs the bending radius is 165 m, and the a maximum angle of incidence of the radiation is 23 mrad. For conservativism in estimating the power density, we ignore the contribution to the height of the synchrotron fan due to the finite emittance. Thus, the minimum height of the illuminated strip is ≈0.5 mm. The corresponding maximum thermal flux at 1.5 A is P_A, 1.14 kW/cm^2, two-thirds of the design value for the present PEP chamber. The corresponding photon flux, which has a typical synchrotron radiation spectrum with a critical energy of 9.8 keV, is 4×10^{19} s^{-1}cm^{-2}. This value provides the basis for the EGS4 calculations of radiation absorption in the chamber.

IV. ABSORPTION OF SYNCHROTRON RADIATION

Depending upon material and thickness of the beam pipe, synchrotron radiation may escape and deposit energy in the surroundings. This radiation can damage magnet insulation, wire insulation and cooling water hoses. The damage threshold for the magnets is a function of the potting compound. The expoxy insulating the PEP magnets is expected to tolerate ≈10^{10} rad. We have adopted 3×10^9 Rads as a conservative criterion, which sets a limit of 10^8 Rads/yr for a magnet lifetime of 30 years. For 6000 hr of operation at the 1.5 A current, the allowed yearly dose translates to 4.9×10^{-19} Rads/e$^-$. This criterion is used to compare with EGS4, which calculates dose *per incident electron*, either in terms of fluences, energy deposited, or Rads (using appropriate conversion factors).

For most calculations the cutoffs for tracking the electromagnetic cascade set at 10 keV (photons) and 1 MeV (electrons). Upper energies for both electrons and photons were 10 MeV. The photon spectrum was sampled uniformly within an energy range from 0.1 ε_{crit} to 10 ε_{crit}. A weight was carried along with each photon (and progeny) for scoring purposes. The final results were later normalized per incident beam electron.

The beam pipe is an octagonal chamber with a copper cooling bar as shown in Fig 2. Our calculations show that only 2.5 mm of Cu is needed to meet the radiation leakage criterion at the point of maximum dose (top and bottom of the beam pipe) for 9-GeV beams. In contrast an octagonal aluminum pipe that is 5 mm thick requires a lead liner. We have adopted 5 mm of Cu as the wall thickness to allow for sufficient shielding at energies as high as 12 GeV.

Using the details of radiation absorption from EGS4, we calculate the temperature distribution in the walls using the thermal analysis program, TOPAZ. For 25° C water flowing at 3 m/s through stainless steel cooling tubes the maximum temperature in the beam tube is 160° C. A 2-D stress analysis with NIKE2D indicates a maximum vertical deflection of 0.021 mm of the flat horizontal faces of the beam tube (an acceptable value). This analysis also shows maximum stresses of 90 MPa, exceeding the yield stress of the 98%Cu-2% Sn alloy in the region where the radiation fan strikes the chamber. This calculation is overly conservative since it does not account for stress relief that would be obtained through bending out of plane axis. We therefore believe that the alloy will actually have sufficient yield strength to withstand the thermal load. We are making a 3-D analysis to evaluate the effects of bending. If the 3-D calculations also indicate that the material yields, we will make a cyclic fatigue analysis to determine if there is a structural problem.

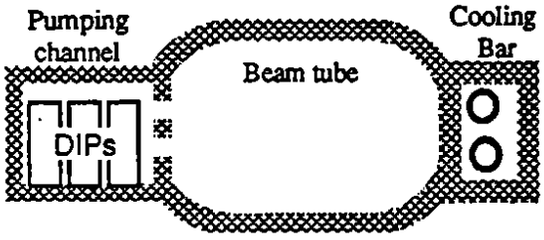

Figure 2. Cross section of the HER arc vacuum chamber.

V. GAS LOAD AND PUMPING

During collider operation photo-desorption from the chamber walls dominates the gas load. Following ref. [2] we can translate the thermal load into a dynamic gas load including the leveling effects due to a non-uniform photo-desorption efficiency, η_F (Fig. 1). Measurements of η_F [3, 4, 5] for well exposed samples of Al, stainless steel and high conductivity, oxygen free Cu indicate minimum values ranging from $<2\times10^{-6}$ for Cu and stainless steel to 2×10^{-5} for Al. Although the beam-gas lifetimes in storage rings with lower ε_{crit} than APIARY suggest that Al may eventually develop an effective $\eta_F \approx 10^{-6}$, we believe a more reliable approach is to adopt Cu or stainless steel as the chamber material despite their higher bulk cost. As the data [5] indicate that pure Cu can attain $\eta_F \le 2\times10^{-6}$, we selected this value as the design basis. Such a low desorp-ion coefficient allows the vacuum chamber to have a conventional shape instead of an ante-chamber configuration that is more difficult and expensive to fabricate. The apparent cost disadvantage of Cu or stainless vis á vis Al is more than offset by the relative simplicity of the chamber shape, by the reduction of the required pumping and by the reduced commissioning time.

With a minimum η_F of 2×10^{-6}, the maximum gas load at 3 A is 1.2×10^{-6} Torr-l/s/m with the profile of Fig. 1.

Such low values of η_F have been measured in pure Cu. Confirming the practicality of our design choice for η_F is a key part of an experimental validation program.

To pump this gas load, we have selected an all sputter ion pump design. We show the inventory of pumping capacities for each pumping element in a typical cell in Table 2. At 1.5 A the desired average pressure (5 nTorr) is maintained with distributed pumping of 125 l/s/m. To achieve these speeds the distributed ion pumping in the dipoles of PEP has been redesigned to operate in a 0.18 T field. The anode was increased to 1.8 cm diameter, and one more row was added, increasing the number of anodes by 33% with a packing factor of about 90%. Distributed ion pumping (DIPs) has been added at the quadrupoles in stainless steel housings to one side of the beam tube and below but none on the top to preclude particles dropping into the beam chamber. As the available space is restrictive, the anodes have been reduced in size. The calculated pumping speed in the beam tube will be about 75 l/s/m from each of the steel housings. However, the total pumping speed for the defocusing and focussing quadrupoles are different owing to their different lengths. To augment the DIPs we have added 60 l/s lumped ion pumps in each of the quadrupole spaces of the cells. Given the low conductance of the beam pipe, larger pumps would not improve system performance. Moreover, the ports are designed to accommodate additional pumps if needed.

Table 2. Pumping inventory of HER arc cell

2 Dipole DIPs	800 l/s
1 Quad DIP	110 l/s
1 Quad DIP	80 l/s
1 Lumped ion pumps	60 l/s
Total distributed pumping	125 l/s/m

VI. STRAIGHT SECTIONS & SPECIAL COMPONENTS

To keep the contribution of the ports to the machine impedance negligible the ports are shielded with perforated screens with longitudinal slots 10 cm long by about 0.2 cm wide. The pumping slots in the septum between the pump channel and beam tube have been calculated as rows of slots 9 cm long by about 0.2 cm wide at a pitch of 10 cm, similar to HERA, giving a conductance of about 500 l/s/m. These slots contribute a negligible amount to machine impedance.

Each bend cell contains a beam position monitor (BPM) located at and anchored to the defocusing quadrupole. The BPM for APIARY follows the HERA design with minor modifications. The housing will be accurately machined from a solid Cu block having recesses on its end faces to index the ends of the beam tube for alignment during brazing. Cooling on both sides will preclude a temperature asymmetry between lateral sides.

Changes in cross section between the arcs of octogonal cross section and the straight sections of circular cross section are made with tapered transition elements. To keep the total contribution to the chamber impedance within the impedance budget, the taper angle is <10°.

A typical cell in the straight sections is 15.125 m in length. The vacuum conduit is a 10 cm diameter, stainless steel tube of circular section sized to clear the 100 mm bore of the magnets. To produce an average pressure <3 nTorr in the straight sections we will install lumped sputter ion pumps rated at 230 l/s spaced by ≈8 m. We have calculated the pump size and spacing assuming a thermal outgassing rate of 10^{-11} torr-l/cm^2/s and a pressure differential in the beam tube of 0.5 nTorr. In situ baking compatibility to 150° C is provided to reduce the initial outgassing and to allow for pressures in the 0.1 nTorr range if such low pressures are required.

To aid in the assembly both bend and straight cells contain bellows designed to permit 130°C of thermal expansion. In their extended position at room temperature, the bellows are 22.9 cm long. They can compress ≈4 cm to 18.9 cm at the maximum temperature (150° C) to which the ring can be baked in situ without disassembly. The inner bellows which carry the surface currents is fabricated as one piece with formed convolutions in the plane of the beam tube flats and has narrow slits at the intersecting corners to permit axial movement. A narrow slit permits synchrotron radiation to shine through to thick-wall, water cooled, Cu absorbers cantilevered from the flanges to carry away the thermal load.

A calculation of a commissioning scenario [2] shows that the time needed to store the design current for >2 hours varies with the initial value of η_F as determined by fabrication procedures. For $\eta_F(0) = 10^{-3}$, commissioning the Cu chamber requires ≈500 hr. For an appropriately cleaned chamber we expect $\eta_F(0) = 10^{-4}$, in which case the full design current can be stored after 150 hours (Fig. 3).

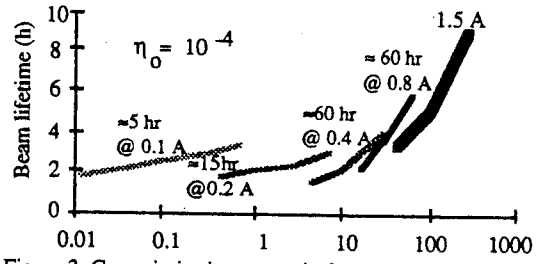

Figure 3. Commissioning scenario for an etched Cu chamber.

The authors thank William Davies-White, Andrew Hutton (SLAC), Henry Halama (BNL), Oswald Gröbner, Alastair Mathewson (CERN), and Michael Zisman (LBL) for their critical comments. Supported by U. S. Dept. of Energy at LLNL under contract W-7405-eng-48 and at SLAC under contract DE-AC03-76SF00515.

VII. References

[1] "An Asymmetric B Factory Based on PEP - Conceptual Design Report", LBL PUB-5263, February, 1991.

[2] W. A. Barletta, Modeling Photo-desorption in High Current Storage Rings, Proceedings, this conference.

[3] C. Foerster, H. Halama, C. Lanni, J. Vac. Sci. Technol. A8 (3)June, 1990, p. 2856.

[4] A. Mathewson et al., "Comparison of Synchrotron Radiation Induced Gas Desorption from Al, Stainless Steel, and Cu Chambers", Proceedings of the Symposium on Vacuum Systems for Synchrotron Radiation Sources, ANL, Nov., 1990.

[5] Ueda et al., "Photo-desorption from Stainless Steel, Aluminum Alloy and Oxygen free Copper Test Chambers", ibid.